eLife

Reviewed Preprint
v1 • September 2, 2026
Not revised

For correspondence:
edward_barker@rush.edu

Competing interests: No competing interests declared

Funding: See page 32

Reviewing editor: Frank Kirchhoff, Ulm University Medical Center, Germany

$CD56^{dim}CD16^{dim}$ NK cells are the dominant effector cells against HIV-infected primary T-cells

William Howell[1], Courtney Branch[1], Jeffrey Ward[2], Zachary Davis[3], Emma Geatches[1], Edward Barker[1]

[1][1]Department of Microbial Pathogens and Immunity, Rush University Medical Center, Chicago, United States • [2]Division of Oncology, Department of Medicine, Washington University in St. Louis, St Louis, United States • [3]Department of Medicine, University of Minnesota, Minneapolis, United States

eLife Assessment

This **valuable** study compares the anti-HIV activity of human natural killer cell subsets and identifies $CD56^{dim}CD16^{dim}$ cells as a potentially key effector population against HIV-infected autologous T cells. The evidence supporting the central conclusions seems **incomplete** because the interpretation may be substantially confounded by activation-induced CD16 downregulation, making it difficult to distinguish intrinsic functional differences from phenotypic changes that occur during target-cell engagement. Additional experiments using purified NK-cell subsets and appropriate controls would substantially strengthen the evidence supporting the major conclusions.

https://doi.org/10.7554/eLife.112322.1.sa3

Abstract

Despite being rare among circulating natural killer (NK) cells and expressing 10-fold less CD16 than the predominant $CD56^{dim}CD16^{bright}$ population, $CD56^{dim}CD16^{dim}$ NK cells are expanded in HIV long-term elite controllers, yet their capacity to kill HIV-infected cells remained untested. Here, we show that these rare cells are the dominant effectors against HIV-infected T-cells, mediating approximately 4-fold higher direct cytotoxicity and 3-4-fold higher antibody-dependent cellular cytotoxicity (ADCC) than $CD56^{dim}CD16^{bright}$ cells, and serially engaging multiple targets. This advantage is intrinsic, unexplained by cytotoxic granule content or inhibitory receptors recognizing MHC class I. Direct killing depends on NKG2D recognition of Vpr-induced ligands, with NKG2D elevated on $CD56^{dim}CD16^{dim}$ cells; ADCC requires both NKG2D and ADAM17-mediated CD16 turnover for serial engagement. These findings explain the elite-controller reorganization, reveal that NK effector dominance is target-tuned rather than fixed ($CD56^{dim}CD16^{negative}$ cells dominate against K562 cells), and identify high-NKG2D $CD56^{dim}CD16^{dim}$ cells as the effector population HIV therapies should reproduce.

Impact Statement

A rare natural killer cell subset that makes up only a few percent of circulating NK cells, yet is enriched in the people who control HIV for years without medication, turns out to be the dominant killer of HIV-infected cells, far outperforming the common subset long assumed to do the job, and this work shows how these cells recognize and repeatedly attack infected targets, pointing to the specific effector that future cell-based therapies might use to help people with HIV stay healthy without lifelong drugs.

Introduction

HIV affects approximately 40.8 million people worldwide [37.0-45.6 million] (UNAIDS 2024), causing a chronic infection that requires antiretroviral therapy (ART) to prevent progression to AIDS. Although ART effectively suppresses viral plasma levels (Antela et al., 2021; Puertas et al., 2025; Sarin & Goldstein, 1995), it cannot eradicate HIV-infected reservoirs that persist in anatomical sites, especially in gut-associated lymphoid tissue and lymph nodes, where ART's access to infected cells appears limited (Belmonte et al., 2007; Chun et al., 2008; Estes et al., 2017; Fletcher et al., 2014; North et al., 2010; Thompson et al., 2017). Moreover, latent reservoirs cause viral rebound within weeks of stopping ART, making lifelong therapy necessary (Finzi et al., 1997; Magombedze et al., 2025; Puertas et al., 2025). Long-term ART has side effects, including accelerated aging, metabolic issues, loss of bone integrity, and cardiovascular problems (Ghandakly et al., 2025; Lagathu et al., 2019; Milburn et al., 2017; Olali et al., 2022; Vos & Venter, 2021). These limitations of ART highlight the urgent need for new, sustainable therapeutic strategies that can target and eliminate infected cells.

Natural killer (NK) cells are cytotoxic lymphocytes that eliminate virus-infected cells through direct cytotoxicity and antibody-dependent cellular cytotoxicity (ADCC) without prior sensitization (Lanier, Chang, et al., 1991; Lanier et al., 1983; Lanier, Yu, et al., 1991; Perussia et al., 1984). NK cell-based immunotherapies have shown success in treating leukemia, and haploidentical NK cell adoptive transfer is safe, does not cause graft-versus-host disease, cytokine release syndrome, or immune effector cell–associated neurotoxicity syndrome, and, under certain circumstances, can be sustained (Bednarski et al., 2022; Bjorklund et al., 2018; Cichocki et al., 2020; Cooley et al., 2019; Geller & Miller, 2011; Miller et al., 2005; Myers & Miller, 2021). However, NK cell-based therapeutic approaches to HIV have demonstrated limited effectiveness (Abeynaike et al., 2023; Kim et al., 2022), possibly due to uncertainty about which NK cell subset provides the best antiviral activity (Alter et al., 2005; Florez-Alvarez et al., 2020; Hu et al., 1995; Ivison et al., 2022; Lichtfuss et al., 2012; Mavilio et al., 2003; Pohlmeyer et al., 2019; Sanchez-Gaona et al., 2024).

Human NK cells comprise distinct subsets with varying functional capacities. The $CD56^{dim}CD16^{bright}$ population, representing ~85% of circulating NK cells, has traditionally been considered the primary cytotoxic subset because of its high CD16 expression, which enables robust ADCC. (Cooper et al., 2001; Jacobs et al., 2001; Nagler et al., 1989). Cells with intermediate CD16 expression have been characterized as transitional or exhausted states in studies of tumors and other contexts, and their low frequency in peripheral blood meant that their potential contribution to HIV-specific responses had not been directly examined (Romee et al., 2013; Yang et al., 2019).

Together with the low frequency of $CD56^{dim}CD16^{dim}$ cells in the peripheral blood of uninfected individuals (<6%), this characterization led therapeutic development to focus on the more abundant $CD56^{dim}CD16^{bright}$ cell subset. However, recent observations have prompted a reexamination of this characterization (Amand et al., 2017; Rallon et al., 2024). Rallon et al. reported that long-term (>10 years since initial infection) HIV elite controllers (LTEC), a rare (<1%) subset of infected individuals who suppress HIV without ART, maintain expanded $CD56^{dim}CD16^{dim}$ populations, suggesting that these cells may contribute to viral control (Rallon et al., 2024). Moreover, the frequency of $CD56^{dim}CD16^{bright}$ NK cells is lower in LTEC than in uninfected controls and in people living with HIV who are on ART. Although this study reports a higher prevalence of $CD56^{dim}CD16^{dim}$ cells in LTEC, the functional capacity of these cells to eliminate HIV-infected targets has not been directly assessed (Rallon et al., 2024).

Here, we systematically compared the ability of NK cell subsets defined by CD16 expression to eliminate HIV-infected cells. We show that $CD56^{dim}CD16^{dim}$ cells, despite their rarity and lower CD16 density, are the dominant NK cell population that targets HIV-infected primary T-cells. This dominance reflects integrated NKG2D and ADAM17-dependent CD16 signaling, which supports

both per-cell efficiency and serial engagement of multiple infected targets. These findings identify the natural effector cells configuration that cellular therapies aimed at an HIV functional cure can build toward.

Results

$CD56^{dim}CD16^{dim}$ NK cells show target-dependent enhanced functional responses

To understand why $CD56^{dim}CD16^{dim}$ NK cell frequencies correlate with HIV clinical outcomes (Amand et al., 2017; Rallon et al., 2024), even though prior work has not shown them to be universally superior effectors against tumor targets, we first validated these findings using the chronic myeloid leukemia cell line, K562, as the target cells (Amand et al., 2017; Herberman & Ortaldo, 1981; Ortaldo et al., 1977). We then specifically examined NK cell responses to autologous HIV-infected T-cells.

We began by characterizing the baseline distribution of NK cell subsets in healthy, uninfected donors. The $CD56^{negative}$ NK cells were identified by NKp80 expression (Figure 1-figure supplement 1). In line with the established literature (Amand et al., 2017; Rallon et al., 2024), $CD56^{dim}$ NK cells constituted the majority [mean=93.38% ± standard deviation (SD)= 0.96%] of circulating NK cells, with $CD56^{bright}$ NK cells (4.46% ± 0.73%) and $CD56^{negative}$ NK cells (2.04% ± 0.32%) accounting for a small fraction (Figure 1-figure supplement 1). Within the $CD56^{dim}$ NK cell population, $CD16^{bright}$ cells were predominant (91.84% ± 0.04%). In comparison, $CD16^{dim}$ cells (4.56% ± 0.24%) and $CD16^{negative}$ cells (3.82% ± 0.22%) were minor $CD56^{dim}$ NK cell subsets (Figure 1-figure supplement 1).

To confirm the previous observations (Amand et al., 2017) regarding $CD56^{dim}CD16^{dim}$ functional capacity, we assessed NK cell degranulation responses against the chronic myeloid leukemia K562 cell line at an effector-to-target (E:T) ratio of 1:1. Consistent with previous findings (Amand et al., 2017), $CD56^{dim}CD16^{negative}$ NK cells showed significantly higher degranulation (surface $CD107a^{positive}$) than $CD56^{dim}CD16^{dim}$ NK cells (Figure 1—figure supplement 2; donor 1, p=0.0018; donor 2, p<0.0001), with $CD56^{dim}CD16^{bright}$ cells showing the lowest responses (donor 1: 20.34 ± 2.39; donor 2: 12.24 ± 0.33; all between-subset comparisons within each donor p≤0.0018 by one-way ANOVA with Tukey's multiple comparisons test; Supplemental Table 1). $CD56^{dim}CD16^{negative}$ NK cells showed the highest degranulation in donors 1 (85.63% ± 1.38%) and 2 (58.78% ± 1.13%), followed by $CD56^{dim}CD16^{dim}$ NK cells in donors 1 (71.17% ± 3.81%) and 2 (48.38% ± 0.56%). These results confirmed (Amand et al., 2017) that $CD56^{dim}CD16^{dim}$ NK cells do not exhibit a functional advantage over $CD56^{dim}CD16^{negative}$ NK cells in response to K562 target cells; on the contrary, $CD56^{dim}CD16^{negative}$ NK cells significantly outperform $CD56^{dim}CD16^{dim}$ NK cells in this context.

Given this knowledge gap between clinical relevance against HIV (Amand et al., 2017; Rallon et al., 2024) and functional capacity against tumor targets (Amand et al., 2017), we hypothesized that $CD56^{dim}CD16^{dim}$ cells might possess HIV-specific functional capacity. To test this, we examined NK cell responses against autologous HIV-infected T-cells using the same degranulation assay at an E:T ratio of 1:1. Notably, despite a low frequency (4.26% ± 0.24%) of $CD56^{dim}CD16^{dim}$ cells amongst the total population of NK cells (Figure 1A), a dramatically higher frequency of $CD56^{dim}CD16^{dim}$ cells that degranulated against HIV-infected targets (25.47% ± 3.75%) compared to all other NK cell subsets, which showed markedly lower responses (0.63% to 13.19%) (Figure 1B; one-way ANOVA $F(6, 14) = 85.96$, p<0.0001; Dunnett's multiple comparisons test against $CD56^{dim}CD16^{dim}$, all p<0.0001; Supplemental Table 2).

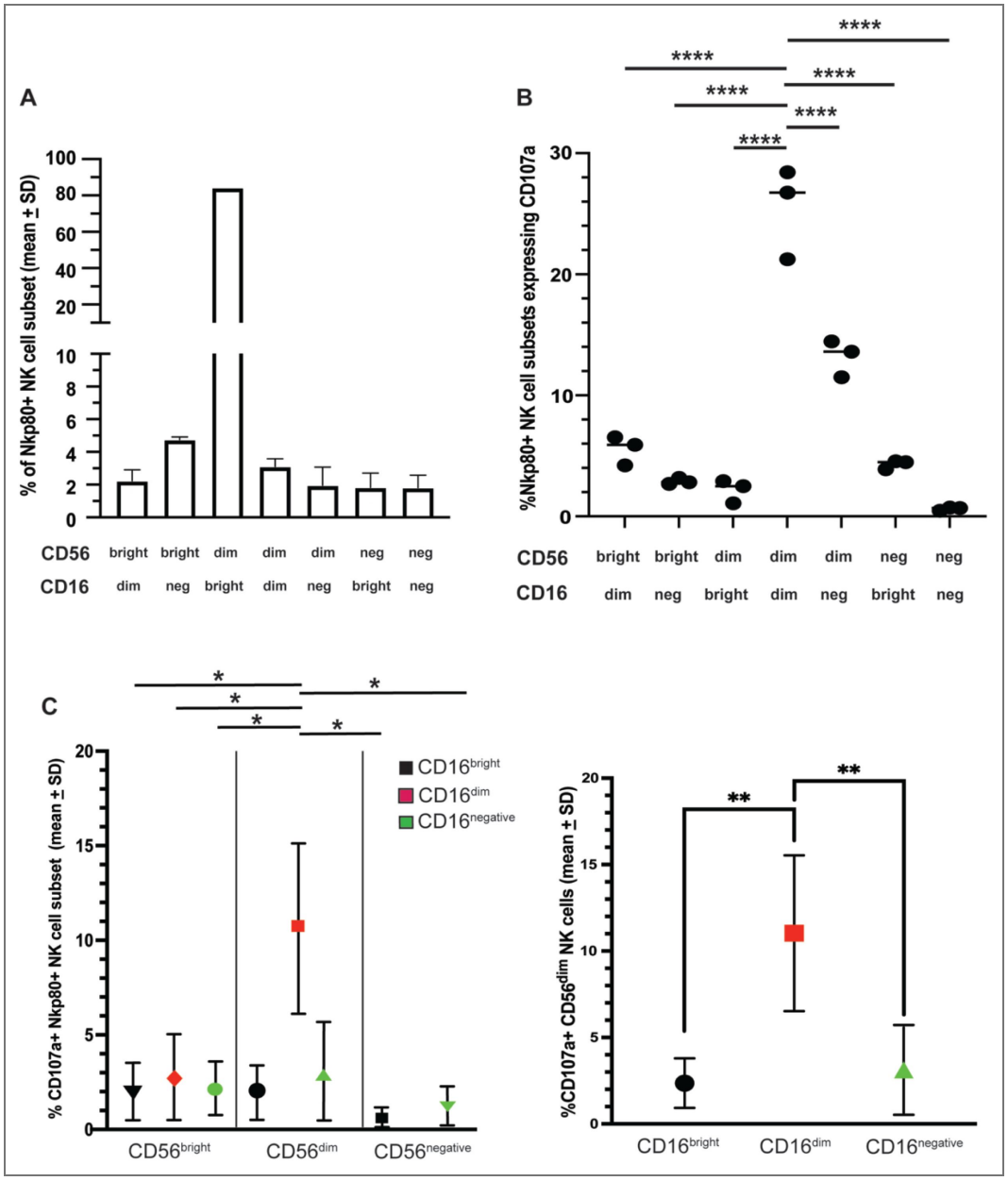

Figure 1. Degranulation of NK cell subsets based on differential expression of CD56 and CD16 in response to purified autologous HIV productively infected T-cells

(A) Frequency of NK cell subsets [mean + standard deviation (SD)] within total peripheral blood NK cells of an HIV-uninfected donor [the donor used for (B)], based on differential CD56 and CD16 expression. NKp80 was used to identify $CD56^{negative}$ NK cell subsets. (B) Frequency of NK cell subsets expressing CD107a following a 4-hour exposure at a 1:1 effector cell to target cell (E:T) ratio to purified autologous productively $HIV\text{-}1_{SHM\text{-}1}$ infected T-cells. Each circle represents a technical replicate; lines indicate mean values. All values are background-subtracted (target-exposed minus unexposed control). (C) Frequency of CD107a expression (mean + SD) on NK cell subsets across six different donors. The $CD56^{negative}$ $CD16^{dim}$ subset was excluded because its frequency in peripheral blood (<0.2% of NK cells; Figure 1-figure supplement 1B) yields event counts insufficient for reliable measurement. (D) Frequency of $CD56^{dim}$ NK cell subsets [from (C)] that were also $CD16^{bright}$, $CD16^{dim}$, or $CD16^{negative}$ across the same six donors. Panels A and B show data from one representative donor with three technical replicates; panels C and D show data from six donors analyzed in separate experiments, with each donor evaluated independently to avoid confounding from KIR and HLA polymorphism. Statistical analyses: one-way ANOVA with Dunnett's post-hoc against $CD56^{dim}CD16^{dim}$ for panel B; repeated-measures one-way ANOVA with donor matching and Dunnett's post-hoc for panels C and D. Full ANOVA tables and post-hoc results are in Supplemental Tables 2 and 3. Significance: * $p < 0.05$, ** $p < 0.01$, *** $p < 0.001$, **** $p < 0.0001$.

The superiority of $CD56^{dim}CD16^{dim}$ to degranulate in response to HIV-infected cells is reproducible and intrinsic

To determine whether the HIV-specific functional superiority of $CD56^{dim}CD16^{dim}$ NK cells was reproducible, we examined NK cell degranulation responses to HIV-infected cells at a 1:1 E:T ratio across six healthy, uninfected donors. The NK cell subsets evaluated were based on nine different populations defined by gates set using fluorescence-minus-one (FMO) staining controls for CD56 and CD16, with gates for $CD56^{bright}CD16^{negative}$ and $CD56^{dim}CD16^{bright}$ NK cells used to determine "bright" NK cell subpopulations, as shown in Figure 1-figure supplement 1 A.

Analysis of NK cell responses to autologous HIV productively infected targets across multiple donors (Figure 1C) confirmed the consistent superiority of $CD56^{dim}CD16^{dim}$ NK cells in the present study. The $CD56^{negative}CD16^{dim}$ subset was excluded from this analysis because its very low frequency in peripheral blood (<0.2% of NK cells; Figure 1-figure supplement 1B) resulted in insufficient event counts for reliable measurement. Within the $CD56^{dim}$ population, a significantly higher frequency of $CD16^{dim}$ cells showed degranulation responses than $CD56^{bright}CD16^{bright}$ (p=0.0110), $CD56^{bright}CD16^{dim}$ (p=0.0200), and $CD56^{bright}CD16^{negative}$ (p=0.0192) NK cells. In other comparisons, $CD56^{dim}CD16^{dim}$ cells showed a significantly higher frequency of degranulating cells than $CD56^{negative}CD16^{bright}$ (p=0.0104) and $CD56^{negative}CD16^{negative}$ (p=0.0145) cells (repeated-measures one-way ANOVA F(1.941, 9.705) = 17.88, p=0.0006; Dunnett's multiple comparisons test against $CD56^{dim}CD16^{dim}$; Supplemental Table 3).

To specifically examine the role of CD16 expression levels within the $CD56^{dim}$ population, we directly compared degranulation responses across the $CD16^{bright}$, $CD16^{dim}$, and $CD16^{negative}$ subsets. $CD56^{dim}CD16^{dim}$ cells exhibited significantly greater HIV-specific degranulation compared to both $CD56^{dim}CD16^{bright}$ (p=0.0043) and $CD56^{dim}CD16^{negative}$ cells (p=0.0040) (Figure 1D). The mean ± SD frequency of degranulating $CD56^{dim}CD16^{dim}$ cells was 11.03 ± 4.51%, which was more than 4-fold higher than the frequency of degranulating $CD56^{dim}CD16^{bright}$ cells (2.36 ± 1.44%) and more than 3-fold higher than $CD56^{dim}CD16^{negative}$ cells (2.93 ± 2.79%).

$CD56^{dim}CD16^{dim}$ cells demonstrate greater cytotoxicity even when purified

To verify that the observed HIV-specific functional superiority was inherent to $CD56^{dim}CD16^{dim}$ NK cells and not influenced by differences in subset frequency in mixed populations, we performed cytotoxicity assays using purified $CD56^{dim}CD16^{bright}$ and $CD56^{dim}CD16^{dim}$ NK cell subsets.

Direct comparison of purified NK cell subsets revealed that $CD56^{dim}CD16^{dim}$ NK cells exhibited significantly higher cytotoxic activity against autologous HIV-infected targets at three of four E:T ratios tested (Figure 2). At the lowest E:T ratio (1:8), $CD56^{dim}CD16^{dim}$ cells showed a 2-fold higher mean ± SD of specific lysis (14.49% ± 2.90%) compared to $CD56^{dim}CD16^{bright}$ cells (7.50% ± 1.05%). This difference approached statistical significance but did not reach it (p=0.0579). At the 1:4 ratio, the functional advantage of $CD56^{dim}CD16^{dim}$ cells reached significance, with 32.63% ± 7.45% specific lysis compared to 16.15% ± 3.16% for $CD56^{dim}CD16^{bright}$ cells (p=0.0002). The advantage increased progressively at higher E:T ratios. At the 1:2 ratio, $CD56^{dim}CD16^{dim}$ cells achieved 59.96% ± 7.39% specific lysis compared to 26.31% ± 2.18% for $CD56^{dim}CD16^{bright}$ cells (p<0.0001). At the 1:1 ratio, $CD56^{dim}CD16^{dim}$ cells achieved 77.58% ± 1.35% specific lysis compared to 39.18% ± 2.05% for $CD56^{dim}CD16^{bright}$ cells (p<0.0001). The overall analysis confirmed significant effects of NK cell subset (F(1, 16) = 195.0, p<0.0001), E:T ratio (F(3, 16) = 148.1, p<0.0001), and their interaction (F(3, 16) = 18.42, p<0.0001), by two-way ANOVA with Šidák's multiple comparisons test (Supplemental Table 4).

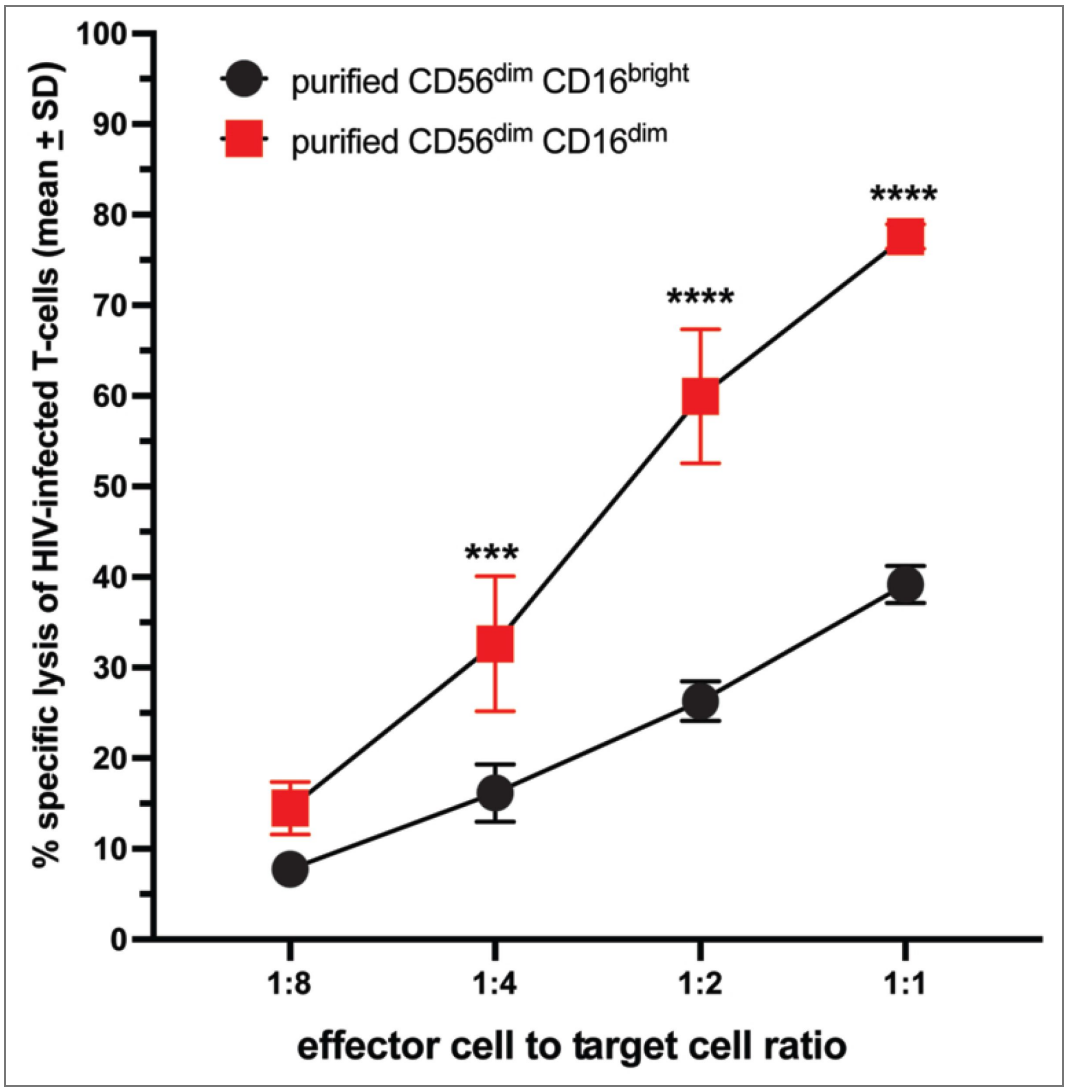

Figure 2. Lysis of autologous HIV-productively infected T-cells by purified CD56^{dim}CD16^{dim} and CD56^{dim}CD16^{bright} NK cells

Purified NK cells from an uninfected individual were sorted into CD56^{dim}CD16^{dim} and CD56^{dim}CD16^{bright} NK cell subsets. Carboxyfluorescein succinimidyl ester (CFSE)-labeled purified autologous productively HIV-1_{SHM-1} infected T-cells generated in vitro were added to the sorted NK cell subsets at various effector-to-target cell (E:T) ratios in triplicate. After 4 hours, cells were surface-stained for CD56 and CD3, then exposed to 7-amino-actinomycin D (7AAD). Mean percent specific lysis ± standard deviation (SD) was calculated as (target cell-exposed minus mean unexposed target cells) / (mean positive control minus mean unexposed target cells) × 100, based on 7AAD staining of CFSE-labeled CD3^{positive}CD56^{negative} cells. The data shown are from one representative donor and are representative of two independent sort experiments performed with separate donors, each yielding similar results. Statistical analysis: two-way ANOVA (E:T ratio × subset) with Šidák's multiple comparisons test between subsets at each E:T ratio. Full ANOVA table and post-hoc results are in Supplemental Table 4 for Figure 2. Significance: * $p < 0.05$, ** $p < 0.01$, *** $p < 0.001$, **** $p < 0.0001$.

$CD56^{dim}CD16^{dim}$ cells exhibit greater degranulation and killing frequency in mixed NK cell populations

To comprehensively characterize the functional differences between $CD56^{dim}CD16^{bright}$ and $CD56^{dim}CD16^{dim}$ cells within mixed NK cell populations, we analyzed both degranulation responses and killing frequency across a range of E:T ratios.

Analysis of the overall NK cell population revealed distinct patterns of degranulation and cytotoxicity as the E:T ratio increased (Figure 3A). Degranulation of $CD56^{dim}CD16^{positive}$ NK cells against autologous HIV-infected cells showed a characteristic decrease from 3.23% ± 0.49% to 1.61% ± 0.05% as E:T ratios increased from 1:4 to 10:1. Specific lysis demonstrated the opposite pattern, rising from 6.23% ± 2.14% to 60.63% ± 1.39% across the same range.

Subset-specific analysis revealed dramatic functional differences between $CD56^{dim}CD16^{bright}$ and $CD56^{dim}CD16^{dim}$ cells (Figure 3B). A minimal percentage of $CD56^{dim}CD16^{bright}$ NK cells degranulated in response to purified productively HIV-infected T-cells (1.57% ± 0.21% to 0.55% ± 0.01%) across all E:T ratios tested. In contrast, a substantially greater percentage of $CD56^{dim}CD16^{dim}$ cells degranulated, peaking at the lowest E:T ratio (10.00% ± 1.21% at 1:4; $p<0.0001$) and decreasing progressively as the E:T ratio increased. The $CD56^{dim}CD16^{dim}$ advantage remained significant at 1:2 ($p<0.0001$), 1:1 ($p=0.0001$), and 3:1 ($p=0.0107$), but was no longer significant at 10:1 (1.99% ± 0.15%; $p=0.0824$). The overall analysis confirmed significant effects of NK cell subset ($F(1, 19) = 254.1$, $p<0.0001$), E:T ratio ($F(4, 19) = 41.18$, $p<0.0001$), and their interaction ($F(4, 19) = 23.94$, $p<0.0001$), by two-way ANOVA with Šidák's multiple comparisons test (Supplemental Table 5).

Two-way ANOVA of killing frequency showed a significant effect of $CD56^{dim}$ NK cell subsets ($F(1,20)=79.47$, $p<0.0001$, 22.20% of variation), a significant effect of E:T ratio ($F(4,20)=48.23$, $p<0.0001$, 53.89%), and a significant subset × E:T interaction ($F(4,20)=16.39$, $p<0.0001$, 18.32%, Supplemental Table 6). At every E:T ratio tested, $CD56^{dim}CD16^{dim}$ cells achieved a higher killing frequency than $CD56^{dim}CD16^{bright}$ cells: at 1:4, 0.990 + 0.214 versus 0.269 + 0.075 (mean diff −0.7215, $p<0.0001$); at 1:2, 0.579 + 0.104 versus 0.138 + 0.020 (mean diff −0.4411, $p<0.0001$); at 1:1, 0.280 + 0.122 versus 0.088 + 0.027 (mean diff −0.1928, $p=0.0147$); at 3:1, 0.083 + 0.012 versus 0.022 + 0.002 (mean diff −0.06046, $p=0.4124$, ns); and at 10:1, 0.033 + 0.003 versus 0.009 + 0.000 (mean diff −0.02375, $p=0.7457$, ns, Figure 3C, Supplemental Table 6). Within $CD56^{dim}CD16^{bright}$ cells, killing frequency at 1:4 was higher than at 3:1 (mean diff 0.2463, $p=0.0274$) and at 10:1 (mean diff 0.2594, $p=0.0181$), with no significant differences among other within-subset E:T comparisons (Figure 3C, Supplemental Table 6). Within $CD56^{dim}CD16^{dim}$ cells, killing frequency at 1:4 was higher than at 1:2 (mean diff 0.4105, $p=0.0001$), 1:1 (mean diff 0.7096, $p<0.0001$), 3:1 (mean diff 0.9073, $p<0.0001$), and 10:1 (mean diff 0.9571, $p<0.0001$); killing frequency at 1:2 was higher than at 1:1 (mean diff 0.2991, $p=0.0050$), 3:1 (mean diff 0.4968, $p<0.0001$), and 10:1 (mean diff 0.5466, $p<0.0001$); and killing frequency at 1:1 was higher than at 10:1 (mean diff 0.2476, $p=0.0263$), with no significant difference between 1:1 vs 3:1 (mean diff 0.1978, $p=0.1197$) or 3:1 vs 10:1 (mean diff 0.04979, $p=0.9990$, Figure 3C, Supplemental Table 6).

In response to HIV-infected cells, $CD56^{dim}CD16^{dim}$ NK cells exhibit greater degranulation and serial degranulation than $CD56^{dim}CD16^{bright}$ NK cells

Having established that $CD56^{dim}CD16^{dim}$ NK cells mediate enhanced killing of HIV-infected targets within mixed NK cell populations, we sought to characterize the kinetics and serial killing capacity of each subset. We measured degranulation over time by exposing purified NK cells to autologous HIV-infected CD4+ T-cells and quantifying CD107a surface expression at multiple time points.

In extended time course experiments (Figure 4-figure supplement 1A), $CD56^{dim}CD16^{dim}$ cells demonstrated significantly greater degranulation than $CD56^{dim}CD16^{bright}$ cells at 30 minutes, 1 hr., 2 hr., and 4 hr. (all $p<0.0001$). $CD56^{dim}CD16^{dim}$ cells reached peak degranulation at 47% at 1

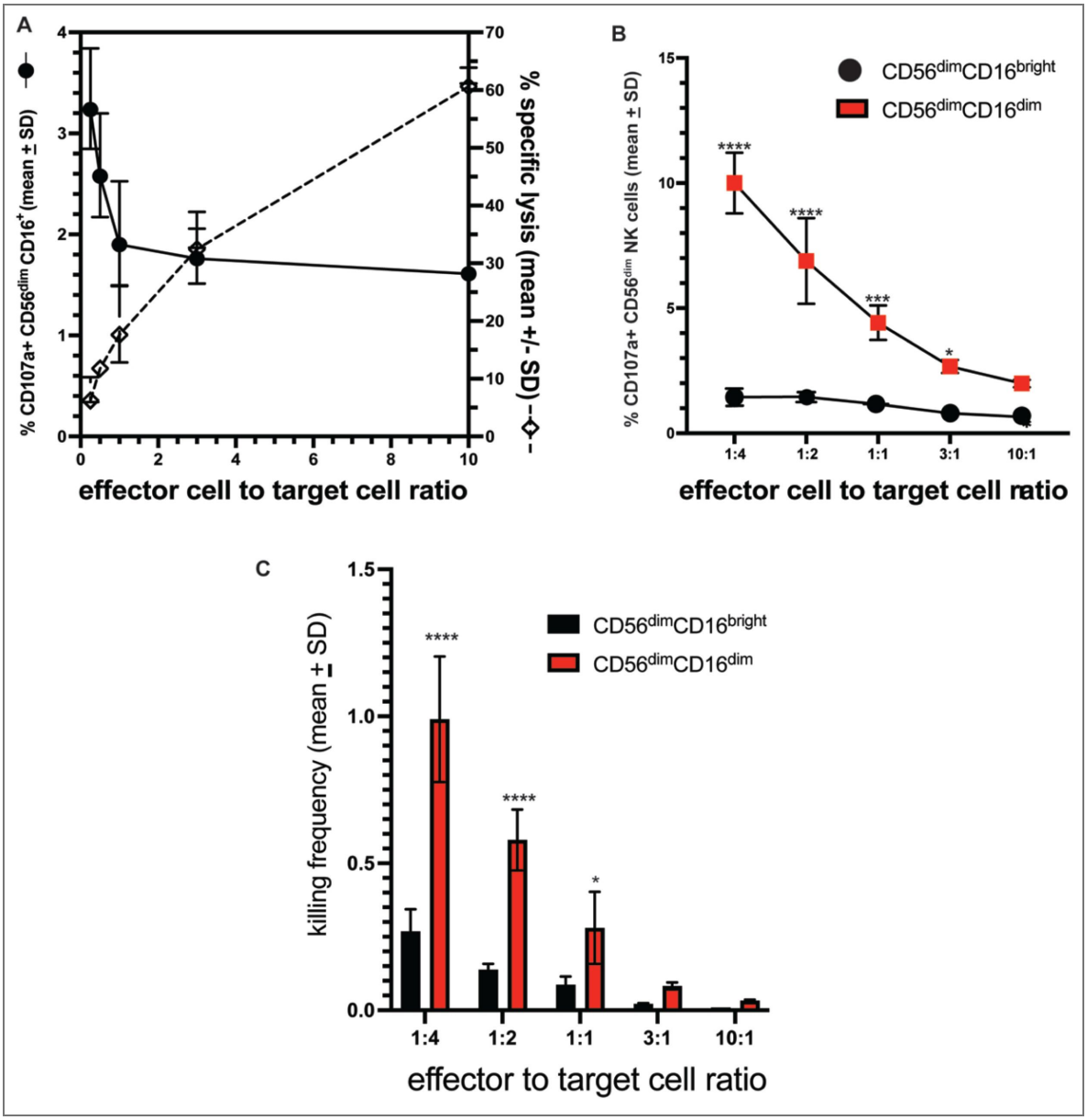

Figure 3. Killing frequency of autologous HIV-productively infected T-cells by $CD56^{dim}CD16^{dim}$ and $CD56^{dim}CD16^{bright}$ NK cells as they naturally exist within the total NK cell population

(A) Percentage of specific lysis and percentage of $CD107a^{+}$ $CD56^{dim}CD16^{+}$ NK cells when exposed to purified autologous HIV-1_{SHM-1} productively infected T-cells across increasing effector cell to target cell (E:T) ratios. Values represent mean ± standard deviation (SD) from three technical replicates. (B) Percentage of CD107a expressing $CD56^{dim}CD16^{bright}$ and $CD56^{dim}CD16^{dim}$ NK cells when exposed to autologous HIV-1_{SHM-1} productively infected T-cells across increasing E:T ratios. (C) NK cell killing frequency (killing frequency = killed targets / active effectors, where killed targets = total targets × % specific lysis / 100 and active effectors = total effectors × % degranulation / 100) calculated from data in panels A and B. Statistical analyses: two-way ANOVA (E:T ratio × subset) with Šidák's multiple comparisons test between subsets at each E:T ratio for panels B and C. Full ANOVA tables and post-hoc results are in Supplemental Tables 5 and 6 for Figure 3B and 3C. Significance: * $p < 0.05$, ** $p < 0.01$, *** $p < 0.001$, **** $p < 0.0001$.

hour, compared to only 11% for $CD56^{dim}CD16^{bright}$ cells (p<0.0001). Degranulation declined in both subsets after the 1 hr. time point, with $CD56^{dim}CD16^{dim}$ cells maintaining approximately 31.9% ± 1.0% CD107a positivity at 4 hrs. compared to 5.9% ± 0.29% for $CD56^{dim}CD16^{bright}$ cells (p<0.0001) (Figure 4-figure supplement 1A; two-way ANOVA: subset F(1, 20) = 2664, p<0.0001; time F(4, 20) = 463.3, p<0.0001; interaction F(4, 20) = 181.3, p<0.0001; Šidák's multiple comparisons test; Supplemental Table 7).

Early kinetic analysis (Figure 4-figure supplement 1B) revealed that $CD56^{dim}CD16^{dim}$ cells began responding by 30 minutes, reaching approximately 15.6% ± 1.3% degranulation by 1 hour, whereas $CD56^{dim}CD16^{bright}$ cells showed minimal early responses, reaching only 2.1% ± 0.4% by 1 hour (p<0.0001). These data indicate that $CD56^{dim}CD16^{dim}$ cells respond more rapidly and with greater magnitude to HIV-infected targets (two-way ANOVA: subset F(1, 20) = 438.3, p<0.0001; time F(4, 20) = 203.4, p<0.0001; interaction F(4, 20) = 120.7, p<0.0001; Šidák's multiple comparisons test; Supplemental Table 8).

To determine whether individual NK cells could sequentially engage multiple targets, we employed a serial degranulation assay that distinguishes cells undergoing zero, one, two, or three degranulation events within 60 minutes (Niemann et al., 2025). This analysis revealed striking differences between the CD16 subsets (Figure 4). The majority of $CD56^{dim}CD16^{bright}$ cells (75.9% ± 1.0%) did not degranulate during the assay period, compared to only 35.2% ± 0.8% of $CD56^{dim}CD16^{dim}$ cells (p<0.0001). Among responding cells, the distribution of degranulation events differed markedly across subsets. 9.40% ± 0.01% of $CD56^{dim}CD16^{bright}$ cells exhibited a single degranulation, with only 3.00% ± 0.23% exhibiting two and 3.89% ± 0.54% exhibiting three degranulations.

In contrast, $CD56^{dim}CD16^{dim}$ cells showed a broader distribution: 19.18% ± 0.89% achieved one degranulation (p<0.0001), 13.94% ± 1.47% achieved two degranulations (p<0.0001), and 29.13% ± 1.36% achieved three degranulations (p<0.0001) (two-way ANOVA: subset F(1, 16) = 12.80, p=0.0025; events F(3, 16) = 3287, p<0.0001; interaction F(3, 16) = 1478, p<0.0001; Šidák's multiple comparisons test; Supplemental Table 9).

$CD56^{dim}CD16^{dim}$ cells exhibit an enhanced activation state and display HIV-specific noncytolytic responses

To investigate the basis of $CD56^{dim}CD16^{dim}$ functional superiority, we examined whether these cells exhibited enhanced HIV-specific non-cytolytic responsiveness compared to $CD56^{dim}CD16^{bright}$ cells and baseline activation. $CD56^{dim}CD16^{positive}$ NK cells can secrete inflammatory cytokines in addition to lysing target cells (De Maria et al., 2011) and are governed by the same mechanisms that control the lysis of target cells (Bryceson et al., 2006; Mandelboim et al., 1998).

IFN-γ production patterns followed a similar trend to the degranulation response (Figure 1-figure supplement 3). A higher frequency of $CD56^{dim}CD16^{dim}$ NK cells produced IFN-γ than $CD56^{dim}CD16^{bright}$ NK cells across all E:T ratios tested (Figure 1-figure supplement 3A). $CD56^{dim}CD16^{dim}$ cells produced IFN-γ at the 1:4 ratio (4.53 ± 0.58%), 1:2 (3.13 ± 0.60%), 1:1 (2.10 ± 0.51%), and 2:1 (0.87 ± 0.34%) ratios. $CD56^{dim}CD16^{bright}$ cells expressed IFN-γ at 1:4 (0.38 ± 0.09%), 1:2 (0.31 ± 0.03%), 1:1 (0.10 ± 0.01%), and 2:1 (0.12 ± 0.19%). Between-subset differences were significant at all E:T ratios (1:4, 1:2, and 1:1, all p<0.0001; 2:1, p=0.0263; two-way ANOVA: subset F(1, 16) = 251.4, p<0.0001; E:T ratio F(3, 16) = 30.08, p<0.0001; interaction F(3, 16) = 21.77, p<0.0001; Šidák's multiple comparisons test; Supplemental Table 10).

At the same time IFN-γ was measured, we also evaluated the same NK cells for their ability to degranulate (Figure 1-figure supplement 3B). $CD56^{dim}CD16^{dim}$ cells degranulated at the 1:4 ratio (15.05 ± 1.70%), 1:2 (11.43 ± 0.91%), 1:1 (7.84 ± 0.30%), and 2:1 (2.56 ± 0.71%) ratios. $CD56^{dim}CD16^{bright}$ cells degranulated at 1:4 (2.91 ± 0.16%), 1:2 (1.92 ± 0.06%), 1:1 (1.16 ± 0.11%), and 2:1 (0.37 ± 0.04%). Between-subset differences were significant at all E:T ratios (1:4, 1:2, and

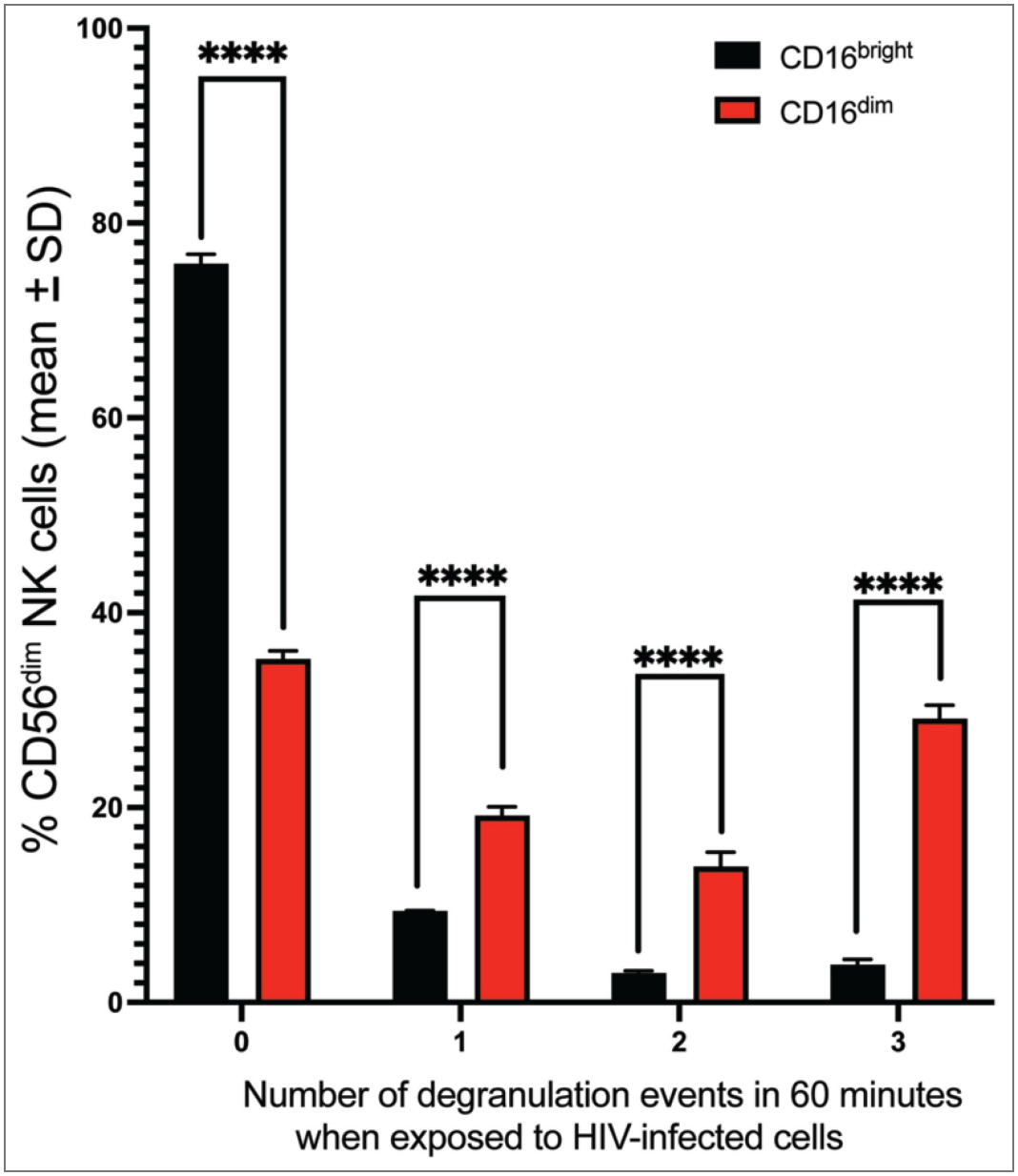

Figure 4. The number of NK cells that degranulated when exposed to HIV-infected cells over a 60-minute period.

Purified NK cells exposed to autologous HIV-1_{SHM-1} productively infected T-cells at an effector cell-to-target cell ratio of 1:1 were treated with a different fluorophore-labeled anti-CD107a antibody every 15 minutes for 60 minutes, blocked with excess unlabeled anti-CD107a, and washed between each labeling step. The number of fluorophores accumulated on $CD56^{dim}CD16^{bright}$ and $CD56^{dim}CD16^{dim}$ NK cells determined how many times each NK cell degranulated during the 60-minute exposure. SD = standard deviation. Statistical analysis: two-way ANOVA (subset × number of degranulation events) with Šidák's multiple comparisons test between subsets at each event category. Full ANOVA tables and post-hoc results are in Supplemental Table 7 for Figure 4. Significance: * $p < 0.05$, ** $p < 0.01$, *** $p < 0.001$, **** $p < 0.0001$.

1:1, all p<0.0001; 2:1, p=0.0086; two-way ANOVA: subset F(1, 16) = 649.1, p<0.0001; E:T ratio F(3, 16) = 114.1, p<0.0001; interaction F(3, 16) = 50.49, p<0.0001; Šidák's multiple comparisons test; Supplemental Table 11).

To determine the baseline activation of $CD56^{dim}CD16^{dim}$ NK cell responses, we compared degranulation of $CD56^{dim}$ subsets against uninfected and HIV-infected target cells (Figure 1—figure supplement 3C). At the 1:4 ratio, 21.32 ± 3.78% of $CD56^{dim}CD16^{dim}$ cells degranulated against HIV-infected targets and 9.19 ± 1.95% degranulated against uninfected targets. $CD56^{dim}CD16^{dim}$ cells responded to HIV-infected cells at 2.3- to 7.3-fold higher percentages than to uninfected cells across all E:T ratios. At the 1:4 ratio, 4.58 ± 0.65% of $CD56^{dim}CD16^{bright}$ NK cells degranulated against infected cells and 1.28 ± 0.04% degranulated against uninfected cells [two-way ANOVA: condition F(3, 40) = 329.9, p<0.0001, 67.31% of variation; E:T ratio F(4, 40) = 64.82, p<0.0001, 17.63%; interaction F(12, 40) = 15.13, p<0.0001, 12.34%; Šidák's multiple comparisons test; Supplemental Table 12].

$CD56^{dim}CD16^{dim}$ NK cell functional superiority is independent of cytotoxic granule protein content and NK cell inhibitory receptors that recognize MHC class I molecules

To determine whether the functional superiority of $CD56^{dim}CD16^{dim}$ cells was due to higher levels of cytotoxic effector molecules, we examined the expression of perforin, granzyme A, and granzyme B in the $CD56^{dim}$ NK cell subsets.

Flow cytometric analysis showed that the expression of cytotoxic proteins was broadly similar between $CD56^{dim}CD16^{bright}$ and $CD56^{dim}CD16^{dim}$ NK cells (Figure 5-figure supplement 1). Perforin was present in nearly all cells of both subsets, with $CD56^{dim}CD16^{bright}$ and $CD56^{dim}CD16^{dim}$ cells exhibiting similar frequencies of perforin-positive cells (99.99% ± 0.01% and 99.27 ± 0.27% cells expressing perforin, respectively). Likewise, granzyme B expression was consistently high across both subsets (100% of cells expressing granzyme B), indicating that all $CD56^{dim}$ NK cells possess this essential cytotoxic protease, regardless of CD16 levels.

Granzyme A expression followed a similar pattern (Figure 5-figure supplement 1), with both $CD56^{dim}CD16^{bright}$ and $CD56^{dim}CD16^{dim}$ NK cells showing similar expression frequencies (99.40 ± 0.31 and 96.84 ± 0.54% of cells expressing granzyme A, respectively). In contrast, $CD56^{dim}CD16^{negative}$ NK cells had slightly lower perforin (87.04 ± 1.95% of cells expressing perforin) and granzyme A expressing cells (74.96 ± 3.04 % of cells expressing granzyme A), while maintaining high granzyme B expression (100% cells expressing granzyme B).

To determine whether $CD56^{dim}CD16^{dim}$ functional superiority resulted from differential KIR3DL1 expression, we evaluated KIR3DL1 frequency and density [geometric mean fluorescent intensity (gMFI)] on $CD56^{dim}$ subsets following 4-hour exposure to purified autologous productively HIV-1_{SHM-1} infected T-cells.

Two-way ANOVA of $KIR3DL1^{positive}$ frequency showed a significant effect of CD16 subset (F(2,18)=54.34, p<0.0001, 77.50% of variation), with no significant effect of E:T ratio (F(2,18)=1.99, p=0.1661) or subset × E:T interaction (F(4,18)=2.39, p=0.0888, Supplemental Table 13). Across the three E:T ratios, $KIR3DL1^{positive}$ frequency was 21.86 ± 0.20% on $CD56^{dim}CD16^{bright}$, 20.16 ± 0.89% on $CD56^{dim}CD16^{dim}$, and 23.37 ± 0.18% on $CD56^{dim}CD16^{negative:}$ cells (Figure 5-figure supplement 2A). At no targets, $CD56^{dim}CD16^{bright}$ differed from $CD56^{dim}CD16^{dim}$ (mean diff 2.400, p=0.0008), $CD56^{dim}CD16^{bright}$ differed from $CD56^{dim}CD16^{negative:}$ (mean diff −1.533, p=0.0301), and $CD56^{dim}CD16^{dim}$ differed from $CD56^{dim}CD16^{negative:}$ (mean diff −3.933, p<0.0001). At the 3:1 E:T ratio, $CD56^{dim}CD16^{bright}$ vs $CD56^{dim}CD16^{negative:}$ (mean diff −1.700, p=0.0153) and $CD56^{dim}CD16^{dim}$ vs $CD56^{dim}CD16^{negative:}$ (mean diff −2.167, p=0.0022) differed, while $CD56^{dim}CD16^{bright}$ vs $CD56^{dim}CD16^{dim}$ did not (mean diff 0.467, p=0.7769). At the 1:1 E:T ratio, $CD56^{dim}CD16^{bright}$ vs $CD56^{dim}CD16^{dim}$ (mean diff 2.233, p=0.0017) and $CD56^{dim}CD16^{dim}$ vs

$CD56^{dim}CD16^{negative:}$ (mean diff −3.533, p<0.0001) differed, while $CD56^{dim}CD16^{bright}$ vs $CD56^{dim}CD16^{negative:}$ did not (mean diff −1.300, p=0.0746, Figure 5-figure supplement 2A, Supplemental Table 13).

Two-way ANOVA of KIR3DL1 density showed a significant effect of CD16 subset (F(2,18)=3970, p<0.0001, 98.68% of variation), a significant effect of E:T ratio (F(2,18)=10.70, p=0.0009, 0.27%), and a significant subset × E:T interaction (F(4,18)=16.78, p<0.0001, 0.83%, Supplemental Table 13). Across the three E:T ratios, KIR3DL1 density on $KIR3DL1^{positive}$ cells was 12686.67 ± 107.31 gMFI for $CD56^{dim}CD16^{bright}$, 8607.44 ± 203.91 gMFI for $CD56^{dim}CD16^{dim}$, and 4630.44 ± 20.36 gMFI for $CD56^{dim}CD16^{negative:}$ (Figure 5-figure supplement 2B). At no targets, $CD56^{dim}CD16^{bright}$ vs $CD56^{dim}CD16^{dim}$ (mean diff 5025, p<0.0001), $CD56^{dim}CD16^{bright}$ vs $CD56^{dim}CD16^{negative:}$ (mean diff 8146, p<0.0001), and $CD56^{dim}CD16^{dim}$ vs $CD56^{dim}CD16^{negative:}$ (mean diff 3121, p<0.0001) all differed. The same pattern was observed at the 3:1 E:T ratio ($CD56^{dim}CD16^{bright}$ vs $CD56^{dim}CD16^{dim}$ mean diff 3666, p<0.0001; $CD56^{dim}CD16^{bright}$ vs $CD56^{dim}CD16^{negative:}$ mean diff 8004, p<0.0001; $CD56^{dim}CD16^{dim}$ vs $CD56^{dim}CD16^{negative:}$ mean diff 4338, p<0.0001) and at the 1:1 E:T ratio ($CD56^{dim}CD16^{bright}$ vs $CD56^{dim}CD16^{dim}$ mean diff 3547, p<0.0001; $CD56^{dim}CD16^{bright}$ vs $CD56^{dim}CD16^{negative:}$ mean diff 8018, p<0.0001; $CD56^{dim}CD16^{dim}$ vs $CD56^{dim}CD16^{negative:}$ mean diff 4472, p<0.0001, Figure 5-figure supplement 2B, Supplemental Table 13).

According to NK licensing theory, $KIR3DL1^{positive}$ cells should show enhanced killing when HLA-Bw4 is downmodulated by HIV-1 Nef (Bonaparte & Barker, 2004; Boudreau et al., 2016; Davis et al., 2016). Two-way ANOVA of KIR3DL1-stratified degranulation showed a significant effect of CD16 subset (F(2,12)=80.34, p<0.0001, 78.25% of variation), a significant effect of KIR3DL1 expression (F(1,12)=12.90, p=0.0037, 6.28%), and a significant subset × KIR3DL1 interaction (F(2,12)=9.88, p=0.0029, 9.62%, Supplemental Table 13). Within $CD56^{dim}CD16^{dim}$ cells, the frequency of $KIR3DL1^{positive}$ cells that degranulated was higher than the frequency of KIR3DL1− cells that degranulated (8.32 ± 1.54% vs 4.50 ± 0.53%, mean diff 3.812, p=0.0001, Figure 5-figure supplement 2C). No difference was observed within $CD56^{dim}CD16^{bright}$ (1.53 ± 0.18% vs 1.63 ± 0.28%, mean diff −0.102, p=0.8822) or $CD56^{dim}CD16^{negative}$ (1.11 ± 0.70% vs 0.63 ± 0.89%, mean diff 0.472, p=0.4958, Figure 5-figure supplement 2C). Among $KIR3DL1^{positive}$ cells, $CD56^{dim}CD16^{dim}$ cells degranulated at a higher frequency than $CD56^{dim}CD16^{bright}$ (mean diff −6.783, p<0.0001) and $CD56^{dim}CD16^{negative}$ (mean diff 7.208, p<0.0001) cells, with no difference between $CD56^{dim}CD16^{bright}$ and $CD56^{dim}CD16^{negative}$ (mean diff 0.426, p=0.9019). Among KIR3DL1− cells, $CD56^{dim}CD16^{dim}$ cells also degranulated at a higher frequency than $CD56^{dim}CD16^{bright}$ (mean diff −2.870, p=0.0033) and $CD56^{dim}CD16^{negative}$ (mean diff 3.869, p=0.0003) cells, with no difference between $CD56^{dim}CD16^{bright}$ and $CD56^{dim}CD16^{negative}$ (mean diff 1.000, p=0.4135, Figure 5-figure supplement 2C, Supplemental Table 13).

Since in our study we used the $HIV\text{-}1_{SHM\text{-}1}$ (a primary isolate strain), which does not down-modulate HLA-C (Davis et al., 2016), we wanted to see whether the greater capacity of $CD56^{dim}CD16^{dim}$ NK cells to degranulate was due to fewer $CD56^{dim}CD16^{dim}$ NK cells expressing KIR2DLs or to lower KIR2DL density than the other CD16 subsets. Two-way ANOVA of $KIR2DL2/3^{positive}$ frequency showed a significant effect of CD16 subset (F(2,18)=54.51, p<0.0001, 81.90% of variation), with no significant effect of E:T ratio (F(2,18)=2.18, p=0.1417) or subset × E:T interaction (F(4,18)=1.18, p=0.7757, Supplemental Table 14). $CD56^{dim}CD16^{bright}$ cells had the highest frequency of $KIR2DL2/3^{positive}$ cells (21.04 ± 1.20%) compared to $CD56^{dim}CD16^{dim}$ (14.47 ± 0.38%, p=0.0002) and $CD56^{dim}CD16^{negative}$ (13.90 ± 1.13%, p<0.0001), with no significant difference between $CD56^{dim}CD16^{dim}$ and $CD56^{dim}CD16^{negative}$ (p=0.9367, Figure 5-figure supplement 3A, Supplemental Table 14). For KIR2DL2/3 density, two-way ANOVA showed a significant effect of CD16 subset (F(2,18)=58.68, p<0.0001, 84.76% of variation), with no significant effect of E:T ratio (F(2,18)=0.65, p=0.5363) or interaction (F(4,18)=0.45, p=0.7685, Supplemental Table 14). KIR2DL2/3 density was significantly higher on $CD56^{dim}CD16^{bright}$ cells (1969.11 ± 55.51 gMFI) compared to $CD56^{dim}CD16^{negative}$ (1340.56 ± 20.71 gMFI, p<0.0001), and higher on $CD56^{dim}CD16^{dim}$ (1665.11 ± 40.84 gMFI) compared to $CD56^{dim}CD16^{negative}$ (p=0.0183), with no significant difference between $CD56^{dim}CD16^{bright}$ and $CD56^{dim}CD16^{dim}$ (p=0.0804, Figure 5-figure supplement 3A, Supplemental Table 14). Two-way ANOVA of $KIR2DL1^{positive}$ frequency

showed a significant effect of CD16 subset (F(2,18)=376.8, p<0.0001, 97.02% of variation), with no significant effect of E:T ratio (F(2,18)=1.40, p=0.2732) or interaction (F(4,18)=0.59, p=0.6753, Supplemental Table 15). KIR2DL1^{positive} cells were most frequent in CD56^{dim}CD16^{bright} (4.69 ± 0.33%) versus CD56^{dim}CD16^{dim} (1.78 ± 0.27%, p<0.0001) and CD56^{dim}CD16^{negative} (0.60 ± 0.10%, p<0.0001) populations, with CD56^{dim}CD16^{dim} higher than CD56^{dim}CD16^{negative} (p=0.0019, Figure 5-figure supplement 4A, Supplemental Table 15). For KIR2DL1 density, two-way ANOVA showed a significant effect of CD16 subset (F(2,18)=151.7, p<0.0001, 87.06% of variation), a significant effect of E:T ratio (F(2,18)=5.82, p=0.0112, 3.35%), and a significant subset × E:T interaction (F(4,18)=3.82, p=0.0204, 4.40%, Supplemental Table 15). Densities were comparable between CD56^{dim}CD16^{bright} (2121.11 ± 10.41 gMFI) and CD56^{dim}CD16^{dim} (2097.45 ± 38.66 gMFI, p=0.1517) when expressing KIR2DL1, with both higher than CD56^{dim}CD16^{negative} (1793.22 ± 17.39 gMFI, p<0.0001 for both comparisons, Figure 5-figure supplement 4B, Supplemental Table 15).

Functionally, two-way ANOVA of KIR2DL2/3-stratified degranulation showed a significant effect of CD16 subset (F(2,12)=67.44, p<0.0001, 83.31% of variation), a significant effect of KIR2DL2/3 expression (F(1,12)=6.95, p=0.0217, 4.29%), and a significant subset × KIR2DL2/3 interaction (F(2,12)=4.03, p=0.0457, 4.98%, Supplemental Table 14). The frequency of KIR2DL2/3^{positive} CD56^{dim}CD16^{dim} cells degranulating was enhanced compared to the frequency of KIR2DL2/3^{negative} counterparts that degranulated (11.16 ± 1.06% vs 7.64 ± 0.70%, p=0.0023, Figure 5-figure supplement 3C, Supplemental Table 14), while only minimal percentages of CD56^{dim}CD16^{bright} (KIR2DL2/3^{positive} 3.65 ± 1.15% vs KIR2DL2/3^{negative} 3.28 ± 0.90%, p=0.6958) and CD56^{dim}CD16^{negative} (KIR2DL2/3^{positive} 2.56 ± 1.80% vs KIR2DL2/3^{negative} 2.27 ± 0.77%, p=0.7512) cells degranulated regardless of KIR2DL2/3 status (Figure 5-figure supplement 3C, Supplemental Table 14). For KIR2DL1-stratified degranulation, two-way ANOVA showed a significant effect of CD16 subset (F(2,12)=46.19, p<0.0001, 80.39% of variation), no significant effect of KIR2DL1 expression (F(1,12)=1.03, p=0.3304), and a significant subset × KIR2DL1 interaction (F(2,12)=4.75, p=0.0302, 8.27%, Supplemental Table 15). The frequency of CD56^{dim}CD16^{negative} cells expressing KIR2DL1 showed paradoxically higher degranulation than the frequency of KIR2DL1^{negative} cells that degranulated (2.02 ± 0.59% vs 0.11 ± 0.11%, p=0.0105, Figure 5-figure supplement 4C, Supplemental Table 15). No significant differences in frequency of cells degranulating were observed between KIR2DL1^{positive} and KIR2DL1^{negatve} cells within CD56^{dim}CD16^{bright} (1.23 ± 0.74% vs 1.31 ± 0.72%, p=0.9063) or CD56^{dim}CD16^{dim} (4.50 ± 1.21% vs 5.23 ± 0.82%, p=0.2711) subsets (Figure 5-figure supplement 4C, Supplemental Table 15). Critically, a significantly higher percentage of CD56^{dim}CD16^{dim} cells degranulated in response to HIV-infected cells compared to both CD56^{dim}CD16^{bright} and CD56^{dim}CD16^{negative} populations within each KIR2DL2/3 stratum (KIR2DL2/3^{positive}: vs CD16^{bright} p<0.0001, vs CD16^{negative} p<0.0001; KIR2DL2/3^{negative}: vs CD16^{bright} p=0.0014, vs CD16^{negative} p=0.0002, Figure 5-figure supplement 3C, Supplemental Table 14) and within each KIR2DL1 stratum (KIR2DL1^{positive}: vs CD16bright p=0.0007, vs CD16^{negative} p=0.0057; KIR2DL1^{negative}: vs CD16bright p=0.0001, vs CD16^{negative} p<0.0001, Figure 5-figure supplement 4C, Supplemental Table 15).

To determine whether CD56^{dim}CD16^{dim} functional superiority resulted from differential NKG2A expression, we evaluated NKG2A frequency and density on CD56^{dim} subsets following 4-hour exposure to autologous HIV-infected cells.

Two-way ANOVA of NKG2A^{positive} frequency showed a significant effect of CD16 subset (F(2,18)=7.362, p=0.0046, 37.33% of variation), with no significant effect of E:T ratio (F(2,18)=0.48, p=0.6248) or subset × E:T interaction (F(4,18)=1.44, p=0.2616, Supplemental Table 16). Across the three E:T ratios, NKG2A^{positive} frequency was 99.54 ± 0.04% on CD56^{dim}CD16^{bright}, 99.61 ± 0.05% on CD56^{dim}CD16^{dim}, and 99.80 ± 0.03% on CD56^{dim}CD16^{negative} cells (Figure 5-figure supplement 5A). At no targets, CD56^{dim}CD16^{bright} differed from CD56^{dim}CD16^{negative} (mean diff −0.367, p=0.0199), with no significant differences between CD56^{dim}CD16^{bright} and CD56^{dim}CD16^{dim} (mean diff −0.167, p=0.4500) or between CD56^{dim}CD16^{dim} and CD56^{dim}CD16^{negative} (mean diff −0.200, p=0.2997). At the 3:1 E:T ratio, no between-subset comparisons reached significance (CD56^{dim}CD16^{bright} vs CD56^{dim}CD16^{dim} p=0.4500; CD56^{dim}CD16^{bright} vs CD56^{dim}CD16^{negative} p=0.2997; CD56^{dim}CD16^{dim} vs CD56^{dim}CD16^{negative} p=0.9899). At the 1:1 E:T ratio, CD56^{dim}CD16^{dim}

differed from CD56^{dim}CD16^{negative} (mean diff −0.333, p=0.0382), with no significant differences between CD56^{dim}CD16^{bright} and CD56^{dim}CD16^{dim} (mean diff 0.133, p=0.6265) or between CD56^{dim}CD16^{bright} and CD56^{dim}CD16^{negative} (mean diff −0.200, p=0.2997, Figure 5-figure supplement 5A, Supplemental Table 16).

Two-way ANOVA of NKG2A density on NKG2A^{positive} cells showed no significant effect of CD16 subset (F(2,18)=1.98, p=0.1676), E:T ratio (F(2,18)=1.07, p=0.3630), or subset × E:T interaction (F(4,18)=0.10, p=0.9804, Supplemental Table 16). Across the three E:T ratios, NKG2A density on NKG2A^{positive} cells was 4046.89 ± 161.10 gMFI for CD56^{dim}CD16^{bright}, 4403.56 ± 114.74 gMFI for CD56^{dim}CD16^{dim}, and 4155.44 ± 88.41 gMFI for CD56^{dim}CD16^{negative} (Figure 5-figure supplement 5B). No between-subset comparisons reached significance at any E:T ratio (Figure 5-figure supplement 5B, Supplemental Table 16).

Two-way ANOVA of NKG2A-stratified degranulation showed a significant effect of CD16 subset (F(2,12)=25.34, p<0.0001, 78.52% of variation), with no significant effect of NKG2A expression (F(1,12)=0.11, p=0.7470) or subset × NKG2A interaction (F(2,12)=0.88, p=0.4410, Supplemental Table 16). Within each CD16 subset, the frequency of NKG2A^{positive} cells degranulating did not differ from the frequency of NKG2A− cells degranulating (CD56^{dim}CD16^{bright} 3.10 ± 1.31% vs 3.81 ± 0.96%, mean diff −0.708, p=0.5963; CD56^{dim}CD16^{dim} 9.26 ± 2.83% vs 8.12 ± 0.61%, mean diff 1.133, p=0.4007; CD56^{dim}CD16^{negative} 2.09 ± 0.72% vs 3.25 ± 1.94%, mean diff −1.169, p=0.3863, Figure 5-figure supplement 5C). Among NKG2A^{positive} cells, CD56^{dim}CD16^{dim} cells degranulated at a higher frequency than CD56^{dim}CD16^{bright} (mean diff −6.157, p=0.0015) and CD56^{dim}CD16^{negative} (mean diff 7.172, p=0.0004) cells, with no difference between CD56^{dim}CD16^{bright} and CD56^{dim}CD16^{negative} (mean diff 1.015, p=0.8339).

Among NKG2A− cells, CD56^{dim}CD16^{dim} cells also degranulated at a higher frequency than CD56^{dim}CD16^{bright} (mean diff −4.316, p=0.0182) and CD56^{dim}CD16^{negative} (mean diff 4.870, p=0.0084) cells, with no difference between CD56^{dim}CD16^{bright} and CD56^{dim}CD16^{negative} (mean diff 0.553, p=0.9666, Figure 5-figure supplement 5C, Supplemental Table 16).

HIV Vpr induces NKG2D ligands on HIV-infected cells and triggers degranulation responses in autologous CD56^{dim}CD16^{dim} NK cells through NKG2D

We and others previously demonstrated that NK cell lysis of HIV-infected cells depends on NKG2D (Cerboni et al., 2007; Ward et al., 2007). To understand how HIV-specific recognition occurs in CD56^{dim} NK cell subsets with differential CD16 expression, we examined whether HIV infection induces the expression of specific ligands recognized by the activating receptor NKG2D. Analysis of NKG2D ligand expression on HIV-infected cells using a soluble NKG2D IgG1 Fc chimeric protein revealed that HIV infection induces expression of these stress-induced molecules (Figure 5A) on the infected cell surface, as previously demonstrated by us and others (Cerboni et al., 2007; Richard et al., 2010; Ward et al., 2009). Uninfected CD4^{positive} T-cells exhibited minimal NKG2D ligand expression, as indicated by overlapping histograms for NKG2D IgG1 Fc chimeric protein staining (blue line) and staining control (red line). Cells infected with wild-type (WT) HIV displayed a rightward shift in NKG2D ligand expression (blue line). Cells infected with HIV lacking the Vpr gene (ΔVpr) had lower NKG2D ligand levels, with histograms resembling those of uninfected cells.

NK cell degranulation occurred only when NKG2D ligands were present, unlike target T-cells infected with Vpr-lacking HIV, which do not express NKG2D ligands (Figure 5B). Flow cytometry confirmed that NKG2D ligand expression correlated with NK cell degranulation (Figure 5A).

To assess the contribution of NKG2D-mediated recognition to direct killing capacity, CD56^{dim} NK cell subsets defined by CD16 expression were tested against HIV-infected targets across E:T ratios (1:4 to 2:1) in the presence of an NKG2D-blocking Ab (Figure 5C). NKG2D blocking reduced degranulation in CD56^{dim}CD16^{dim} cells across all E:T ratios tested: 1:4 (p<0.0001), 1:2 (p<0.0001), 1:1 (p<0.0001), and 2:1 (p<0.0001), with degranulation decreasing from 20.49 ± 0.56% to 5.88 ±

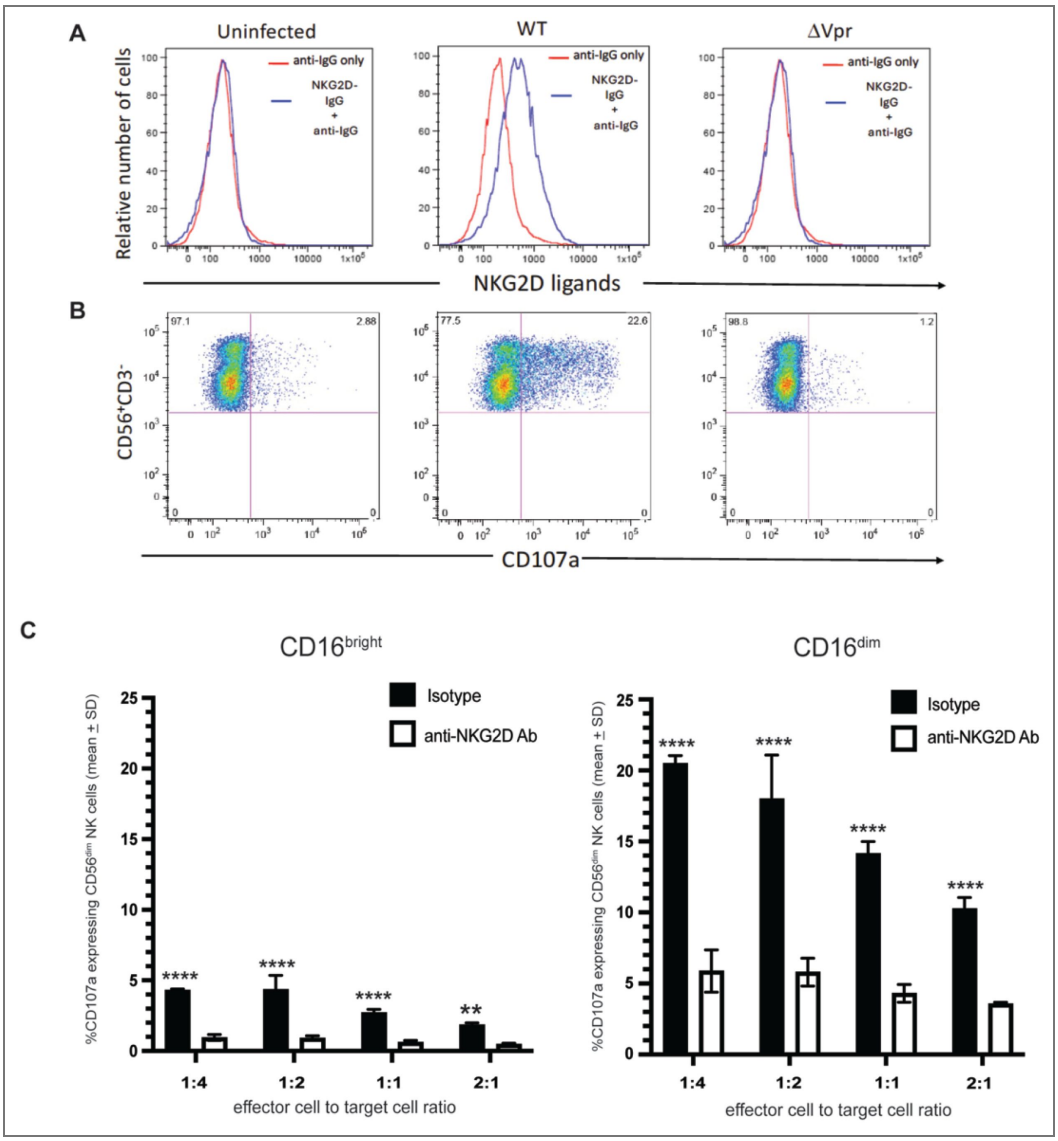

Figure 5. Role of NKG2D in the ability of NK cell subsets to degranulate in response to autologous HIV-productively infected T-cells

(A) CD3 and CD28-stimulated $CD4^+$ T-cells remained uninfected or were infected with VSV-G pseudotyped DHIV3, which possessed (wild-type; WT) or lacked (ΔVpr) Vpr. Following infection, cells were stained with a recombinant human soluble NKG2D/IgG1 Fc chimera protein, followed by a fluorochrome-conjugated anti-human IgG1 Fc-specific antibody (Ab). The staining control consisted of cells stained only with the anti-human IgG1 Fc-specific Ab. Cells were then stained with fluorochrome-conjugated antibodies against surface CD4 and intracellular HIV-1 p24 capsid and analyzed by flow cytometry. (B) NK cells were isolated from healthy uninfected donors by negative selection from peripheral blood mononuclear cells and exposed for 4 hours to uninfected $CD4^{positive}$ T-cells or purified HIV-infected cells possessing or lacking Vpr. Cells were stained with fluorochrome-conjugated antibodies against CD56, CD3, and CD107a and analyzed by flow cytometry. Dot plots show CD107a versus CD56 expression on CD3− gated cells, with quadrants set by FMO controls; the upper-right quadrant indicates degranulating (CD107a+) CD56+ NK cells, with the percentage shown. (C) NK cells in triplicate wells were treated with blocking antibodies to NKG2D or an isotype-specific control antibody, then exposed to purified autologous $HIV\text{-}1_{SHM\text{-}1}$ productively infected T-cells at various effector-to-target (E:T) ratios for 4 hours. Cells were stained with antibodies against CD107a, CD56, CD16, and CD3 and analyzed by flow cytometry. All values represent background-subtracted percentages (target-exposed minus mean unexposed controls). Statistical analysis: separate two-way ANOVAs (E:T ratio × treatment) for $CD56^{dim}CD16^{bright}$ and $CD56^{dim}CD16^{dim}$ subsets, with Šidák's multiple comparisons test between isotype and anti-NKG2D treatment at each E:T ratio. Full ANOVA tables and post-hoc results are in Supplemental Table 17 for Figure 5C. Significance: * $p < 0.05$, ** $p < 0.01$, *** $p < 0.001$, **** $p < 0.0001$.

0.98% CD107a^{positive} at the lowest E:T ratio tested (two-way ANOVA: treatment F(1, 16) = 543.0, p<0.0001; E:T ratio F(3, 16) = 36.30, p<0.0001; interaction F(3, 16) = 13.18, p=0.0001; Šidák's multiple comparisons test; Supplemental Table 17). NKG2D blocking also reduced degranulation in CD56^{dim}CD16^{bright} cells across all E:T ratios: 1:4 (p<0.0001), 1:2 (p<0.0001), 1:1 (p<0.0001), and 2:1 (p=0.0018), with responses decreasing from 4.30 ± 0.09% to 0.95 ± 0.21% CD107a^{positive} at the 1:4 E:T ratio (two-way ANOVA: treatment F(1, 16) = 266.4, p<0.0001; E:T ratio F(3, 16) = 21.54, p<0.0001; interaction F(3, 16) = 10.06, p=0.0006; Šidák's multiple comparisons test; Supplemental Table 17).

NKG2D expression levels correlate with subset-specific degranulation capacity

To determine whether differential NKG2D receptor expression on CD56^{dim}CD16^{dim} and CD56^{dim}CD16^{bright} cells could account for the NKG2D-dependent subset-specific degranulation responses to HIV-infected cells, we measured NKG2D surface expression (gMFI) following 4-hour exposure to HIV-infected targets across a range of E:T ratios (Figure 6A). Two-way ANOVA of NKG2D gMFI showed a significant effect of CD56^{dim} NK cell subset (F(1,20)=1897, p<0.0001, 70.97% of variation), a significant effect of E:T ratio (F(4,20)=139.0, p<0.0001, 20.80%), and a significant subset × E:T interaction (F(4,20)=49.98, p<0.0001, 7.48%, Supplemental Table 18). CD56^{dim}CD16^{dim} cells showed significantly higher NKG2D gMFI than CD56^{dim}CD16^{bright} cells at every E:T ratio tested: at no targets (mean diff −1182, p<0.0001), 1:2 (mean diff −501.0, p<0.0001), 1:1 (mean diff −558.3, p<0.0001), 2:1 (mean diff −679.3, p<0.0001), and 4:1 (mean diff −826.0, p<0.0001, Figure 6A, Supplemental Table 18). Across the five E:T ratios, CD56^{dim}CD16^{dim} NKG2D gMFI was 2521.5 ± 17.35, and CD56^{dim}CD16^{bright} NKG2D gMFI was 1772.2 ± 9.07.

To verify that the differential NKG2D expression observed between CD16 subsets was receptor-specific and not due to general differences in surface receptor levels, we measured NKp46 expression on the same CD56^{dim}CD16^{bright} and CD56^{dim}CD16^{dim} NK cells from identical experimental wells (Figure 6B). NKp46 was selected because it does not participate in NK cell lysis of HIV-infected cells (Ward et al., 2007). Two-way ANOVA of NKp46 gMFI showed a significant effect of CD56^{dim} NK cell subset (F(1,20)=321.1, p<0.0001, 50.30% of variation), a significant effect of E:T ratio (F(4,20)=64.89, p<0.0001, 40.66%), and a significant subset × E:T interaction (F(4,20)=9.432, p=0.0002, 5.91%, Supplemental Table 18). In contrast to NKG2D, NKp46 gMFI did not differ between CD56^{dim}CD16^{dim} and CD56^{dim}CD16^{bright} cells at no targets (mean diff 45.67, p=0.0668), and showed smaller absolute differences at the higher E:T ratios than those observed for NKG2D (1:2 mean diff 178.3, p<0.0001; 1:1 mean diff 160.7, p<0.0001; 2:1 mean diff 148.3, p<0.0001; 4:1 mean diff 144.3, p<0.0001, Figure 6B, Supplemental Table 18). Across the five E:T ratios, CD56^{dim}CD16^{bright} NKp46 gMFI was 1119.7 ± 11.58, and CD56^{dim}CD16^{dim} NKp46 gMFI was 984.2 ± 11.83.

As all CD56^{dim}CD16^{bright} and CD56^{dim}CD16^{dim} NK cells expressed NKG2D receptors, we examined the proportion of cells within each subset that degranulated after exposure to HIV-infected targets (Figure 6C). Two-way ANOVA of % CD107a^{positive} cells showed a significant effect of CD56^{dim} NK cell subset (F(1,16)=1434, p<0.0001, 65.24% of variation), a significant effect of E:T ratio (F(3,16)=179.7, p<0.0001, 24.53%), and a significant subset × E:T interaction (F(3,16)=69.57, p<0.0001, 9.50%, Supplemental Table 18). At every E:T ratio tested, a higher percentage of CD56^{dim}CD16^{dim} cells degranulated than CD56^{dim}CD16^{bright} cells: at 1:4, 26.53 ± 1.67% of CD56^{dim}CD16^{dim} cells degranulated compared to 6.11 ± 0.47% of CD56^{dim}CD16^{bright} cells (mean diff −20.42, p<0.0001); at 1:2, 21.46 ± 1.59% versus 4.92 ± 0.17% (mean diff −16.54, p<0.0001); at 1:1, 13.96 ± 0.17% versus 3.51 ± 0.08% (mean diff −10.45, p<0.0001); and at 2:1, 8.91 ± 0.78% versus 1.86 ± 0.05% (mean diff −7.047, p<0.0001, Figure 6C, Supplemental Table 18). Both subsets showed decreasing degranulation frequency as E:T ratios increased. To evaluate whether NKp46 expression affects the differential degranulation capacities observed among CD16 subsets, we analyzed degranulation responses according to NKp46 status within each CD56^{dim} subset at the 1:1 E:T ratio (Figure 6D). Two-way ANOVA showed a significant effect of CD56^{dim} NK cell subset (F(1,8)=176.2, p<0.0001, 94.96% of variation), with no significant effect of NKp46 expression status (F(1,8)=0.963, p=0.3552) or subset × NKp46 interaction (F(1,8)=0.388, p=0.5507, Supplemental Table

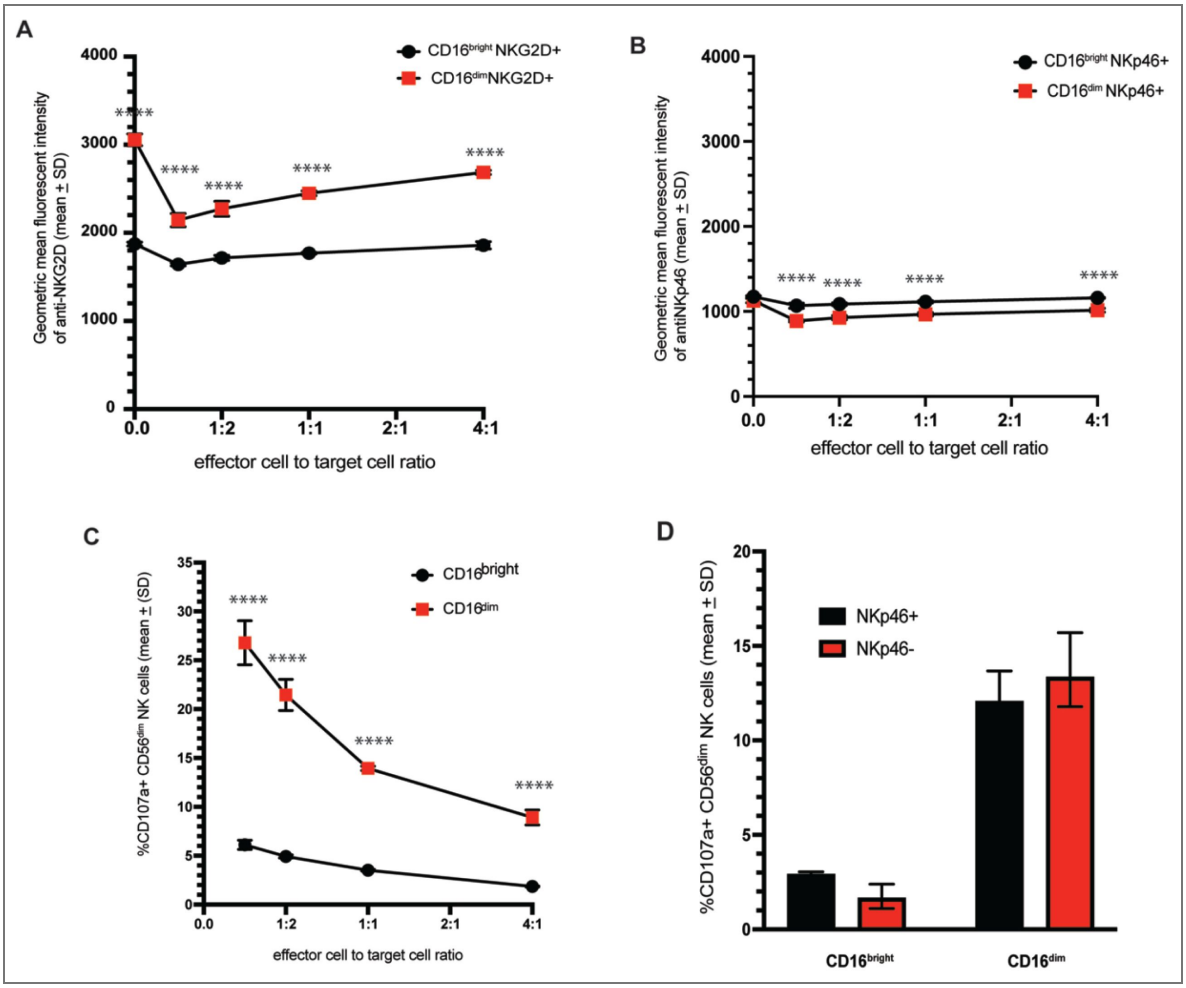

Figure 6. NKG2D and NKp46 surface expression and degranulation responses of CD56^{dim}CD16^{bright} and CD56^{dim}CD16^{dim} NK cell subsets following HIV-infected T-cell recognition

(A) Geometric mean fluorescence intensity (gMFI) of NKG2D surface expression on CD56^{dim}CD16^{bright} and CD56^{dim}CD16^{dim} NK cells following 4-hour exposure to purified autologous HIV-1$_{SHM-1}$ productively infected T-cells across different effector cell-to-target cell ratios. (B) gMFI of NKp46 surface expression on the NKp46-positive cells within the CD56^{dim}CD16^{bright} and CD56^{dim}CD16^{dim} NK cell subsets under the same conditions as (A). (C) CD107a degranulation responses of CD56^{dim}CD16^{bright} and CD56d^{im}CD16^{dim} NK cells from (A) across different effector cell-to-target cell ratios. (D) CD107a degranulation responses of CD56^{dim}CD16^{bright} and CD56^{dim}CD16^{dim} NK cells stratified by NKp46 expression (NKp46+ vs NKp46–) at a 1:1 effector-to-target cell ratio. Values represent mean ± standard deviation (SD). All CD107a values represent background-subtracted percentages (target-exposed minus mean unexposed controls). Statistical analyses: two-way ANOVA (effector cell-to-target cell ratio × subset) with Šidák's multiple comparisons test between subsets at each effector cell-to-target cell ratio for panels A, B, and C; two-way ANOVA (subset × NKp46 status) with Šidák's multiple comparisons test for panel D. Full ANOVA tables and post-hoc results are in Supplemental Table 18 for Figure 6. Significance: * p < 0.05, ** p < 0.01, *** p < 0.001, **** p < 0.0001.

18). Within CD56^{dim}CD16^{bright} cells, NKp46^{positive} cells exhibited 2.857 ± 0.119% CD107a^{positive} compared to 1.669 ± 0.622% CD107a^{positive} in NKp46− cells, with no significant difference between groups (mean diff 1.188, p=0.4952). Within CD56^{dim}CD16^{dim} cells, NKp46^{positive} cells showed 12.227 ± 1.594% CD107a^{positive} compared to 11.961 ± 1.910% in NKp46^{negative} cells, again with no significant difference (mean diff 0.265, p=0.9625, Figure 6D, Supplemental Table 18).

CD56^{dim}CD16^{dim} NK cells exhibit an enhanced antibody-dependent cell-mediated cytotoxic response against anti-gp120-coated HIV-infected cells

To thoroughly evaluate the functional capacity of CD56^{dim}CD16^{dim} NK cells, we assessed their ability to mediate ADCC using anti-gp120 broadly neutralizing Ab (clone VRC01)-coated HIV-1$\sim_{SHM-1}$ productively infected autologous primary CD4^{positive} T-cells, and compared these responses with the patterns of direct cytotoxicity.

Dose-response analysis of ADCC against anti-gp120 Ab-coated targets at a 1:1 E:T ratio showed that a higher frequency of CD56^{dim}CD16^{dim} NK cells exhibited Ab-mediated degranulation responses across all tested VRC01 concentrations (Figure 7A). Two-way ANOVA showed a significant effect of NK cell subset (F(1,16)=424.0, p<0.0001, 85.91% of variation), a significant effect of VRC01 concentration (F(3,16)=16.74, p<0.0001, 10.18%), and no significant subset × VRC01 interaction (F(3,16)=1.112, p=0.3732, 0.68%, Supplemental Table 19). At 0 µg/mL VRC01, CD56^{dim}CD16^{dim} cells degranulated at 12.19 cells ± 0.97% CD107a^{positive} compared to 2.92 + 0.06% CD107a^{positive} for CD56^{dim}CD16^{bright} (mean diff −9.268, p<0.0001). At 0.5 µg/mL, CD56^{dim}CD16^{dim} cells reached 13.17 ± 1.04% versus 3.99 ± 0.06% for CD56^{dim}CD16^{bright} (mean diff −9.174, p<0.0001). At 1 µg/mL, CD56^{dim}CD16^{dim} cells reached 15.22 ± 2.19% versus 4.94 ± 0.60% for CD56^{dim}CD16^{bright} cells (mean diff −10.29, p<0.0001). At 2 µg/mL, CD56^{dim}CD16^{dim} cells reached 17.82 ± 1.86% versus 6.45 ± 0.88% for CD56^{dim}CD16^{bright} (mean diff −11.37, p<0.0001, Figure 7A, Supplemental Table 19).

To confirm that CD56^{dim}CD16^{bright} cells retain the capacity for CD16-mediated degranulation despite their limited response against antibody-coated HIV-infected cells, we tested both subsets under direct CD16 cross-linking conditions using anti-CD16 antibody (clone 3G8). One-way ANOVA across the four treatment conditions (CD56^{dim}CD16^{bright} isotype, CD56^{dim}CD16^{bright} 3G8, CD56^{dim}CD16^{dim} isotype, CD56^{dim}CD16^{dim} 3G8) showed a significant effect of treatment (F(3,8)=1887, p<0.0001, R^2 = 0.9986, Supplemental Table 20). Both subsets demonstrated robust degranulation in response to 3G8, with CD56^{dim}CD16^{bright} cell reaching 41.00 ± 2.08% CD107a^{positive} compared to 0.12 $^{\pm}$ 0.02% with isotype (mean diff −40.89, p<0.0001) and CD56^{dim}CD16^{dim} cells reaching 61.27 ± 0.30% CD107a+ compared to 3.43 ± 1.08% with isotype (mean diff −57.84, p<0.0001). CD56^{dim}CD16^{dim} cells degranulated at a higher frequency than CD56^{dim}CD16^{bright} cell under 3G8 cross-linking (mean diff −20.27, p<0.0001, Figure 7-figure supplement 1, Supplemental Table 20).

ADAM17 enhances the ability of CD56^{dim}CD16^{dim} NK cells to degranulate in response to anti-HIV-1 gp120 antibody-coated HIV-infected cells

ADAM17 mediates CD16 shedding from the NK cell surface following engagement of antibody-coated targets, thereby influencing the NK cell's serial killing capacity (Lajoie et al., 2014; Romee et al., 2013). Thus, we investigated how ADAM17's impact on CD16 shedding affects the function of CD56^{dim}CD16^{dim} NK cells against anti-HIV-1 gp120 Ab-labeled HIV-infected targets (Figure 7B). We also determined the extent of changes in the frequency of CD16^{bright} and CD16^{dim} among the CD56^{dim} that degranulated when these cells were exposed to anti-gap120 Ab-coated HIV-infected cells in the absence or presence of ADAM17 inhibition.

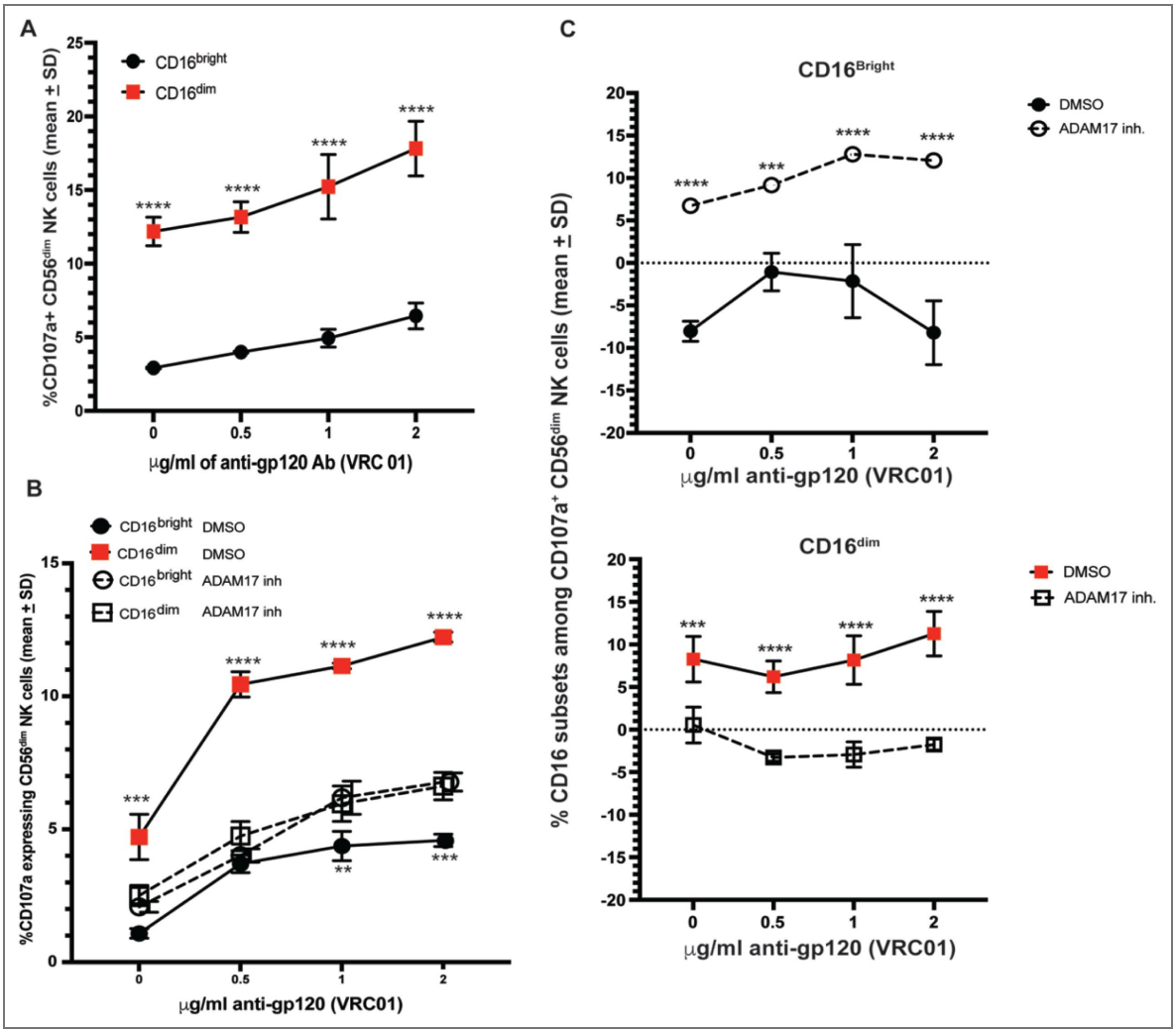

Figure 7. Degranulation of NK cell subsets in response to anti-gp120 labeled autologous HIV productively infected T-cells in the presence or absence of ADAM17 inhibition.

(A) Mean percentage ± standard deviation (SD) of CD56dimCD16bright and CD56dimCD16dim NK cells degranulating following 4-hour exposure at an effector-to-target ratio of 1:1 to purified autologous HIV-1SHM-1 productively infected T-cells pretreated with varying concentrations of anti-gp120 broadly neutralizing antibody (VRC01). All values represent background-subtracted percentages (target-exposed minus mean unexposed controls). (B) CD107a degranulation of CD56dimCD16bright (upper sub-panel) and CD56dimCD16dim (lower sub-panel) NK cells following exposure to VRC01-coated autologous HIV-1SHM-1 productively infected T-cells in the presence of an ADAM17 inhibitor in DMSO or DMSO vehicle alone. p-values next to the symbols are comparisons of the vehicle versus an ADAM17 inhibitor for each VRC01 concentration. (C) Change in the percentage of each CD16 subset following 4-hour exposure to purified autologous HIV-1_{SHM-1} productively infected T-cells across VRC01 concentrations, calculated as the percentage of the subset under target exposure minus the percentage of the same subset without target exposure, under either DMSO vehicle or ADAM17 inhibition, shown for $CD56^{dim}CD16^{bright}$ (upper sub-panel) and $CD56^{dim}CD16^{dim}$ (lower sub-panel) NK cells. p-values next to the symbols are comparisons between the vehicle and the ADAM17 inhibitor at each VRC01 concentration. Statistical analyses: two-way ANOVA (subset × VRC01 concentration) with Šidák's multiple comparisons test between subsets at each VRC01 concentration for panel A; three-way ANOVA (subset × treatment × VRC01 concentration) with Šidák's multiple comparisons test between DMSO and ADAM17 inhibition at each VRC01 concentration within each sub-panel for panel B; separate two-way ANOVAs (treatment × VRC01 concentration) for the $CD56^{dim}CD16^{bright}$ and $CD56^{dim}CD16^{dim}$ sub-panels, with Šidák's multiple comparisons test between DMSO and ADAM17 inhibition at each VRC01 concentration, for panel C. Full ANOVA tables and post-hoc results are in Supplemental Tables 19, 21, and 22 for Figures 7A, 7B, and 7C. Significance: * $p < 0.05$, ** $p < 0.01$, *** $p < 0.001$, **** $p < 0.0001$.

Three-way ANOVA of CD107a^{positive} degranulation responses (NK cell subset × treatment × VRC01 concentration) showed a significant effect of NK cell subset ($F(1,16)=557.9$, $p<0.0001$, 26.25% of variation), treatment ($F(1,16)=178.1$, $p<0.0001$, 7.18%), and VRC01 concentration ($F(3,16)=309.0$, $p<0.0001$, 37.38%), as well as a significant treatment × subset interaction ($F(1,16)=492.6$, $p<0.0001$, 23.18%), VRC01 × treatment interaction ($F(3,16)=11.68$, $p=0.0003$, 1.41%), VRC01 × subset interaction ($F(3,16)=8.962$, $p=0.0010$, 1.27%), and VRC01 × treatment × subset interaction ($F(3,16)=13.72$, $p<0.0001$, 1.94%, Supplemental Table 21). Within CD56^{dim}CD16^{bright} cell, ADAM17 inhibition did not significantly change the percentage of cells degranulating at 0 μg/mL VRC01 (DMSO 1.082 ± 0.181% vs ADAM17 inhibitor 2.084 ± 0.204%, mean diff −1.001, $p=0.7204$) or at 0.5 μg/mL (DMSO 3.700 ± 0.330% vs ADAM17 inhibitor 4.013 ± 0.251%, mean diff −0.313, $p>0.9999$), but significantly increased degranulation at 1.0 μg/mL (DMSO 4.371 ± 0.553% vs ADAM17 inhibitor 6.188 ± 0.622%, mean diff −1.817, $p=0.0029$) and at 2.0 μg/mL (DMSO 4.582 ± 0.231% vs ADAM17 inhibitor 6.776 ± 0.340%, mean diff −2.194, $p=0.0002$, Figure 7B, Supplemental Table 21). Conversely, within CD56^{dim}CD16^{dim} cells, ADAM17 inhibition significantly decreased the percentage of cells degranulating at every VRC01 concentration tested: at 0 μg/mL (DMSO 4.711 ± 0.853% vs ADAM17 i inhibition 2.509 ± 0.378%, mean diff 2.202, $p=0.0001$), 0.5 μg/mL (DMSO 10.446 ± 0.475% vs ADAM17 inhibition 4.742 ± 0.550%, mean diff 5.704, $p<0.0001$), 1.0 μg/mL (DMSO 11.141 ± 0.108% vs ADAM17 inhibition 5.959 ± 0.665%, mean diff 5.182, $p<0.0001$), and 2.0 μg/mL (DMSO 12.226 + 0.183% vs ADAM17 inhibition 6.621 ± 0.516%, mean diff 5.605, $p<0.0001$, Figure 7B, Supplemental Table 21).

Ab concentration-dependent analysis revealed ADAM17-mediated phenotypic transitions among CD56^{dim} NK cell subsets (Figure 7C). For CD56^{dim}CD16^{bright} cells, two-way ANOVA (treatment × VRC01 concentration) showed a significant effect of treatment ($F(1,16)=179.7$, $p<0.0001$, 80.93% of variation), a significant effect of VRC01 concentration ($F(3,16)=5.437$, $p=0.0090$, 7.35%), and a significant treatment × concentration interaction ($F(3,16)=3.338$, $p=0.0459$, 4.51%, Supplemental Table 22).

Under DMSO conditions, the change in CD56^{dim}CD16^{bright} frequency upon exposure to Ab-coated targets was negative across the concentration range (−8.03 ± 1.18% at 0 μg/mL, −1.07 ± 2.21% at 0.5 μg/mL, −2.13 ± 4.31% at 1.0 μg/mL, and −8.20 ± 3.76% at 2.0 μg/mL), whereas ADAM17 inhibition shifted these values positive (6.73 ± 3.76%, 9.17 ± 0.17%, 12.80 ± 2.10%, and 12.07 ± 1.73%, respectively). The difference between DMSO and ADAM17 inhibitor was significant at every concentration: 0 μg/mL (mean diff −14.77, $p<0.0001$), 0.5 μg/mL (mean diff −10.23, $p=0.0003$), 1.0 μg/mL (mean diff −14.93, $p<0.0001$), and 2.0 μg/mL (mean diff −20.27, $p<0.0001$, Figure 7C, Supplemental Table 22).

For CD56^{dim}CD16^{dim} cells, two-way ANOVA showed a significant effect of treatment ($F(1,16)=156.3$, $p<0.0001$, 82.96% of variation), a significant effect of VRC01 concentration ($F(3,16)=3.495$, $p=0.0402$, 5.57%), and no significant treatment × concentration interaction ($F(3,16)=1.871$, $p=0.1751$, Supplemental Table 22). Under DMSO conditions, the change in CD56^{dim}CD16^{dim} frequency upon exposure to Ab-coated targets was positive across the concentration range (8.27 ± 2.68% at 0 μg/mL, 6.20 ± 1.85% at 0.5 μg/mL, 8.17 ± 2.85% at 1.0 μg/mL, and 11.27 ± 2.61% at 2.0 μg/mL), whereas ADAM17 inhibition held these values at or below zero (0.53 ± 2.11%, −3.28 ± 0.43%, −2.93 ± 1.49%, and −1.77 ± 0.66%, respectively). The difference between DMSO and ADAM17 inhibitor was significant at every concentration: 0 μg/mL (mean diff 7.733, $p=0.0003$), 0.5 μg/mL (mean diff 9.483, $p<0.0001$), 1.0 μg/mL (mean diff 11.10, $p<0.0001$), and 2.0 μg/mL (mean diff 13.03, $p<0.0001$, Figure 7C, Supplemental Table 22).

CD56^{dim}CD16^{dim} NK cells require coordinated NKG2D signaling and ADAM17 activity for optimal anti-HIV response during antibody-dependent T-cell cytotoxicity of HIV-1-infected T-cells

To evaluate the functional impact of NKG2D and/or ADAM17 on CD56^{dim} NK cell subsets during ADCC, we analyzed the degranulation responses of CD56^{dim}CD16^{bright} and CD56^{dim}CD16^{dim} NK cells against HIV-infected T-cells opsonized with 1 μg/mL of anti-gp120 Ab (VRC01) at a 1:1 E:T ratio

(Figure 8). Two distinct response patterns were observed among the CD56^{dim} NK cell subsets.

Two-way ANOVA of CD107a^{positive} degranulation showed a significant effect of CD56^{dim} NK cell subset ($F(1,16)=245.2$, $p<0.0001$, 32.59% of variation), a significant effect of treatment ($F(3,16)=97.33$, $p<0.0001$, 38.81%), and a significant subset × treatment interaction ($F(3,16)=66.39$, $p<0.0001$, 26.47%, Supplemental Table 23). Under DMSO control conditions, CD56^{dim}CD16^{dim} cells degranulated at 12.604 ± 0.376% CD107a^{positive} compared to 2.583 ± 0.163% for CD56^{dim}CD16^{bright} cell (mean diff −10.02, $p<0.0001$, Figure 8A). Within CD56^{dim}CD16^{dim} cells, all three perturbations reduced degranulation relative to DMSO: anti-NKG2D blockade reduced degranulation to 5.241 ± 0.926% (mean diff 7.363, $p<0.0001$), ADAM17 inhibition reduced degranulation to 5.048 ± 0.814% (mean diff 7.556, $p<0.0001$), and the ADAM17 inhibitor + anti-NKG2D combination reduced degranulation to 2.026 ± 1.249% (mean diff 10.58, $p<0.0001$). The combination treatment reduced degranulation further than either single perturbation: ADAM17 inhibition vs combination mean diff 3.022, $p=0.0001$; anti-NKG2D vs combination mean diff 3.215, $p<0.0001$. Anti-NKG2D and ADAM17 inhibition alone did not differ from each other (mean diff 0.193, $p=0.9821$, Figure 8A, Supplemental Table 23).

Within CD56^{dim}CD16^{bright} cell, the pattern differed. Anti-NKG2D blockade reduced degranulation from 2.583 ± 0.163% to 0.918 ± 0.060% (mean diff 1.666, $p=0.0263$). ADAM17 inhibition increased degranulation to 3.993 ± 0.113% (mean difference −1.410, $p = 0.0679$, ns). The ADAM17 inhibitor ± anti-NKG2D combination reduced degranulation to 1.074 ± 0.084% (DMSO vs combination mean diff 1.509, $p=0.0472$; ADAM17 inhibition vs combination mean diff 2.919, $p=0.0002$). Anti-NKG2D alone and the combination did not differ (mean diff −0.157, $p=0.9903$, Figure 8A, Supplemental Table 23). Between subsets, CD56^{dim}CD16^{dim} cells degranulated at higher frequencies than CD56^{dim}CD16^{bright} cell under DMSO (mean diff −10.02, $p<0.0001$) and anti-NKG2D (mean diff −4.323, $p<0.0001$), with no significant difference under ADAM17 inhibition (mean diff −1.055, $p=0.0604$) or under the combination treatment (mean diff −0.952, $p=0.0871$, Figure 8A, Supplemental Table 23).

Analysis of the change in CD56^{dim} NK cell subset frequency when exposed to Ab-coated HIV-infected T-cells (relative to no-target controls) revealed activation-induced phenotypic transitions (Figure 8B). Two-way ANOVA showed a significant effect of CD56^{dim} subset ($F(1,16)=805.3$, $p<0.0001$, 31.09% of variation), a significant effect of treatment ($F(3,16)=23.83$, $p<0.0001$, 2.77%), and a significant subset × treatment interaction ($F(3,16)=565.8$, $p<0.0001$, 65.52%, Supplemental Table 24). Under DMSO conditions, CD56^{dim}CD16^{bright} frequency decreased by 5.20 ± 0.36% while CD56^{dim}CD16^{dim} frequency increased by 3.55 ± 0.15% (between-subset mean diff −8.747, $p<0.0001$). ADAM17 inhibition reduced these shifts: CD56^{dim}CD16^{bright} Δ −1.13 ± 0.35% and CD56^{dim}CD16^{dim} Δ 0.30 ± 0.10% (between-subset mean difference −1.430, $p<0.0001$). Anti-NKG2D blockade and the anti-NKG2D + ADAM17 inhibitor combination effectively abolished the shifts: under anti-NKG2D, CD56^{dim}CD16^{bright} Δ 0.13 ± 0.25% and CD56^{dim}CD16^{dim} Δ −0.03 ± 0.06% (between-subset mean diff 0.163, $p=0.3703$); under the combination, CD56^{dim}CD16^{bright} Δ 0.07 ± 0.15% and CD56^{dim}CD16^{dim} Δ 0.11 ± 0.05% (between-subset mean diff −0.043, $p=0.8099$, Figure 8B, Supplemental Table 24).

Within CD56^{dim}CD16^{bright} cell, the change in subset frequency differed significantly between DMSO and each of the three perturbations: DMSO vs ADAM17 inhibition (mean diff −4.067, $p<0.0001$), DMSO vs anti-NKG2D (mean diff −5.333, $p<0.0001$), DMSO vs anti-NKG2D + ADAM17 inhibition (mean diff −5.267, $p<0.0001$). ADAM17 inhibition also differed from anti-NKG2D (mean diff −1.267, $p<0.0001$) and from the combination (mean diff −1.200, $p<0.0001$), with no significant difference between anti-NKG2D and the combination (mean diff 0.067, $p=0.9994$, Figure 8B, Supplemental Table 24). Within CD56^{dim}CD16^{dim} cells, DMSO differed significantly from all three perturbations: vs ADAM17 inhibition (mean diff 3.250, $p<0.0001$), vs anti-NKG2D (mean diff 3.577, $p<0.0001$), vs anti-NKG2D + ADAM17 inhibition (mean diff 3.437, $p<0.0001$), with no significant differences among the three perturbations themselves (Figure 8B, Supplemental Table 24).

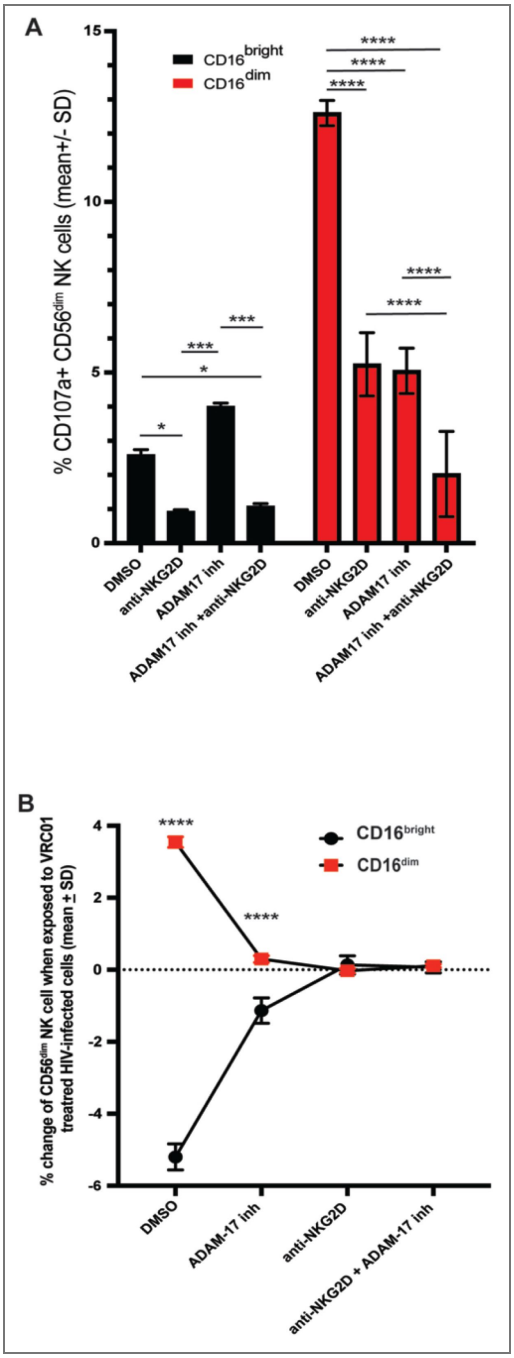

Figure 8. Degranulation of NK cell subsets in response to anti-gp120 labeled autologous HIV productively infected T-cells in the presence or absence of NKG2D blocking antibodies and/or ADAM17 inhibition

(A) Mean percentage ± standard deviation (SD) of $CD56^{dim}CD16^{bright}$ and $CD56^{dim}CD16^{dim}$ NK cells degranulating following 4-hour exposure at an effector-to-target ratio of 1:1 to purified autologous HIV-1_{SHM-1} productively infected T-cells pretreated with 1 µg/mL of anti-gp120 broadly neutralizing antibody (VRC01). NK cells were treated with DMSO vehicle, anti-NKG2D blocking antibody, ADAM17 inhibitor, or anti-NKG2D blocking antibody combined with ADAM17 inhibitor before being added to VRC01-coated HIV-infected T-cells. All values represent background-subtracted percentages (target-exposed minus mean unexposed controls). (B) Change in the frequency of $CD56^{dim}CD16^{bright}$ and $CD56^{dim}CD16^{dim}$ NK cells under each treatment condition, calculated as the percentage of the subset following 4-hour exposure to VRC01-coated HIV-infected T-cells minus the percentage of the same subset under matched treatment in the absence of target cells and antibody. Statistical analyses: two-way ANOVA (subset × treatment) with Tukey's multiple comparisons test for panel A; two-way ANOVA (subset × treatment) with Šidák's multiple comparisons test for panel B. Full ANOVA tables and post-hoc results are in Supplemental Tables 23 and 24 for Figures 8A and 8B. Significance: * $p < 0.05$, ** $p < 0.01$, *** $p < 0.001$, **** $p < 0.0001$

$CD56^{dim}CD16^{dim}$ NK cells perform serial ADCC against anti-gp120-coated HIV-infected cells via ADAM17-dependent CD16 turnover

To determine whether $CD56^{dim}CD16^{dim}$ NK cells could engage in repeated degranulation against anti-gp120 antibody-coated HIV-infected T-cells, and whether this serial ADCC required ADAM17-mediated CD16 turnover, we employed sequential CD107a labeling at 15-minute intervals over 60 minutes against VRC01-coated autologous HIV-infected T-cells. NK cells were treated with either DMSO vehicle control or an ADAM17 inhibitor before exposure to anti-gp120 antibody-coated targets, and the number of degranulation events per cell within the 60-minute window was quantified.

For $CD56^{dim}CD16^{bright}$ NK cells, two-way ANOVA (treatment × number of degranulations) showed a significant effect of the number of degranulations ($F(3,16)=6145$, $p<0.0001$, 99.60% of variation), with no significant effect of treatment ($F(1,16)=0.13$, $p=0.7233$) and a significant degranulations × treatment interaction ($F(3,16)=19.50$, $p<0.0001$, 0.32%, Supplemental Table 25). Under DMSO conditions, 91.06 ± 0.68% of $CD56^{dim}CD16^{bright}$ cells failed to degranulate, 5.17 ± 0.20% degranulated once, 3.10 ± 0.36% degranulated twice, and 0.79 ± 0.18% degranulated three times. Under ADAM17 inhibition, the distribution shifted to 84.48 ± 2.34% non-degranulating cells, 6.64 ± 0.07% single events, 4.65 ± 1.54% double events, and 5.12 ± 2.26% triple events. Šidák's comparisons of DMSO vs ADAM17 inhibition at each degranulation count showed a significant difference at 0 degranulations (mean diff 6.581, $p<0.0001$) and at 3 degranulations (mean diff −4.326, $p=0.0009$), with no significant differences at 1 degranulation (mean diff −1.471, $p=0.1866$) or 2 degranulations (mean diff −1.553, $p=0.1645$, Figure 9 $CD56^{dim}CD16^{bright}$ panel, Supplemental Table 25).

For $CD56^{dim}CD16^{dim}$ NK cells, two-way ANOVA showed a significant effect of the number of degranulations ($F(3,16)=2619$, $p<0.0001$, 91.74% of variation), no significant effect of treatment ($F(1,16)=0.0007$, $p=0.9788$), and a significant degranulations × treatment interaction ($F(3,16)=230.6$, $p<0.0001$, 8.08%, Supplemental Table 26). Under DMSO conditions, 61.56 ± 1.94% of $CD56^{dim}CD16^{dim}$ cells failed to degranulate, 13.55 ± 1.97% achieved one degranulation, 9.95 ± 3.30% achieved two degranulations, and 15.16 ± 0.80% achieved three degranulations within the 60-minute window. Under ADAM17 inhibition, the population shifted toward non-degranulation: 92.13 ± 1.21% non-degranulating cells, 3.57 ± 0.50% single events, 2.19 ± 0.96% double events, and 2.24 ± 0.30% triple events. Šidák's comparisons of DMSO vs ADAM17 inhibition at each degranulation count showed significant differences at every level: 0 degranulations (mean diff −30.57, $p<0.0001$), 1 degranulation (mean diff 9.98, $p<0.0001$), 2 degranulations (mean diff 7.75, $p<0.0001$), and 3 degranulations (mean diff 12.92, $p<0.0001$, Figure 9 $CD56^{dim}CD16^{dim}$ panel, Supplemental Table 26).

Discussion

Cellular immunotherapy has emerged as a promising strategy for HIV functional cure, and its development benefits from identifying which effector cells are most capable of eliminating HIV-infected cells. Knowing which population mediates the dominant response informs cell selection for adoptive transfer. The relevant effector cells for HIV control are likely those that are naturally selected during successful immune containment of the virus. HIV elite controllers maintain undetectable viremia and preserved $CD4^{positive}$ T-cell counts for at least 10 years without antiretroviral therapy, and this control is associated with a reorganization of the $CD56^{dim}$ NK cell compartment, with expansion of the $CD56^{dim}CD16^{dim}$ subset and corresponding decrease in the $CD56^{dim}CD16^{bright}$ subset compared to people living with HIV on ART and uninfected controls (Rallon et al., 2024). Whether this compartmental reorganization contributes mechanistically to control or simply correlates with it has been unclear. Here, we addressed this question by characterizing the responses of $CD56^{dim}CD16^{dim}$ and $CD56^{dim}CD16^{bright}$ NK cells to purified autologous productively HIV-infected primary T-cells, a major physiologically relevant target for HIV control. Our findings demonstrate that the minor $CD56^{dim}CD16^{dim}$ subset, despite

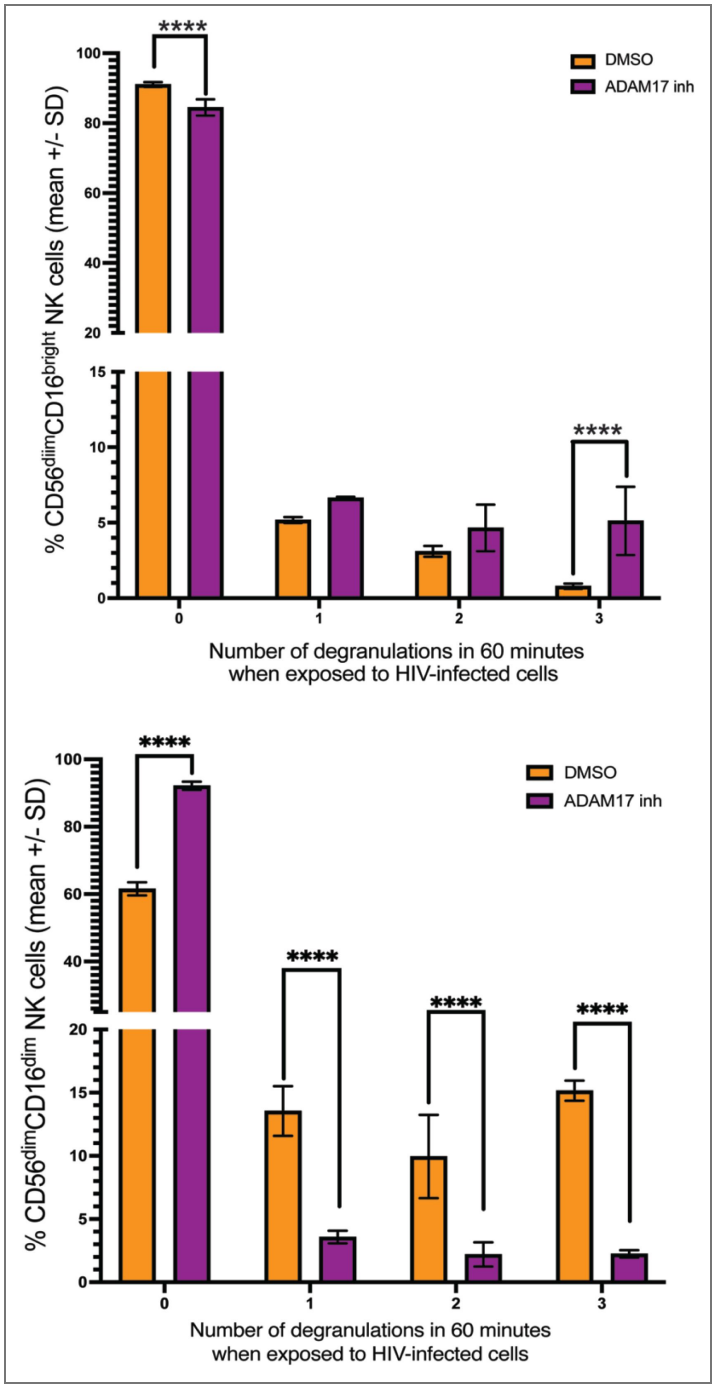

Figure 9. The number of NK cell subsets that degranulated when exposed to anti-gp120 Ab-coated HIV-infected cells over 60 minutes.

Purified autologous HIV-1_{SHM-1} productively infected T-cells were coated with 1 μg/mL of the broadly neutralizing anti-gp120 antibody VRC01. NK cells, pretreated with DMSO vehicle or an ADAM17 inhibitor dissolved in DMSO, were exposed to the coated target cells at an effector-to-target cell ratio of 1:1 and treated with a different fluorophore-labeled anti-CD107a antibody every 15 minutes for 60 minutes, with each labeling step blocked by excess unlabeled anti-CD107a and washed between steps. The number of fluorophores accumulated on $CD56^{dim}CD16^{bright}$ (upper panel) and $CD56d^{im}CD16^{dim}$ (lower panel) NK cells determined how many times each cell degranulated during the 60-minute exposure. SD = standard deviation. Statistical analyses: separate two-way ANOVAs (treatment × number of degranulations) for the $CD56^{dim}CD16^{bright}$ panel (with Šidák's multiple comparisons test) and the $CD56^{dim}CD16^{dim}$ panel (with Dunnett's multiple comparisons test), comparing DMSO and ADAM17 inhibition at each degranulation count. Full ANOVA tables and post-hoc results are in Supplemental Tables 25 and 26 for Figure 9. Significance: * $p < 0.05$, ** $p < 0.01$, *** $p < 0.001$, **** $p < 0.0001$.

representing less than 6% of circulating NK cells in uninfected subjects, mediates the dominant cytolytic response against HIV-infected cells, whereas the numerically dominant $CD56^{dim}CD16^{bright}$ population contributes minimally, even when HIV-infected cells are coated with antibodies that trigger CD16 activation on NK cells. We found that the $CD56^{dim}CD16^{dim}$ functional advantage stems from higher NKG2D expression, which is critical for $CD56^{dim}CD16^{dim}$ NK cells to mediate both direct killing and ADCC of HIV-infected T-cells, and from a greater capacity for serial killing. The $CD56^{dim}CD16^{dim}$ functional advantage is independent of inhibitory KIR repertoire and cytotoxic granule content. These findings provide a mechanistic basis for the compartmental reorganization observed in elite controllers, with expanded $CD56^{dim}CD16^{dim}$ cells providing the relevant effector capacity, while the contracted $CD56^{dim}CD16^{bright}$ population contributes minimally to HIV-infected cell killing under any condition. Thus, our data support the identification of $CD56^{dim}CD16^{dim}$ NK cells as the relevant effector population for cellular therapeutic strategies aimed at achieving functional cure of HIV.

Previous studies (Amand et al., 2017), as well as our own, have shown that the relatively rare $CD56^{dim}CD16^{negative}$ cells are more effective against the chronic myeloid leukemia, K562 cell line than other $CD56^{dim}$ subsets (Figure 1-figure supplement 2). Our findings demonstrate that $CD56^{dim}CD16^{dim}$ NK cells, comprising ~3-6% of peripheral blood NK cells and expressing 10-fold lower CD16 levels than $CD56^{dim}CD16^{bright}$ cell, are the primary effectors that eliminate HIV-infected T-cells, outperforming both $CD56^{dim}CD16^{bright}$ and $CD56^{dim}CD16^{negative}$ NK cells (Figure 1).

Despite their low frequency in uninfected subjects, $CD56^{dim}CD16^{dim}$ NK cells mediate disproportionate anti-HIV activity. This HIV-specific functional advantage was consistent across multiple donors (Figs. 1C and D), indicating an inherent characteristic rather than donor-specific variation. The killing frequency measurements (Figure 3) confirmed that $CD56^{dim}CD16^{dim}$ NK cells achieved significantly higher per-cell killing rates than $CD56^{dim}CD16^{bright}$ NK cells, translating enhanced degranulation into effective target elimination. At a 1:4 E:T ratio, one $CD56^{dim}CD16^{dim}$ cell could kill one HIV-infected cell, whereas four $CD56^{dim}CD16^{bright}$ cells were required for equivalent T-cell killing.

The functional advantage of $CD56^{dim}CD16^{dim}$ NK cells against HIV-infected cells emerges in a target system that has not traditionally been a focus of NK cell characterization, where $CD56^{dim}CD16^{dim}$ cells have been characterized as transitional or exhausted states (Romee et al., 2013; Yang et al., 2019). Our observations indicate that $CD56^{dim}CD16^{dim}$ cells, rather than being transitional or exhausted in the HIV context, drive the optimal NK cell response against HIV-infected cells. At matched effector cell-to-target cell ratios, purified $CD56^{dim}CD16^{dim}$ cells also lysed substantially more HIV-infected T-cells than purified $CD56^{dim}CD16^{bright}$ cell (Figure 2), confirming through sorted populations what bulk per-cell killing frequency analysis (Figure 3) demonstrated: the cytotoxic advantage is intrinsic to $CD56^{dim}CD16^{dim}$ cells rather than a reflection of subset composition. Moreover, $CD56d^{im}CD16^{dim}$ cells exhibited lower activation thresholds than $CD56^{dim}CD16^{bright}$ cells, evident even in responses to uninfected targets (Figure 1—figure supplement 3C). Notably, $CD56^{dim}CD16^{dim}$ cells responding to uninfected targets showed 2.0-fold higher degranulation than $CD56^{dim}CD16^{bright}$ cells at a 1:4 E:T ratio when responding to HIV-infected targets, indicating a naturally primed state. Furthermore, the 2.3- to 7.3-fold higher responses of $CD56^{dim}CD16^{dim}$ against infected versus uninfected targets indicate pathogen-specific recognition rather than generalized hyperreactivity.

We found in our study that $CD56^{dim}CD16^{dim}$ NK cells not only degranulate 4-6 times more frequently than $CD56^{dim}CD16^{bright}$ NK cells, but also respond to HIV-infected cells multiple times within one hour. The data presented in Figure 4 reveal two distinct response patterns in $CD56^{dim}CD16^{bright}$ cells. First, the majority of $CD56^{dim}CD16^{bright}$ cells did not initiate degranulation despite exposure to HIV-infected targets. Second, among the minority of $CD56^{dim}CD16^{bright}$ cells that do respond, most achieve only a single degranulation event and fail to continue killing. In contrast, the majority of $CD56^{dim}CD16^{dim}$ cells not only respond to HIV-infected targets but also undergo multiple rounds of degranulation, with approximately 15% achieving three degranulation events within one hour. Collectively, approximately 25% of

$CD56^{dim}CD16^{dim}$ cells achieved two or more degranulations, compared with only approximately 4% of $CD56^{dim}CD16^{bright}$ cells, demonstrating that $CD56^{dim}CD16^{dim}$ cells are more effective serial killers of HIV-infected cells. The greater capacity of $CD56^{dim}CD16^{dim}$ NK cells to respond to HIV-infected cells across multiple rounds of degranulation may explain why they are more effective than $CD56^{dim}CD16^{bright}$ cells at lysing HIV-infected cells over a given period.

The HIV-specific cytotoxic advantage of $CD56^{dim}CD16^{dim}$ cells is not attributable to higher cytotoxic protein content, as $CD56^{dim}CD16^{bright}$ and $CD56^{dim}CD16^{dim}$ subsets contain similar levels of perforin, granzyme A, and B (Figure 5-figure supplement 1). These functional differences likely stem from enhanced target recognition, serial killing, and more efficient degranulation. The consistently higher frequency of responding $CD56^{dim}CD16^{dim}$ cells across degranulation (Figure 1), IFN-γ production (Figure 1-figure supplement 3A and B), and cytotoxicity (Figure 2) measures indicates that the $CD56^{dim}CD16^{dim}$ subset has greater potential for activation against productively HIV-infected cells.

Our profiling of inhibitory receptors revealed an unexpected paradox that argues against differential inhibition by MHC class I molecules as the mechanism underlying the functional advantage of $CD56^{dim}CD16^{dim}$ cells. Despite $CD56^{dim}CD16^{bright}$ cells expressing the highest frequency and density of HLA-C-restricted KIRs, while $CD56^{dim}CD16^{negative}$ cells express the lowest, both subsets exhibit equivalently poor degranulation compared to $CD56^{dim}CD16^{dim}$ cells (Figure 5-figure supplement 3A and Figure 5-figure supplement 4A). This functional hierarchy of $CD56^{dim}CD16^{dim}$ > $CD56^{dim}CD16^{negative}$ and $CD56^{dim}CD16^{bright}$ persists even when comparing KIR-negative populations (Figure 5-figure supplement 3C and Figure 5-figure supplement 4C), indicating that inhibitory receptor expression does not account for the observed differences. Further evidence against differential inhibition as the mechanism comes from our analysis of KIR3DL1-mediated education (Kim et al., 2005). When HLA-A and - B molecules containing the HLA-Bw4 serological epitope are downmodulated by HIV Nef (Bonaparte & Barker, 2004; Boudreau et al., 2016; Schwartz et al., 1996), removing KIR3DL1-mediated inhibition, only educated $KIR3DL1^{positive}$ $CD56^{dim}CD16^{dim}$ cells showed enhanced degranulation compared to their $KIR3DL1^{negative}$ counterparts (Figure 5-figure supplement 2C), consistent with NK cell licensing (Boudreau et al., 2016; Kim et al., 2005). Remarkably, this education-derived advantage was absent in $CD56^{dim}CD16^{bright}$ cells (Figure 5-figure supplement 2A): they remained poorly functional despite greater education and disinhibition. NKG2A expression and HLA-E-mediated inhibition showed only minor differences between $CD56^{dim}$ NK cell subsets that do not account for the observed functional differences (Figure 5-figure supplement 5). This is consistent with our previous demonstration that HIV-infected cells present an HLA-E-bound HIV peptide that fails to engage NKG2A/CD94 productively (Davis et al., 2016), effectively neutralizing this inhibitory pathway. These findings collectively demonstrate that NK cell inhibitory receptor signaling is secondary to intrinsic subset-specific properties in determining NK cell effectiveness against HIV-infected cells. A caveat applies to this interpretation. The stratifications in Figure 5-figure supplement 2C through Figure 5-figure supplement 5C each evaluate degranulation according to a single inhibitory receptor at a time (KIR3DL1, KIR2DL2/3, KIR2DL1, or NKG2A), comparing receptor-positive with receptor-negative cells within each $CD56^{dim}$ subset. Because individual NK cells frequently co-express more than one inhibitory receptor, a cell scored as receptor-negative in any one of these analyses may still carry one or more of the others. These single-receptor stratifications therefore cannot resolve the combined inhibitory input of co-expressed receptors, nor can they formally exclude the possibility that specific combinations of inhibitory receptors influence degranulation in ways not captured when each receptor is analyzed in isolation.

We show in our study that HIV-1 Vpr induces expression of ligands for the NK cell activation receptor NKG2D on infected cells, and $CD56^{dim}CD16^{dim}$ cells respond more robustly to these stress ligands than $CD56^{dim}CD16^{bright}$ cells (Figure 5). The hierarchy of HIV-specific responses was consistent across NKG2D expression analysis (Figure 6) and blocking studies (Figure 5C), confirming that $CD56^{dim}CD16^{dim}$ cells were optimized for NKG2D-mediated recognition. While both $CD56^{dim}CD16^{bright}$ and $CD56^{dim}CD16^{dim}$ subsets show heavy dependence on NKG2D for HIV-

specific responses, with NKG2D blockade reducing degranulation by approximately 65-75% in both subsets, the higher baseline activation of $CD56^{dim}CD16^{dim}$ cells (Figure 1-figure supplement 3C) renders them the more effective HIV-specific $CD56^{dim}$ NK cell subset. This functional difference correlates with 1.3-1.5 fold higher NKG2D surface expression on $CD56^{dim}CD16^{dim}$ versus $CD56^{dim}CD16^{bright}$ cells, while NKp46 expression remains equivalent (Figure 6), suggesting that NKG2D receptor density contributes to HIV-specific functional capacity.

Beyond NKG2D, we examined the expression of other activating receptors implicated in NK cell recognition of infected or stressed cells, namely NKp30, NKp44, NKG2C, DNAM-1, 2B4, and NTB-A, across the $CD56^{dim}$ subsets, and none showed a between-subset difference (data not shown) comparable to that seen with NKG2D. This suggests that the elevated NKG2D on $CD56^{dim}CD16^{dim}$ cells distinguishes these subsets among the activating receptors surveyed, although expression analysis alone cannot exclude a functional contribution from these receptors.

In our studies, we observed that, despite CD16 being 10-fold less abundant, $CD56^{dim}CD16^{dim}$ NK cells mediated ADCC against productively HIV-infected T-cells 3-4 times more effectively than $CD56^{dim}CD16^{bright}$ NK cells (Figure 7A). The ADCC advantage of $CD56^{dim}CD16^{dim}$ NK cells was dependent on ADAM17. Inhibition of the enzyme significantly decreased ADCC mediated by $CD56^{dim}CD16^{dim}$ NK cells (Figs. 7B, 7C). In contrast, $CD56^{dim}CD16^{bright}$ NK cells showed increased ADCC when ADAM17 was inhibited, indicating that ADAM17 dampens the ability of $CD56^{dim}CD16^{bright}$ NK cells to function. This asymmetric dependence reframes ADAM17 not as a uniform brake on NK cell function but as a context-dependent regulator that enables serial engagement in $CD56^{dim}CD16^{dim}$ cells (Fig 9) while constraining sustained activation in $CD56^{dim}CD16^{bright}$ cells.

The inverse relationship between CD16 density and NKG2D expression on these subsets further suggests a compensatory mechanism: the higher NKG2D levels on $CD56^{dim}CD16^{dim}$ cells (Figure 6) may offset their lower CD16, enabling sustained recognition of HIV-infected cells through dual receptor engagement (Figure 8). This compensation is likely critical given the low surface density of gp120 on HIV-infected primary T-cells (~6.4×10^2 molecules per cell (Vasiliver-Shamis et al., 2008)) relative to high-density antigens such as CD20 on Raji cells (~5×10^4 molecules per cell (Lallemand et al., 2017)). Meeting a specific degranulation threshold against HIV-infected cells may therefore require NKG2D engagement regardless of CD16 expression (Figure 7A). Consistent with this, ADAM17 inhibition reduced $CD56^{dim}CD16^{dim}$ degranulation even at 0 µg/mL VRC01 (Figure 7B and C), where no antibody is present to engage CD16, suggesting that NKG2D-driven activation triggers ADAM17 activity independently of CD16 engagement and positioning ADAM17 as an enabler of sustained $CD56^{dim}CD16^{dim}$ function downstream of NKG2D signaling rather than solely a regulator of antibody-engaged CD16.

Previous studies have shown that ADAM17-mediated CD16 shedding facilitates NK cell detachment for serial killing (Srpan et al., 2018; Zambarda et al., 2025), an outcome that aligns with serial killing optimization models (Anft et al., 2020) and enables effective ADCC followed by rapid detachment via ADAM17-mediated synapse disassembly (Lorenzen et al., 2016). Our data (Figure 9) extend these findings to HIV-infected targets and suggest that $CD56^{dim}CD16^{dim}$ cells depend on efficient CD16 shedding to disengage from one target and engage the next. When shedding is blocked, sustained CD16 expression may prolong antibody-target tethering, which can explain why ADAM17 inhibition enhances otherwise modest $CD56^{dim}CD16^{bright}$ responses (Figs. 7B and 8A) but collapses $CD56^{dim}CD16^{dim}$ serial degranulation. A receptor-level mechanism for this asymmetry is provided by ADAM17 cleavage of CD16 at Valine 158 (Lajoie et al., 2014; Romee et al., 2013; Valipour et al., 2024), which releases CD2 from the central supramolecular activation cluster (cSMAC) of the immunological synapse, where CD2 is held by a cis interaction with CD16 mediated by Leucine 66 on CD16 (Grier et al., 2012). The release of CD2 from this cis interaction likely permits CD2 to move to the corolla of the immune synapse, where it signals 77x more strongly when it engages CD58 on T-cells (Siokis et al., 2021), thereby contributing to sustained activation of $CD56^{dim}CD16^{dim}$ cells during serial engagement (Figure 9).

This study has several significant limitations. Our studies primarily used cells from healthy donors in vitro. Validation in clinical cohorts, particularly elite controllers and patients across disease stages, is essential (Amand et al., 2017; Rallon et al., 2024). Most experiments used HIV-1_{SHM-1}, a primary clade B isolate, except for Vpr deletion studies (Figs. 4a-b), which used VSV-G pseudotyped DHIV3 to avoid Vpr strain growth disadvantages (Cohen et al., 1990). Validation across non-clade B isolates is crucial. In vitro-to-in vivo translation uncertainty persists, particularly because peripheral NK cells may not reach HIV reservoir sites, such as lymph nodes or the gastrointestinal tract (Estes et al., 2017). Chronic HIV markedly alters NK cell phenotypes and functions (Jost & Altfeld, 2012), potentially limiting the applicability of healthy donor findings described in this study. Despite limitations, our results identify $CD56^{dim}CD16^{dim}$ NK cells as specialized anti-HIV effector cells and provide a mechanistic framework for understanding clinical relevance (Amand et al., 2017; Rallon et al., 2024).

An important consideration in interpreting our results is that NK cells were rested overnight in 100 U/mL IL-2 following isolation, as detailed in the Materials and Methods section. This standard practice maintains NK cell viability while also providing activation signals that could normalize dysfunctional markers and reduce exhaustion phenotypes. Indeed, the dramatic functional differences between $CD56^{dim}CD16$ subsets observed after cytokine rest likely underestimate the disparities present in vivo, where dysfunctional cells would not receive this restorative signal.

Our CD107a degranulation assays were performed without the protein transport inhibitor brefeldin A, to preserve physiological intracellular trafficking conditions (Doms et al., 1989) during NK cell activation. This methodological choice preserves the natural dynamics of both degranulation and CD107a recycling during serial target engagement (Cohnen et al., 2013; Li et al., 2011; Liu et al., 2009). The decline in CD107a surface expression observed at higher E:T ratios in our study has been consistently reported across studies, regardless of inhibitor use, indicating that this reflects authentic NK cell functional kinetics (Vanherberghen et al., 2013). Moreover, since we measure intracellular interferon gamma and surface CD107a at the same time, we found that even in the presence of monensin, $CD56^{dim}CD16^{dim}$ NK cells display a higher ability to degranulate than $CD56^{dim}CD16^{bright}$ NK cells (Figure 1-figure supplement 3).

An important limitation of the present study is that we did not evaluate trafficking, sustainability, or homing of $CD56^{dim}CD16^{dim}$ cells to HIV reservoir sites such as mucosal tissues, which would be required for therapeutic translation. Peripheral blood NK cells naturally lack receptors for gut trafficking such as CCR9 and α4β7 (Lachota et al., 2023), and engineering approaches to add these features and to generate memory-like NK cells capable of sustained response without continuous cytokine treatment (Bednarski et al., 2022; Fehniger et al., 1999; Romee et al., 2012) will be necessary to translate the natural anti-HIV configuration of $CD56^{dim}CD16^{dim}$ cells into a durable therapeutic platform.

The findings presented here demonstrate that $CD56^{dim}CD16^{dim}$ NK cells, a rare population expanded in HIV elite controllers, are the dominant effectors against HIV-infected primary CD4+ T-cells, and that their effectiveness depends on the integration of NKG2D and CD16-ADAM17 signaling. This combination of dominant per-cell cytotoxicity, NKG2D-dependent threshold activation against low-density gp120, and ADAM17-mediated serial engagement provides a mechanistic basis for the correlation between expansion of this subset and the loss of the dominant $CD56^{dim}CD16^{bright}$ population in elite controllers, who maintain long-term viral control without ART. More broadly, the observation that different NK cell subsets dominate against different targets, with $CD56^{dim}CD16^{dim}$ cells against HIV-infected primary T-cells and $CD56^{dim}CD16^{negative}$ cells against K562 (Figure 1-figure supplement 2), suggests that the dominant effector population is not a fixed property of the NK cell compartment but is matched to the activating and inhibitory signal profile of the target. Primary tumors also show substantial heterogeneity in NK cell ligand and antibody target expression (Shembrey et al., 2019), and antigen heterogeneity is recognized as a central challenge for current CAR-NK cell engineering against solid tumors (Qutub et al., 2026). Whether the dual receptor logic operating in

$CD56^{dim}CD16^{dim}$ cells against HIV-infected T-cells generalizes to other limiting-antigen and heterogeneous-target contexts, including other intracellular pathogens and antigenically heterogeneous tumors, remains an open question that the framework developed here can address.

Materials and Methods

Human subjects

All primary cells, including NK cells and $CD4^{positive}$ T-cells, used in this study were isolated from the peripheral blood of healthy HIV-1-seronegative donors following informed written consent obtained in accordance with the Declaration of Helsinki. The Institutional Review Board at Rush University Medical Center approved the study under protocol 20062305-IRB01 (Chicago, IL, USA).

Cell isolation and NK cell subset purification

NK cells and $CD4^{positive}$ T-cells were isolated from peripheral blood in separate draws as described by Davis et al. (Davis et al., 2011). Briefly, $CD4^{positive}$ T-cells were isolated from PBMCs using positive selection with anti-CD4 magnetic beads (Miltenyi Biotec) and stimulated for 3 days with anti-CD3 and CD28 Ab beads (Miltenyi Biotec) before HIV infection. NK cells were isolated from PBMCs using the NK cell negative selection kit (Miltenyi Biotec) and cultured in RPMI-1640 medium supplemented with 10% FBS, 2mM glutamine, 100U/ml penicillin, and 100 mg/ml of streptomycin (complete media). We then added 100 IU/ml of recombinant human IL-2 (Peprotech) to the cells and allowed them to rest overnight at 37 °C in a 5% CO_2 incubator (Fisher). In the cytotoxicity assay, CD16 NK cell subsets were sorted for purity using a Beckman Coulter MoFlo Astrios EQ (flow core facility, University of Illinois at Chicago). The purity of $CD4^{positive}$ and NK cells was greater than 97%, and sorted NK cells (the two subsets evaluated in Figure 2) exceeded 99.9% positivity in our studies.

HIV infection of primary $CD4^{positive}$ T-cells

Anti-CD3 and anti-CD28 Ab coupled to bead-stimulated primary $CD4^{positive}$ T-cells were infected with either a primary isolate ($HIV\text{-}1_{SHM\text{-}1}$) or an HIV-1 strain lacking the envelope protein (DHIV3). These envelope-defective viruses were pseudotyped with the vesicular stomatitis virus G protein. For Vpr deletion studies (Figs. 5A and B), VSV-G pseudotyped DHIV3 (wild-type and ΔVpr) were used as target cells in the degranulation assay as described (Davis et al., 2011). All other studies used $HIV\text{-}1_{SHM\text{-}1.}$ HIV infection was carried out by spin-inoculation at an MOI of 0.5, as detailed by O'Doherty et al. (O'Doherty et al., 2000). Following infection, cells were cultured at 1.5×10^6/mL in RPMI complete medium supplemented with 200 IU/mL recombinant IL-2 (Peprotech). Cells were split 1:2 every three days with fresh complete medium containing 200 U/ml of IL-2. Between days 7 and 10 post-infection, the infected cells were processed for target cells as described (Davis et al., 2011). Purified infected cells were verified by flow cytometry using anti-CD4 surface staining and intracellular HIV-1 p24 staining (Supplemental Table 27). Representative dot plots (Figure 1-figure supplement 4) showing CD4 and HIV-1 p24 staining of uninfected (left) and HIV-infected (right) primary T-cells. Across all preparations used in this study, the purity of infected T-cells was greater than 92% p24 antigen-positive.

Functional assays and flow cytometry

The purified infected cells were added to a U-bottom 96-well plate at a final cell count of 5×10^4 cells per well. In some studies, uninfected $CD4^{positive}$ T-cells, cultured alongside infected cells (Figure 1-figure supplement 3), or K562 (ATCC) cells (Figure 1-figure supplement 2) were used as target cells instead of purified HIV-infected cells. In Ab-dependent cell-mediated cytotoxicity assays, the VRC01 clone of an anti-HIV-1 gp120-specific broadly neutralizing Ab (BEI Resources Repository) was used. VRC01 was added to the infected cells at various concentrations and incubated for 30 minutes at room temperature before the addition of NK cells (Figs. 7, 8, and 9) In some cases the NK cells were either pretreated with 10 μg/ml of anti-NKG2D blocking Ab (R&D Systems; Supplemental Table 27) and/or the ADAM17 inhibitor GW280264X (Aobious)

suspended in ^{dim}ethyl sulfoxide (DMSO) (Supplemental Table 27) and used at a final concentration of 1.74 mM (Figs. 6 and 7). Controls consisted of adding DMSO to the same final volume as the DMSO used to resuspend the ADAM17 inhibitor (Figs. 7 and 8). Following the incubation period with blocking reagents, NK cells were added to the target cells at NK cell E:T ratios ranging from 1:8 to 10:1, depending on the experiment. All groups were performed in triplicate wells at each E:T ratio, with a final volume of 200 µL. For controls of CD107a surface and intracellular IFNg expression, NK cells were added to wells without target cells. For the cytotoxicity controls, infected target-cells were added without NK cells. The 96-well U-bottom plates containing cells were centrifuged at 20 x g for 2 minutes and incubated at 37 °C in a 5% CO_2 incubator for 4 hours. For intracellular IFNγ expression by NK cells, we added Monensin (Becton Dickinson) to a final concentration of 2.05 mM, 1 hour into the 4-hour incubation (Supplemental Table 27). At the end of the incubation period, the cells were surface-stained with anti-CD56, CD16, and anti-CD3 antibodies, and then further stained for CD107a to assess NK cell surface expression according to the procedures described by Davis et al. (Davis et al., 2011). All Abs used for flow-based assays are listed in Supplemental Table 27. NK cell intracellular expression of IFN-γ (Figure 1-figure supplement 3A) was determined using the methods described by Cogswell et al. (Cogswell et al., 2022). For the cytotoxicity assessment of HIV-infected cells (Figure 2), we followed the manufacturer's (Abcam) protocol and control cell treatments for the flow-based cytotoxicity assay (reagents listed in Supplemental Table 27), which used 7-amino-actinomycin D (7AAD) to stain infected cells killed by NK cells.

The flow cytometer used in our study was a Becton Dickinson $LSR_{Fortessa}$, equipped with four lasers set up for Violet (405nm), Blue (488 nm), Yellow (561 nm), and Red (637 nm) emission. All samples collected were analyzed using FlowJo Software, Version 10.9.0. (Becton, Dickinson). Cells were stained with live-dead stain (Supplemental Table 27) followed by cell surface staining with fluorochrome-conjugated Ab against CD3, CD56, and CD16 (Supplemental Table 27). In some studies (Figure 1 and Figure 1-figure supplement 1) fluorochrome-conjugated Ab to NKp80 (Supplemental Table 27) was used. Fluorescence-minus-one (FMO) controls were also set up for all stains and fluorochrome-conjugated antibodies. All cells used in the analysis were viable singlet $CD3^{negative}$ lymphocytes (Figure 1-figure supplement 5) except for cytotoxicity assays, where CD3 was used to identify the infected T-cells (Figure 2). Nine NK cell populations were identified based on differential expression of CD16 and CD56 (Figure 1-figure supplement 1). Fluorescence-minus-one (FMO) controls were used to set negative (neg) gates for CD16 and CD56 (Figure 1-figure supplement 1). Anti-NKp80 staining was used as an NK cell marker to identify $CD56^{negative}$ NK cells (Figure 1-figure supplement 1). $CD56^{bright}$ gates were set based on cells in quadrant 3, and $CD16^{bright}$ gates were set based on cells in quadrant 4 (Figure 1-figure supplement 1).

For functional assays, event acquisition varied with the E:T ratio, reflecting the number of NK cells plated per well. For the $CD56^{dim}CD16^{dim}$ subset (3-6% of total NK cells), the average event acquisition ranged from 384 events per well at E:T 1:4 to 3,029 events per well at E:T 4:1 (Figure 1-figure supplement 6). At E:T ratios of 1:2 and 1:4, fewer than 1,000 $CD56^{dim}CD16^{dim}$ events were acquired per well. Event numbers for each subset reflected their normal frequencies within the $CD56^{dim}$ population, with $CD56^{dim}CD16^{bright}$ (~80-85% of NK cells) yielding 3,974-63,369 mean events collected per well and $CD56^{dim}$CD16neg (1-3%) yielding 283-5,820 mean events collected per well across all E:T ratios.

Serial degranulation assay

This flow-based serial degranulation assay is based on the protocol by Niemann et al. (Niemann et al., 2025). Briefly, purified autologous HIV-infected T-cell targets were added to V-bottomed 96-well plates at 5×10^4 cells and pelleted before the addition of 2.5×10^4 NK cells. Under ADCC conditions, 1 µg/ml VRC01 antibody is pre-incubated with the target cells for 30 minutes at 4 °C before NK cells are added to the wells. Control wells consisted of NK cells without target cells. All groups were performed in triplicate wells, with a final volume of 50 µL of RPMI-1640, 10% FBS, 2 mM glutamine, 100 U/ml penicillin, and 100 µg/ml streptomycin (complete medium). The 96-well V-bottom plates were then centrifuged at 500 x g for 10 seconds and incubated at 37 °C in a 5% CO_2

incubator for 10 minutes. Following the incubation step, the pellets were resuspended in 5 µL of anti-CD107a BV421-conjugated antibody (Table 1) and incubated at 37 °C for 5 minutes. This step fluorescently labels all CD107a present on NK cells at the initial 15-minute exposure. Next, we added 5 µL of non-conjugated anti-

CD107a antibody (Table 1), and incubated for another 5 minutes at 37°C. Blocking allows for only newly externalized CD107a molecules to be stained in the subsequent staining. Following the blocking step, the wells were diluted with 100 µL complete medium, and plates were centrifuged at 500 x g for 5 minutes before being resuspended in a final volume of 50 µL of complete medium. The 96-well V-bottom plates were then centrifuged at 500 x g for 10 seconds and incubated at 37 °C in a 5% CO_2 incubator for 10 minutes. Following the incubation step, the pellets were resuspended in 5 µL of an anti-CD107a FITC-conjugated antibody (Table 1) and incubated at 37 °C for 5 min. Next, we added 5 µL of non-conjugated anti-CD107a antibody (Table 1), and incubated for another 5 minutes at 37°C. Following the blocking step, the wells were diluted with 100 µL complete medium, and plates were centrifuged at 500 x g for 5 minutes before being resuspended in a final volume of 50 µL of complete medium. The 96-well V-bottom plates were then centrifuged at 500 x g for 10 seconds and incubated at 37 °C in a 5% CO_2 incubator for 10 minutes. Following the incubation step, the pellets were resuspended in 5 µL of an anti-CD107a PE conjugated antibody (Table 1) and incubated at 37 °C for 5 min. The unconjugated anti-CD107a incubation step is unnecessary during the final stage. At the end of the one-hour incubation, the cells were washed with 100 µL of PBS and centrifuged at 500 × g for 5 minutes. The pellet was then stained for viability and surface markers (anti-CD56, CD16, and CD3) as described above under “Functional assays and flow cytometry.”

Statistical Analyses

Statistical analyses were performed using GraphPad Prism version 10.6.1 (GraphPad Software). Data are presented as mean ± standard deviation (SD) with n = 3 per group for all functional studies. This sample size reflects the practical yield of purified, productively HIV-infected primary CD4+ T-cells, donor-to-donor variability in HIV infection efficiency, and the requirement that p24 purity be verified for every functional study before NK cell exposure. A donor-matched design was used throughout to control for between-donor variation in KIR and HLA polymorphism, recent infections, diet, sleep, and stress, which can influence baseline NK cell phenotype and function.

For Figure 1 and Figure 1-figure supplement 1, comparisons across the three $CD56^{dim}$ NK cell subsets ($CD56^{dim}CD16^{bright}$, $CD56^{dim}CD16^{dim}$, and $CD56^{dim}CD16^{negative}$) were performed using one-way ANOVA with Dunnett’s multiple comparisons test for between-subset contrasts. For Figure 1C and Figure 1D, donor-matched comparisons were performed using repeated-measures one-way ANOVA with donor matching. Based on these data and consistent with Rallon et al. (Rallon et al., 2024), subsequent analyses focused on direct comparisons between the $CD56^{dim}CD16^{bright}$ and $CD56^{dim}CD16^{dim}$ subsets, which show the most pronounced alterations in HIV elite controllers relative to people living with HIV on antiretroviral therapy and uninfected donors. The $CD56^{dim}CD16^{negative}$ subset was retained as a comparator for the inhibitory receptor analyses (KIR3DL1, KIR2DL2/3, KIR2DL1, and NKG2A; Figure 5-figure supplement 2 through Figure 5-figure supplement 5).

Two-way ANOVA with Šidák’s multiple comparisons test was used for the majority of analyses involving two independent factors, including Figures 2, 3B, 3C, 4, 5C, 6A, 6B, 6C, 6D, 7A, 7C, 8B, and 9 ($CD56^{dim}CD16^{bright}$ and $CD56^{dim}CD16^{dim}$ panels), and figure supplements: Figure 4-figure supplement 1A, Figure 4-figure supplement 1B, Figure 1-figure supplement 3A, Figure 1-figure supplement 3B, Figure 1-figure supplement 3C, Figure 5-figure supplement 2A, Figure 5-figure supplement 2C, Figure 5-figure supplement 3A, Figure 5-figure supplement 3B, Figure 5-figure supplement 3C, Figure 5-figure supplement 4A, Figure 5-figure supplement 4B, Figure 5-figure supplement 4C, Figure 5-figure supplement 5A, Figure 5-figure supplement 5B, and Figure 5-figure supplement 5C. Two-way ANOVA with Tukey’s multiple comparisons test was used where all pairwise contrasts among groups were of interest, specifically Figure 5-figure supplement 2B (KIR3DL1 density) and Figure 8A (NKG2D and

ADAM17 combined effects on ADCC). One-way ANOVA with Šidák's multiple comparisons test for preselected pairwise contrasts was used for Figure 7-figure supplement 1 (anti-CD16 3G8 cross-linking). Three-way ANOVA with Šidák's multiple comparisons test was used for Figure 7B (NK cell subset × treatment × VRC01 concentration).

For all ANOVA analyses, F-statistics, degrees of freedom, percentage of total variation, and adjusted p-values are reported in the Results section and in the corresponding Supplemental Tables (Supplemental Tables 1 through 26). Statistical significance was defined as $p < 0.05$, with exact adjusted p-values reported throughout. Post-hoc multiple comparisons p-values are reported as adjusted values.

Data availability

All data generated and analyzed during this study are included in the manuscript, figure supplements, and supplemental statistical tables. Additional raw donor-level data and source files are available from the corresponding author upon reasonable request. Flow cytometry data files will be deposited in FlowRepository upon acceptance.

Acknowledgements

We thank Kerry Campbell, Ph.D., of Fox Chase Cancer Center, for his helpful insights into experimental design throughout this study. We also thank the Flow Cytometry Cores at Rush University and the University of Illinois at Chicago for technical support.

Additional information

Funding

This work was supported by the National Institutes of Health/National Institute of Allergy and Infectious Diseases (NIH/NIAID) grant R01AI161816 to David T. Evans and Edward Barker.

Author contributions

William Howell: Data curation, Formal analysis, Investigation, Methodology, Validation, Writing – original draft.
Courtney Branch: Data curation, Formal analysis, Investigation.
Jeffrey Ward: Conceptualization, Data curation, Formal analysis, Investigation.
Zachary Davis: Conceptualization, Data curation, Formal analysis, Investigation.
Emma Geatches: Data curation, Formal analysis, Investigation.
Edward Barker: Formal analysis, Funding acquisition, Investigation, Project administration, Supervision, Writing – original draft, Writing – review & editing.

Funding

Funder	Grant reference number	Author
HHS | NIH | National Institute of Allergy and Infectious Diseases (NIAID)	R01AI161816	Edward Barker

Author ORCID iDs

Edward Barker: https://orcid.org/0000-0003-3773-9565

Additional files

Supplemental Table 1

Supplemental Table 2

Supplemental Table 3

Supplemental Table 4
Supplemental Table 5
Supplemental Table 6
Supplemental Table 7
Supplemental Table 8
Supplemental Table 9
Supplemental Table 10
Supplemental Table 11
Supplemental Table 12
Supplemental Table 13
Supplemental Table 14
Supplemental Table 15
Supplemental Table 16
Supplemental Table 17
Supplemental Table 18
Supplemental Table 19
Supplemental Table 20
Supplemental Table 21
Supplemental Table 22
Supplemental Table 23
Supplemental Table 24
Supplemental Table 25
Supplemental Table 26
Supplemental Table 27
Figure 1-figure supplement 1
Figure 1-figure supplement 2
Figure 1-figure supplement 3
Figure 1-figure supplement 4
Figure 1-figure supplement 5
Figure 1-figure supplement 6
Figure 4-figure supplement 1
Figure 5-figure supplement 1
Figure 5-figure supplement 2
Figure 5-figure supplement 3
Figure 5-figure supplement 4
Figure 5-figure supplement 5
Figure 7-figure supplement 1

References

Abeynaike SA, Huynh TR, Mehmood A, Kim T, Frank K, Gao K, Zalfa C, Gandarilla A, Shultz L, Paust S (2023) Human hematopoietic stem cell engrafted IL-15 transgenic NSG mice support robust NK cell responses and sustained HIV-1 infection. *Viruses* **15**:e365 https://doi.org/10.3390/v15020365 | PubMed

Alter G, Teigen N, Davis BT, Addo MM, Suscovich TJ, Waring MT, Streeck H, Johnston MN, Staller KD, Zaman MT, *et al.* (2005) Sequential deregulation of NK cell subset distribution and function starting in acute HIV-1 infection. *Blood* **106**:3366-3369 https://doi.org/10.1182/blood-2005-03-1100 | PubMed

Amand M, Iserentant G, Poli A, Sleiman M, Fievez V, Sanchez IP, Sauvageot N, Michel T, Aouali N, Janji B, *et al.* (2017) Human CD56dimCD16dim cells as an individualized natural killer cell subset. *Frontiers in Immunology* **8**:699 https://doi.org/10.3389/fimmu.2017.00699 | PubMed

Anft M, Netter P, Urlaub D, Prager I, Schaffner S, Watzl C (2020) NK cell detachment from target cells is regulated by successful cytotoxicity and influences cytokine production. *Cellular & Molecular Immunology* **17**:347-355 https://doi.org/10.1038/s41423-019-0277-2 | PubMed

Antela A, Rivero A, Llibre JM, Moreno S, Group RET (2021) Redefining therapeutic success in HIV patients: an expert view. *Journal of Antimicrobial Chemotherapy* **76**:2501-2518 https://doi.org/10.1093/jac/dkab168 | PubMed

Bednarski JJ, Zimmerman C, Berrien-Elliott MM, Foltz JA, Becker-Hapak M, Neal CC, Foster M, Schappe T, McClain E, Pence PP, *et al.* (2022) Donor memory-like NK cells persist and induce remissions in pediatric patients with relapsed AML after transplant. *Blood* **139**:1670-1683 https://doi.org/10.1182/blood.2021013972 | PubMed

Belmonte L, Olmos M, Fanin A, Parodi C, Bare P, Concetti H, Perez H, de Bracco MM, Cahn P (2007) The intestinal mucosa as a reservoir of HIV-1 infection after successful HAART. *Aids* **21**:2106-2108 https://doi.org/10.1097/QAD.0b013e3282efb74b | PubMed

Bjorklund AT, Carlsten M, Sohlberg E, Liu LL, Clancy T, Karimi M, Cooley S, Miller JS, Klimkowska M, Schaffer M, *et al.* (2018) Complete remission with reduction of high-risk clones following haploidentical NK-cell therapy against MDS and AML. *Clinical Cancer Research* **24**:1834-1844 https://doi.org/10.1158/1078-0432.CCR-17-3196 | PubMed

Bonaparte MI, Barker E (2004) Killing of human immunodeficiency virus-infected primary T-cell blasts by autologous natural killer cells is dependent on the ability of the virus to alter the expression of major histocompatibility complex class I molecules. *Blood* **104**:2087-2094 https://doi.org/10.1182/blood-2004-02-0696 | PubMed

Boudreau JE, Mulrooney TJ, Le Luduec JB, Barker E, Hsu KC (2016) KIR3DL1 and HLA-B density and binding calibrate NK education and response to HIV. *The Journal of Immunology* **196**:3398-3410 https://doi.org/10.4049/jimmunol.1502469 | PubMed

Bryceson YT, March ME, Ljunggren HG, Long EO (2006) Synergy among receptors on resting NK cells for the activation of natural cytotoxicity and cytokine secretion. *Blood* **107**:159-166 https://doi.org/10.1182/blood-2005-04-1351 | PubMed

Cerboni C, Zingoni A, Cippitelli M, Piccoli M, Frati L, Santoni A (2007) Antigen-activated human T lymphocytes express cell-surface NKG2D ligands via an ATM/ATR-dependent mechanism and become susceptible to autologous NK-cell lysis. *Blood* **110**:606-615 https://doi.org/10.1182/blood-2006-10-052720 | PubMed

Chun TW, Nickle DC, Justement JS, Meyers JH, Roby G, Hallahan CW, Kottilil S, Moir S, Mican JM, Mullins JI, *et al.* (2008) Persistence of HIV in gut-associated lymphoid tissue despite long-term antiretroviral therapy. *The Journal of Infectious Diseases* **197**:714-720 https://doi.org/10.1086/527324 | PubMed

Cichocki F, Bjordahl R, Gaidarova S, Mahmood S, Abujarour R, Wang H, Tuininga K, Felices M, Davis ZB, Bendzick L, *et al.* (2020) iPSC-derived NK cells maintain high cytotoxicity and enhance in vivo tumor control in concert with T cells and anti-PD-1 therapy. *Science Translational Medicine* **12**:eaaz5618 https://doi.org/10.1126/scitranslmed.aaz5618 | PubMed

Cogswell A, Jo S, Ferguson N, Gupta K, Barker E (2022) Presence of natural killer B cells in simian immunodeficiency virus-infected colon that have properties and functions similar to those of natural killer cells and B cells but are a distinct cell population. *Journal of Virology* **96**:e0023522 https://doi.org/10.1128/jvi.00235-22 | PubMed

Cohen EA, Terwilliger EF, Jalinoos Y, Proulx J, Sodroski JG, Haseltine WA (1990) Identification of HIV-1 vpr product and function. *Journal of Acquired Immune Deficiency Syndromes* **3**:11-18 PubMed

Cohnen A, Chiang SC, Stojanovic A, Schmidt H, Claus M, Saftig P, Janssen O, Cerwenka A, Bryceson YT, Watzl C (2013) Surface CD107a/LAMP-1 protects natural killer cells from degranulation-associated damage. *Blood* **122**:1411-1418 https://doi.org/10.1182/blood-2012-07-441832 | PubMed

Cooley S, He F, Bachanova V, Vercellotti GM, DeFor TE, Curtsinger JM, Robertson P, Grzywacz B, Conlon KC, Waldmann TA, *et al.* (2019) First-in-human trial of rhIL-15 and haploidentical natural killer cell therapy for advanced acute myeloid leukemia. *Blood Advances* **3**:1970-1980 https://doi.org/10.1182/bloodadvances.2018028332 | PubMed

Cooper MA, Fehniger TA, Caligiuri MA (2001) The biology of human natural killer-cell subsets. *Trends in Immunology* **22**:633-640 https://doi.org/10.1016/s1471-4906(01)02060-9 | PubMed

Davis ZB, Cogswell A, Scott H, Mertsching A, Boucau J, Wambua D, Le Gall S, Planelles V, Campbell KS, Barker E (2016) A conserved HIV-1-derived peptide presented by HLA-E renders infected T-cells highly susceptible to attack by NKG2A/CD94-bearing natural killer cells. *PLOS Pathogens* **12**:e1005421 https://doi.org/10.1371/journal.ppat.1005421 | PubMed

Davis ZB, Ward JP, Barker E (2011) Preparation and use of HIV-1 infected primary CD4+ T-cells as target cells in natural killer cell cytotoxic assays. *Journal of Visualized Experiments* **49**:2668 https://doi.org/10.3791/2668 | PubMed

De Maria A, Bozzano F, Cantoni C, Moretta L (2011) Revisiting human natural killer cell subset function revealed cytolytic CD56dimCD16+ NK cells as rapid producers of abundant IFN-gamma on activation. *Proceedings of the National Academy of Sciences of the United States of America* **108**:728-732 https://doi.org/10.1073/pnas.1012356108 | PubMed

Doms RW, Russ G, Yewdell JW (1989) Brefeldin A redistributes resident and itinerant Golgi proteins to the endoplasmic reticulum. *Journal of Cell Biology* **109**:61-72 https://doi.org/10.1083/jcb.109.1.61 | PubMed

Estes JD, Kityo C, Ssali F, Swainson L, Makamdop KN, Del Prete GQ, Deeks SG, Luciw PA, Chipman JG, Beilman GJ, *et al.* (2017) Defining total-body AIDS-virus burden with implications for curative strategies. *Nature Medicine* **23**:1271-1276 https://doi.org/10.1038/nm.4411 | PubMed

Fehniger TA, Shah MH, Turner MJ, VanDeusen JB, Whitman SP, Cooper MA, Suzuki K, Wechser M, Goodsaid F, Caligiuri MA (1999) Differential cytokine and chemokine gene expression by human NK cells following activation with IL-18 or IL-15 in combination with IL-12: implications for the innate immune response. *The Journal of Immunology* **162**:4511-4520 https://doi.org/10.4049/jimmunol.162.8.4511 | PubMed

Finzi D, Hermankova M, Pierson T, Carruth LM, Buck C, Chaisson RE, Quinn TC, Chadwick K, Margolick J, Brookmeyer R, *et al.* (1997) Identification of a reservoir for HIV-1 in patients on highly active antiretroviral therapy. *Science* **278**:1295-1300 https://doi.org/10.1126/science.278.5341.1295 | PubMed

Fletcher CV, Staskus K, Wietgrefe SW, Rothenberger M, Reilly C, Chipman JG, Beilman GJ, Khoruts A, Thorkelson A, Schmidt TE, *et al.* (2014) Persistent HIV-1 replication is associated with lower antiretroviral drug concentrations in lymphatic tissues. *Proceedings of the National Academy of Sciences of the United States of America* **111**:2307-2312 https://doi.org/10.1073/pnas.1318249111 | PubMed

Florez-Alvarez L, Blanquiceth Y, Ramirez K, Ossa-Giraldo AC, Velilla PA, Hernandez JC, Zapata W (2020) NK cell activity and CD57+/NKG2Chigh phenotype are increased in men who have sex with men at high risk for HIV. *Frontiers in Immunology* **11**:537044 https://doi.org/10.3389/fimmu.2020.537044 | PubMed

Geller MA, Miller JS (2011) Use of allogeneic NK cells for cancer immunotherapy. *Immunotherapy* **3**:1445-1459 https://doi.org/10.2217/imt.11.131 | PubMed

Ghandakly E, Moudgil R, Holman K (2025) Cardiovascular disease in people living with HIV: risk assessment and management. *Cleveland Clinic Journal of Medicine* **92**:159-167 https://doi.org/10.3949/ccjm.92a.24055 | PubMed

Grier JT, Forbes LR, Monaco-Shawver L, Oshinsky J, Atkinson TP, Moody C, Pandey R, Campbell KS, Orange JS (2012) Human immunodeficiency-causing mutation defines CD16 in spontaneous NK cell cytotoxicity. *The Journal of Clinical Investigation* **122**:3769-3780 https://doi.org/10.1172/JCI64837 | PubMed

Herberman RB, Ortaldo JR (1981) Natural killer cells: their roles in defenses against disease. *Science* **214**:24-30 https://doi.org/10.1126/science.7025208 | PubMed

Hu PF, Hultin LE, Hultin P, Hausner MA, Hirji K, Jewett A, Bonavida B, Detels R, Giorgi JV (1995) Natural killer cell immunodeficiency in HIV disease is manifest by profoundly decreased numbers of CD16+CD56+ cells and expansion of a population of CD16dimCD56- cells with low lytic activity. *Journal of Acquired Immune Deficiency Syndromes and Human Retrovirology* **10**:331-340 https://doi.org/10.1097/00042560-199511000-00005 | PubMed

Ivison GT, Vendrame E, Martinez-Colon GJ, Ranganath T, Vergara R, Zhao NQ, Martin MP, Bendall SC, Carrington M, Cyktor JC, *et al.* (2022) Natural killer cell receptors and ligands are associated with markers of HIV-1 persistence in chronically infected ART suppressed patients. *Frontiers in Cellular and Infection Microbiology* **12**:757846 https://doi.org/10.3389/fcimb.2022.757846 | PubMed

Jacobs R, Hintzen G, Kemper A, Beul K, Kempf S, Behrens G, Sykora KW, Schmidt RE (2001) CD56bright cells differ in their KIR repertoire and cytotoxic features from CD56dim NK cells. *European Journal of Immunology* **31**:3121-3127 https://doi.org/10.1002/1521-4141(2001010)31:10<3121::aid-immu3121>3.0.co;2-4 | PubMed

Jost S, Altfeld M (2012) Evasion from NK cell-mediated immune responses by HIV-1. *Microbes and Infection* **14**:904-915 https://doi.org/10.1016/j.micinf.2012.05.001 | PubMed

Kim JT, Zhang TH, Carmona C, Lee B, Seet CS, Kostelny M, Shah N, Chen H, Farrell K, Soliman MSA, *et al.* (2022) Latency reversal plus natural killer cells diminish HIV reservoir in vivo. *Nature Communications* **13**:121 https://doi.org/10.1038/s41467-021-27647-0 | PubMed

Kim S, Poursine-Laurent J, Truscott SM, Lybarger L, Song YJ, Yang L, French AR, Sunwoo JB, Lemieux S, Hansen TH, *et al.* (2005) Licensing of natural killer cells by host major histocompatibility complex class I molecules. *Nature* **436**:709-713 https://doi.org/10.1038/nature03847 | PubMed

Lachota M, Zielniok K, Palacios D, Kanaya M, Penna L, Hoel HJ, Wiiger MT, Kveberg L, Hautz W, Zagozdzon R, *et al.* (2023) Mapping the chemotactic landscape in NK cells reveals subset-specific synergistic migratory responses to dual chemokine receptor ligation. *EBioMedicine* **96**:104811 https://doi.org/10.1016/j.ebiom.2023.104811 | PubMed

Lagathu C, Bereziat V, Gorwood J, Fellahi S, Bastard JP, Vigouroux C, Boccara F, Capeau J (2019) Metabolic complications affecting adipose tissue, lipid and glucose metabolism associated with HIV antiretroviral treatment. *Expert Opinion on Drug Safety* **18**:829-840 https://doi.org/10.1080/14740338.2019.1644317 | PubMed

Lajoie L, Congy-Jolivet N, Bolzec A, Gouilleux-Gruart V, Sicard E, Sung HC, Peiretti F, Moreau T, Vie H, Clemenceau B, *et al.* (2014) ADAM17-mediated shedding of FcgammaRIIIA on human NK cells: identification of the cleavage site and relationship with activation. *The Journal of Immunology* **192**:741-751 https://doi.org/10.4049/jimmunol.1301024 | PubMed

Lallemand C, Liang F, Staub F, Simansour M, Vallette B, Huang L, Ferrando-Miguel R, Tovey MG (2017) A novel system for the quantification of the ADCC activity of therapeutic antibodies. *Journal of Immunology Research* **2017**:3908289 https://doi.org/10.1155/2017/3908289 | PubMed

Lanier LL, Chang C, Azuma M, Ruitenberg JJ, Hemperly JJ, Phillips JH (1991) Molecular and functional analysis of human natural killer cell-associated neural cell adhesion molecule (N-CAM/CD56). *The Journal of Immunology* **146**:4421-4426 https://doi.org/10.4049/jimmunol.146.12.4421 | PubMed

Lanier LL, Le AM, Phillips JH, Warner NL, Babcock GF (1983) Subpopulations of human natural killer cells defined by expression of the Leu-7 (HNK-1) and Leu-11 (NK-15) antigens. *The Journal of Immunology* **131**:1789-1796 https://doi.org/10.4049/jimmunol.131.4.1789 | PubMed

Lanier LL, Yu G, Phillips JH (1991) Analysis of Fc gamma RIII (CD16) membrane expression and association with CD3 zeta and Fc epsilon RI-gamma by site-directed mutation. *The Journal of Immunology* **146**:1571-1576 https://doi.org/10.4049/jimmunol.146.5.1571 | PubMed

Li P, Katirai F, Zheng F, Gong F (2011) Recycling and reutilization of cytotoxic molecules, a new type of energy conservation of NK cells?. *Medical Hypotheses* **76**:293-295 https://doi.org/10.1016/j.mehy.2010.10.027 | PubMed

Lichtfuss GF, Cheng WJ, Farsakoglu Y, Paukovics G, Rajasuriar R, Velayudham P, Kramski M, Hearps AC, Cameron PU, Lewin SR, *et al.* (2012) Virologically suppressed HIV patients show activation of NK cells and persistent innate immune activation. *The Journal of Immunology* **189**:1491-1499 https://doi.org/10.4049/jimmunol.1200458 | PubMed

Liu D, Bryceson YT, Meckel T, Vasiliver-Shamis G, Dustin ML, Long EO (2009) Integrin-dependent organization and bidirectional vesicular traffic at cytotoxic immune synapses. *Immunity* **31**:99-109 https://doi.org/10.1016/j.immuni.2009.05.009 | PubMed

Lorenzen I, Lokau J, Korpys Y, Oldefest M, Flynn CM, Kunzel U, Garbers C, Freeman M, Grotzinger J, Dusterhoft S (2016) Control of ADAM17 activity by regulation of its cellular localisation. *Scientific Reports* **6**:35067 https://doi.org/10.1038/srep35067 | PubMed

Magombedze G, Vendrame E, SenGupta D, Geleziunas R, Little S, Smith D, Walker B, Routy JP, Hecht FM, Chun TW, *et al.* (2025) Early viral dynamics predict human immunodeficiency virus posttreatment control after analytic treatment interruption. *The Journal of Infectious Diseases* **231**:e419-e428 https://doi.org/10.1093/infdis/jiae551 | PubMed

Mandelboim O, Kent S, Davis DM, Wilson SB, Okazaki T, Jackson R, Hafler D, Strominger JL (1998) Natural killer activating receptors trigger interferon gamma secretion from T cells and natural killer cells. *Proceedings of the National Academy of Sciences of the United States of America* **95**:3798-3803 https://doi.org/10.1073/pnas.95.7.3798 | PubMed

Mavilio D, Benjamin J, Daucher M, Lombardo G, Kottilil S, Planta MA, Marcenaro E, Bottino C, Moretta L, Moretta A, *et al.* (2003) Natural killer cells in HIV-1 infection: dichotomous effects of viremia on inhibitory and activating receptors and their functional correlates. *Proceedings of the National Academy of Sciences of the United States of America* **100**:15011-15016 https://doi.org/10.1073/pnas.2336091100 | PubMed

Milburn J, Jones R, Levy JB (2017) Renal effects of novel antiretroviral drugs. *Nephrology Dialysis Transplantation* **32**:434-439 https://doi.org/10.1093/ndt/gfw064 | PubMed

Miller JS, Soignier Y, Panoskaltsis-Mortari A, McNearney SA, Yun GH, Fautsch SK, McKenna D, Le C, Defor TE, Burns LJ, *et al.* (2005) Successful adoptive transfer and in vivo expansion of human haploidentical NK cells in patients with cancer. *Blood* **105**:3051-3057 https://doi.org/10.1182/blood-2004-07-2974 | PubMed

Myers JA, Miller JS (2021) Exploring the NK cell platform for cancer immunotherapy. *Nature Reviews Clinical Oncology* **18**:85-100 https://doi.org/10.1038/s41571-020-0426-7 | PubMed

Nagler A, Lanier LL, Cwirla S, Phillips JH (1989) Comparative studies of human FcRIII-positive and negative natural killer cells. *The Journal of Immunology* **143**:3183-3191 https://doi.org/10.4049/jimmunol.143.10.3183 | PubMed

Niemann J, Claus M, Imsirovic V, Watzl C (2025) Repeated CD107a staining enables identification of serial degranulating NK cells. *European Journal of Immunology* **55**:e202451642 https://doi.org/10.1002/eji.202451642 | PubMed

North TW, Higgins J, Deere JD, Hayes TL, Villalobos A, Adamson L, Shacklett BL, Schinazi RF, Luciw PA (2010) Viral sanctuaries during highly active antiretroviral therapy in a nonhuman primate model for AIDS. *Journal of Virology* **84**:2913-2922 https://doi.org/10.1128/JVI.02356-09 | PubMed

O'Doherty U, Swiggard WJ, Malim MH (2000) Human immunodeficiency virus type 1 spinoculation enhances infection through virus binding. *Journal of Virology* **74**:10074-10080 https://doi.org/10.1128/jvi.74.21.10074-10080.2000 | PubMed

Olali AZ, Carpenter KA, Myers M, Sharma A, Yin MT, Al-Harthi L, Ross RD (2022) Bone quality in relation to HIV and antiretroviral drugs. *Current HIV/AIDS Reports* **19**:312-327 https://doi.org/10.1007/s11904-022-00613-1 | PubMed

Ortaldo JR, Oldham RK, Cannon GC, Herberman RB (1977) Specificity of natural cytotoxic reactivity of normal human lymphocytes against a myeloid leukemia cell line. *Journal of the National Cancer Institute* **59**:77-82 https://doi.org/10.1093/jnci/59.1.77 | PubMed

Perussia B, Trinchieri G, Jackson A, Warner NL, Faust J, Rumpold H, Kraft D, Lanier LL (1984) The Fc receptor for IgG on human natural killer cells: phenotypic, functional, and comparative studies with monoclonal antibodies. *The Journal of Immunology* **133**:180-189 https://doi.org/10.4049/jimmunol.133.1.180 | PubMed

Pohlmeyer CW, Gonzalez VD, Irrinki A, Ramirez RN, Li L, Mulato A, Murry JP, Arvey A, Hoh R, Deeks SG, *et al.* (2019) Identification of NK cell subpopulations that differentiate HIV-infected subject cohorts with diverse levels of virus control. *Journal of Virology* **93**:e01790-18 https://doi.org/10.1128/JVI.01790-18 | PubMed

Puertas MC, Bailon L, Urrea V, Garcia-Guerrero MC, Alarcon-Soto Y, Rivero A, Mothe B, Molto J, Martinez-Picado J, study group DUALITY (2025) Rapid clearance of inducible HIV-1 proviruses after initiation of antiretroviral therapy. *PLOS Pathogens* **21**:e1013466 https://doi.org/10.1371/journal.ppat.1013466 | PubMed

Qutub M, Premchandani T, Bhagat S, Tatode A, Taksande J, Umekar M, Hussain UM, Khan R (2026) CAR-NK cell therapy for overcoming antigen heterogeneity and immunosuppressive tumor microenvironments. *Human Immunology* **87**:111728 https://doi.org/10.1016/j.humimm.2026.111728 | PubMed

Rallon N, Jimenez-Carretero D, Restrepo C, Ligos JM, Valentin-Quiroga J, Mahillo I, Cabello A, Lopez-Collazo E, Sanchez-Cabo F, Gorgolas M, *et al.* (2024) A specific natural killer cells phenotypic signature associated to long term elite control of HIV infection. *Journal of Medical Virology* **96**:e29646 https://doi.org/10.1002/jmv.29646 | PubMed

Richard J, Sindhu S, Pham TN, Belzile JP, Cohen EA (2010) HIV-1 Vpr up-regulates expression of ligands for the activating NKG2D receptor and promotes NK cell-mediated killing. *Blood* **115**:1354-1363 https://doi.org/10.1182/blood-2009-08-237370 | PubMed

Romee R, Foley B, Lenvik T, Wang Y, Zhang B, Ankarlo D, Luo X, Cooley S, Verneris M, Walcheck B, *et al.* (2013) NK cell CD16 surface expression and function is regulated by a disintegrin and metalloprotease-17 (ADAM17). *Blood* **121**:3599-3608 https://doi.org/10.1182/blood-2012-04-425397 | PubMed

Romee R, Schneider SE, Leong JW, Chase JM, Keppel CR, Sullivan RP, Cooper MA, Fehniger TA (2012) Cytokine activation induces human memory-like NK cells. *Blood* **120**:4751-4760 https://doi.org/10.1182/blood-2012-04-419283 | PubMed

Sanchez-Gaona N, Gallego-Cortes A, Astorga-Gamaza A, Rallon N, Benito JM, Ruiz-Mateos E, Curran A, Burgos J, Navarro J, Suanzes P, *et al.* (2024) NKG2C and NKG2A coexpression defines a highly functional antiviral NK population in spontaneous HIV control. *JCI Insight* **9**:e182660 https://doi.org/10.1172/jci.insight.182660 | PubMed

Sarin PS, Goldstein AL (1995) Treatment of AIDS with drugs targeted to inhibit different stages of the HIV life cycle. *Immunopharmacology and Immunotoxicology* **17**:217-245 https://doi.org/10.3109/08923979509019748 | PubMed

Schwartz O, Marechal V, Le Gall S, Lemonnier F, Heard JM (1996) Endocytosis of major histocompatibility complex class I molecules is induced by the HIV-1 Nef protein. *Nature Medicine* **2**:338-342 https://doi.org/10.1038/nm0396-338 | PubMed

Shembrey C, Huntington ND, Hollande F (2019) Impact of tumor and immunological heterogeneity on the anti-cancer immune response. *Cancers* **11**:1217 https://doi.org/10.3390/cancers11091217 | PubMed

Siokis A, Robert PA, Demetriou P, Kvalvaag A, Valvo S, Mayya V, Dustin ML, Meyer-Hermann M (2021) Characterization of mechanisms positioning costimulatory complexes in immune synapses. *iScience* **24**:103100 https://doi.org/10.1016/j.isci.2021.103100 | PubMed

Srpan K, Ambrose A, Karampatzakis A, Saeed M, Cartwright ANR, Guldevall K, De Matos G, Onfelt B, Davis DM (2018) Shedding of CD16 disassembles the NK cell immune synapse and boosts serial engagement of target cells. *Journal of Cell Biology* **217**:3267-3283 https://doi.org/10.1083/jcb.201712085 | PubMed

Thompson CG, Gay CL, Kashuba ADM (2017) HIV persistence in gut-associated lymphoid tissues: pharmacological challenges and opportunities. *AIDS Research and Human Retroviruses* **33**:513-523 https://doi.org/10.1089/AID.2016.0253 | PubMed

Valipour B, Mohammadi SM, Abedelahi A, Charoudeh HN (2024) The inhibition of ADAM17 in cord blood stem cell-derived CD16+ NK cells to enhance their cytotoxicity against acute lymphoblastic leukemia cells. *Human Immunology* **85**:110769 https://doi.org/10.1016/j.humimm.2024.110769 | PubMed

Vanherberghen B, Olofsson PE, Forslund E, Sternberg-Simon M, Khorshidi MA, Pacouret S, Guldevall K, Enqvist M, Malmberg KJ, Mehr R, *et al.* (2013) Classification of human natural killer cells based on migration behavior and cytotoxic response. *Blood* **121**:1326-1334 https://doi.org/10.1182/blood-2012-06-439851 | PubMed

Vasiliver-Shamis G, Tuen M, Wu TW, Starr T, Cameron TO, Thomson R, Kaur G, Liu J, Visciano ML, Li H, *et al.* (2008) Human immunodeficiency virus type 1 envelope gp120 induces a stop signal and virological synapse formation in noninfected CD4+ T cells. *Journal of Virology* **82**:9445-9457 https://doi.org/10.1128/JVI.00835-08 | PubMed

Vos AG, Venter WDF (2021) Cardiovascular toxicity of contemporary antiretroviral therapy. *Current Opinion in HIV and AIDS* **16**:286-291 https://doi.org/10.1097/COH.0000000000000702 | PubMed

Ward J, Bonaparte M, Sacks J, Guterman J, Fogli M, Mavilio D, Barker E (2007) HIV modulates the expression of ligands important in triggering natural killer cell cytotoxic responses on infected primary T-cell blasts. *Blood* **110**:1207-1214 https://doi.org/10.1182/blood-2006-06-028175

Ward J, Davis Z, DeHart J, Zimmerman E, Bosque A, Brunetta E, Mavilio D, Planelles V, Barker E (2009) HIV-1 Vpr triggers natural killer cell-mediated lysis of infected cells through activation of the ATR-mediated DNA damage response. *PLOS Pathogens* **5**:e1000613 https://doi.org/10.1371/journal.ppat.1000613 | PubMed

Yang C, Siebert JR, Burns R, Gerbec ZJ, Bonacci B, Rymaszewski A, Rau M, Riese MJ, Rao S, Carlson KS, *et al.* (2019) Heterogeneity of human bone marrow and blood natural killer cells defined by single-cell transcriptome. *Nature Communications* **10**:3931 https://doi.org/10.1038/s41467-019-11947-7 | PubMed

Zambarda C, Guldevall K, Breunig C, Toullec D, Sandoz PA, Carannante V, Xu S, Ross P, Kuhnigk K, Sandstrom N, *et al.* (2025) CD16A shedding regulates innate cell engager-induced serial killing by natural killer cells. *European Journal of Immunology* **55**:e70078 https://doi.org/10.1002/eji.70078 | PubMed

Peer reviews

Reviewer #1 (Public review):

Howell et al investigate the functional capacities of CD16dim CD56dim NK cells, including their activity against HIV-1-infected T cells. The authors provide an extensive characterization of the functional activity of different NK cell subsets derived from peripheral blood. CD16 is an important receptor expressed on NK cells, and previous studies have demonstrated that CD16 expression changes depending on the activation status of NK cells - one important regulator of CD16 expression is proteolytic shedding/cleavage of CD16 on activated NK cells by the metalloprotease ADAM17. In vitro activation of NK cells, for

example in response to K562 cells or other target cells, results in a rapid downregulation of the expression of CD16 on the surface of NK cells, unless an ADAM17 inhibitor is added. This is an important point to consider in the interpretation of the presented results. Overall, the manuscript includes many data in nine figures plus supplemental figures, and would benefit from some focusing of the results.

(1) Figure 1

The observation that CD16dim NK cells responded more strongly by degranulation to K562 cells and HIV-1-infected cells could be due to the shedding of CD16 following activation. In other words, more strongly activated NK cells express higher levels of CD107 but also shed CD16, resulting in higher CD107 expression in CD16low NK cells. The authors should investigate this, for example by performing the degranulation assays shown in Figure 1 in the presence and absence of an ADAM17 inhibitor.

(2) Figure 2

The authors sorted CD16dim and bright NK cells for these experiments and observed higher lysis of HIV-1-infected CD4+ T cells. Important controls should be included in these experiments - how strong was the lysis of HIV-1-uninfected CD4+ T cells by these different NK cell subsets? It also appears that the results shown were derived using NK cells from one donor, and "representative of two independent sort experiments performed with separate donors, each yielding similar results". Why are the authors now showing the respective data? One or two experiments appear too few to come to these conclusions. To support the broad conclusions drawn by the reviewers, the experiments should be performed in a larger number of individuals.

(3) Figure 3

It appears that experiments were performed again using bulk NK cell populations, and superior degranulation and killing frequencies by CD16dim NK cells might reflect different levels of activation again, as described above for Figure 1. The same applies to Figure 4 - lower degranulation events in CD16bright NK cells are consistent with lower activation of these cells, resulting in less CD16 downregulation. Also, it is not clear to the reviewer why CD107a expression and killing frequencies decrease with higher effector-to-target ratios (Figure 3).

(4) Pages 19-25

It would be helpful if the authors could provide some conclusions regarding their findings - it is very difficult for the reader to follow the many reported frequencies and p-values. What does this actually mean? Overall, the results appear to follow prior observations that licensed (KIR3DL+) NK cells respond more strongly than unlicensed (KIR3DL1neg) NK cells. The consistent observation within these different subanalyses that CD16dim NK cells degranulate more than CD16bright NK cells is probably the result of activation-induced CD16 downregulation in these assays, as mentioned above. Providing two-way ANOVA analysis results for these very many observations would furthermore require, in the opinion of the reviewer, adjustments for multiple comparisons.

(5) Figures 5 and 6

These figures demonstrate that NK cell-mediated activation by HIV-1-infected cells depends on NKG2D ligands and can be inhibited by blocking this interaction - this is consistent with data presented by the Barker group and others previously, and does not provide new information.

(6) Figure 7

The authors extended their functional analyses of NK cells to ADCC function. It is very well established that CD16 is downregulated in the context of ADCC following activation of NK cells. Consistent with this, higher degranulation is observed by CD16dim NK cells.

(7) The data using ADAM17 inhibition in the final figures of the manuscript

These data are of interest, but should be presented in a more structured way. First of all, does the addition of ADAM17 inhibitors change the overall proportion of CD16bright and dim NK cells following activation, independent of whether these cells degranulate or not? Overall, the proportion of CD16dim NK cells that degranulate appears to be reduced in the presence of the ADAM inhibitor, which is consistent with reduced CD16 shedding and maintenance of CD16 expression on activated NK cells - and this is supported by the increase in CD107a-positive NK cells that express CD16 (Figure 8a). Overall, the differences between CD16bright and dim NK cells in their level of activation appear to disappear in the presence of an ADAM17 inhibitor, based on the data shown in Figure 8b, suggesting that CD16 downregulation is occurring in response to activation of NK cells as a consequence of CD16 shedding, and can be inhibited by an ADAM17 inhibitor.

Taken together, many of the data presented in the manuscript are consistent with the very well-established downregulation of CD16 expression on activated NK cells, suggesting that the observed association between reduced CD16 expression on CD56dim NK cells and enhanced effector functions is a consequence of higher activation of these NK cells.

https://doi.org/10.7554/eLife.112322.1.sa2

Reviewer #2 (Public review):

Summary:

This study investigates the cytotoxic activity of human NK-cell subsets against autologous HIV-1-infected CD4 T cells and identifies CD56dimCD16dim NK cells as the dominant effector population. The authors propose that this subset possesses superior cytotoxic activity compared with CD56dimCD16bright NK cells and could therefore represent an attractive target for HIV cure strategies. While the study addresses an important and clinically relevant question, several of its major conclusions rely on assumptions that are not adequately supported by the experimental design. In particular, CD16 is treated as a stable phenotypic marker throughout most of the study despite its well-established and rapid downregulation following NK cell activation.

Strengths:

(1) The study addresses an important and clinically relevant question regarding which NK cell subset is responsible for the elimination of autologous HIV-1-infected cells. To the best of my knowledge, this is the first study directly comparing the anti-HIV functional activities of CD56dimCD16dim vs CD56dimCD16bright NK cells.

(2) The experiments performed with purified NK cell subset (Figure 2) provide some evidence that CD56dimCD16dim NK cells possess enhanced cytotoxic activity relative to CD56dimCD16bright NK cells. This experimental approach is considerably more convincing than the analyses performed on mixed NK cell populations and should be expanded throughout the study.

Weaknesses:

(1) The central conclusion is weakened by the use of CD16 as a stable phenotypic marker. CD16 is well established to be rapidly downregulated following NK-cell activation and target cell (K562 or infected cells) engagement through ADAM17-mediated shedding. NK cell

shedding regulates NK cell effector functions by promoting target cell detachment, boosting serial killing capacity, and preventing overstimulation. Therefore, NK cells displaying a CD56dimCD16dim phenotype after co-culture cannot be assumed to represent a pre-existing subset with intrinsically superior cytotoxic activity, but may instead correspond to activated CD56dimCD16bright NK cells that have downregulated CD16 during the assay. Because the vast majority of the functional experiments classified NK cell subsets based on post-assay CD16 expression, it is difficult to distinguish intrinsic functional differences between NK cell subsets from activation-induced phenotypic conversion. This limitation affects the interpretation of most of the study's principal findings.

(2) The "killing frequency" analysis presented in Figure 3 is based on a mathematical estimate rather than a direct experimental measurement. Since total target cell killing is measured in mixed NK cell populations, it cannot be attributed to individual NK cell subsets. This experiment must be repeated using purified NK cell subsets.

(3) The serial degranulation assay presented in Figure 4 does not directly measure serial target cell killing and therefore does not support the conclusion that CD56dimCD16dim NK cells possess superior serial killing capacity. Furthermore, the increased serial degranulation observed in the CD16dim population could simply reflect activation-induced CD16 downregulation rather than an intrinsic property of this subset. This experiment should therefore be repeated using purified NK cell subsets.

(4) The finding that CD56dimCD16dim NK cells exhibit greater ADCC activity is somewhat counterintuitive given the central role of CD16 in mediating ADCC. Moreover, these experiments are likely confounded by activation-induced CD16 downregulation, which is expected to be even more pronounced during ADCC. Thus, the apparent superiority of the CD56dimCD16dim subset may simply reflect the conversion of activated CD56dimCD16bright NK cells into the CD16dim gate rather than intrinsically greater ADCC activity. To directly compare the intrinsic ADCC capacity of each subset, these experiments should be repeated using purified NK cell populations prior to target-cell stimulation.

https://doi.org/10.7554/eLife.112322.1.sa1

Author response:

We thank the editors and all three reviewers for their careful and constructive evaluation of our manuscript. We recognize that a single concern, the possibility that cells classified as $CD56^{dim}CD16^{dim}$ after co-culture represent activated $CD56^{dim}CD16^{bright}$ cells that have shed CD16 rather than a pre-existing subset, underlies the majority of the comments. We therefore address this concern first, in a central response, and then respond to each reviewer and editor comment in turn. Where a comment relates to this shared concern, we point to the central response rather than repeating the argument.

The analytical and presentational revisions described below are complete: the statistical analyses have been re-run with corrections for multiple comparisons, the Discussion has been rewritten, the figures and supplemental tables have been renumbered and corrected, and existing data on pre-stimulation receptor expression and NKp30 have been incorporated. These will appear in the revised manuscript. The new experiments described will be completed within approximately six to eight weeks and provided with the revised manuscript.

Central are $CD56^{dim}CD16^{dim}$ cells a pre-existing subset, or activated $CD56^{dim}CD16^{bright}$ cells that have shed CD16?

We agree with the premise that CD16 is rapidly shed by ADAM17 upon activation, and that classifying subsets by post-assay CD16 expression alone cannot, on its own, distinguish a pre-

existing subset from activation-induced conversion. For this reason, our conclusion does not rest on post-assay classification. The evidence below, from experiments already in the manuscript, argues against activation-induced conversion, and we will strengthen it with the expanded sorted-subset experiments described at the end.

Cells sorted before target exposure establish the advantage independently of any during-assay shedding (Fig. 2, unchanged in the revised manuscript).

The most direct evidence comes from subsets purified before the assay. In Fig. 2, NK cells were sorted into $CD56^{dim}CD16^{dim}$ and $CD56^{dim}CD16^{bright}$ populations before any exposure to target cells, and their cytolytic function was measured as specific lysis of autologous HIV-infected T cells. Purified $CD16^{dim}$ cells lysed infected targets approximately twice as efficiently as purified $CD16^{bright}$ cells across the effector-to-target range, reaching 77.58% versus 39.18% at 1:1. The difference was significant at 1:4 ($p = 0.0008$), 1:2 and 1:1 (both $p < 0.0001$); at the lowest ratio tested, 1:8, specific lysis was low in both subsets and the difference did not reach significance ($p = 0.2121$; Supplemental Table 4). The additional donors described below will allow this comparison to be made across a larger data set, including at the lowest ratios where specific lysis is low in both subsets.

Because the subsets are defined by sorting before target contact, and because the readout is direct target lysis rather than post-assay CD16 gating, this advantage cannot arise from activation-induced CD16 shedding during the assay. Public reviewer 2 and the peer reviewer both identified this experiment as the strongest evidence in the manuscript. Its interpretation is secure; what it requires is additional donors for statistical robustness, which we provide in the planned expansion below.

The two subsets respond to ADAM17 inhibition in opposite directions (Figs. 7 and 9, now Figures 6 and 8).

If $CD56^{dim}CD16^{dim}$ cells were simply $CD56^{dim}CD16^{bright}$ cells that had shed CD16, the two would be one population sampled at different points along a shedding continuum, and inhibiting ADAM17 would move them in the same direction. Instead, ADAM17 inhibition moves them in opposite directions. In the antibody-dependent degranulation assay (Fig. 7B, now Figure 6B), ADAM17 inhibition increased $CD56^{dim}CD16^{bright}$ degranulation but decreased $CD56^{dim}CD16^{dim}$ degranulation across VRC01 concentrations. The same opposition is seen when serial degranulation is resolved by the number of degranulation events per cell (Fig. 9, now Figure 8): ADAM17 inhibition increased multiple degranulation events in $CD56^{dim}CD16^{bright}$ cells, with cells undergoing three events rising from 0.79% to 5.12%, while in $CD56^{dim}CD16^{dim}$ cells it reduced them, with three events falling from 15.16% to 2.24% and the non-degranulating fraction rising from 61.56% to 92.13%.

A single population would not be expected to respond to the same perturbation in opposite directions, and these observations are difficult to reconcile with the $CD16^{dim}$ cells being activated $CD16^{bright}$ cells; rather, they point to two functionally distinct subsets with opposite dependence on ADAM17 activity. This is consistent with our model, in which $CD16^{dim}$ cells use ADAM17-mediated shedding to detach and serially re-engage, whereas $CD16^{bright}$ cells are hindered by the loss of CD16.

The $CD16^{dim}$ degranulation advantage is driven by NKG2D through a mechanism separable from ADAM17 (Fig. 8, now Figure 7).

The change in subset frequency on exposure to VRC01-treated infected cells (Fig. 8B, now Figure 7B) is abolished by anti-NKG2D even though VRC01 and ADAM17 remain present, indicating that this frequency shift is driven by NKG2D-dependent activation rather than by antibody-CD16 engagement alone.

The degranulation data in Fig. 8A (now Figure 7A) show that the two perturbations act differently in the two subsets. In $CD56^{dim}CD16^{dim}$ cells, both reduce the response, and the combination reduces it further than either alone: from 12.60% under vehicle to 5.24% with anti-NKG2D ($p < 0.0001$), 5.05% with ADAM17 inhibition ($p < 0.0001$), and 2.03% with both ($p < 0.0001$ versus vehicle; $p < 0.0001$ versus anti-NKG2D alone; $p = 0.0001$ versus ADAM17 inhibition alone). If anti-NKG2D acted only by removing the activation trigger for ADAM17, that is, if NKG2D and ADAM17 lay on a single linear pathway, blocking the pathway at two points would not be expected to add to the effect of either alone. The further reduction therefore indicates that NKG2D and ADAM17 contribute through separable mechanisms.

In $CD56^{dim}CD16^{bright}$ cells the two perturbations act in opposite directions. Anti-NKG2D reduced degranulation from 2.58% to 0.92% ($p = 0.0263$), whereas ADAM17 inhibition increased it to 3.99% ($p = 0.0679$). NKG2D therefore supports the response of $CD56^{dim}CD16^{bright}$ cells while ADAM17 activity constrains it, the reverse of the pattern in $CD56^{dim}CD16^{dim}$ cells, where ADAM17 activity is required. Two populations differing only in the extent to which they have shed CD16 would not be expected to respond to the same two perturbations in opposite ways.

Supporting evidence: pre-sorted subsets are stable and differ before stimulation.

Two further observations support a pre-existing subset. First, we have directly tracked the fate of each subset sorted before target exposure. NK cells were sorted into $CD16^{bright}$ and $CD16^{dim}$ subsets, exposed to HIV-infected cells for one hour, and reanalyzed for CD16 expression. One hour is the point at which we observe the highest frequency of degranulating cells in both subsets (Figure 3—Figure Supplement 1A in the revised manuscript), and therefore the point at which activation-induced shedding would be most likely to be detected. Sorted $CD16^{bright}$ cells remained predominantly $CD16^{bright}$ (approximately 62%); of those that lost CD16, most became $CD16^{negative}$ (approximately 35%) rather than $CD16^{dim}$ (approximately 4%). Sorted $CD16^{dim}$ cells likewise shifted predominantly to a $CD16^{negative}$ phenotype (approximately 75%). Activation-induced CD16 shedding therefore directs cells of both subsets toward the $CD16^{negative}$ gate rather than generating the $CD16^{dim}$ population from $CD16^{bright}$ cells. These data are presented in Author response image 1.

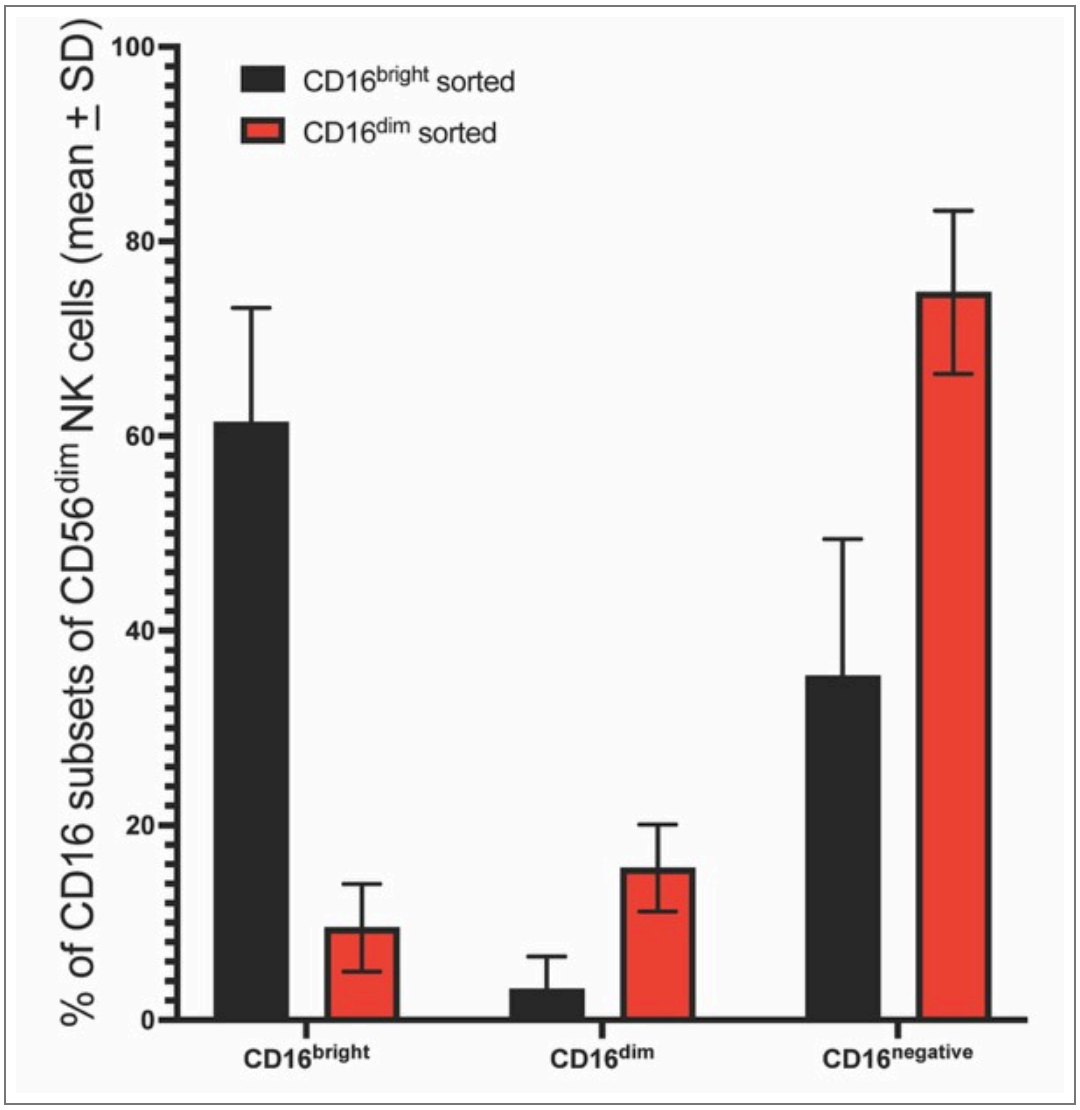

Author response image 1.

Phenotype of sorted $CD56^{dim}CD16^{bright}$ and $CD56^{dim}CD16^{dim}$ NK cells after exposure to HIV-infected T-cells. NK cells were sorted into $CD56^{dim}CD16^{bright}$ and $CD56^{dim}CD16^{dim}$ subsets, exposed to purified autologous productively HIV-1^{SHM-1}-infected T cells for 1 hour at a 1:1 effector-to-target cell ratio, and reanalyzed for CD16 expression. Bars show the percentage of each sorted NK cell population ($CD56^{dim}CD16^{bright}$ and $CD56^{dim}CD16^{dim}$) falling into the $CD16^{bright}$, $CD16^{dim}$, and $CD16^{negative}$ gates after exposure, as the mean ± standard deviation (SD) of three replicates. One hour is when the highest frequency of degranulating cells is observed in both subsets.

Second, the subsets differ before any stimulation. $CD56^{dim}CD16^{dim}$ cells express higher NKG2D than $CD56^{dim}CD16^{bright}$ cells before any target-cell contact. In the no-target condition, NKG2D was 1182 gMFI higher on $CD56^{dim}CD16^{dim}$ cells ($p < 0.0001$), a difference of approximately 1.6-fold; across all conditions tested the subset means were 2521.5 versus 1772.2 gMFI, or 1.42-fold (two-way ANOVA: subset $F(1, 20) = 1897$, $p < 0.0001$, 70.97% of the total variation; Fig. 6, now Figure 5; Supplemental Table 18). This difference is specific to NKG2D: NKp46, measured on the same cells in the same wells, did not differ between the subsets in the no-target condition (mean difference 45.67 gMFI, $p = 0.0668$), and was higher on $CD56^{dim}CD16^{bright}$ cells when targets were present. The subsets therefore differ in NKG2D density before activation, and not in activating receptor density generally.

Planned strengthening.

To place this beyond doubt, we will expand the sorted-subset experiments, performing the specific-lysis assay (Fig. 2) and the antibody-dependent degranulation assay on subsets purified before target exposure across additional donors, together with uninfected-target controls. If cell yields from the sort permit, we will also perform the serial degranulation assay on sorted subsets; because the $CD56^{dim}CD16^{dim}$ subset constitutes fewer than 5% of $CD56^{dim}$ NK cells and the serial degranulation assay requires four sequential labelling and washing steps, we cannot commit to this in advance of the sort. These experiments require sorting and primary-cell work and will be completed within approximately six to eight weeks and provided with the revised manuscript.

We note that performing every functional assay in this study on sorted subsets is not feasible within the scope of this revision. Sorting the $CD56^{dim}CD16^{dim}$ subset, which constitutes fewer than 5% of $CD56^{dim}$ NK cells, from a sufficient number of donors to repeat the full panel of assays would require resources beyond those currently available to us. We have therefore prioritized the specific-lysis and antibody-dependent degranulation assays, which bear most directly on the concern raised by the reviewers and the editor, and will extend the approach to the remaining assays as resources allow.

> ***Public Reviews:***
>
> ***Reviewer #1 (Public review):***
>
> *Overall organization*
>
> *Overall, the manuscript includes many data in nine figures plus supplemental figures, and would benefit from some focusing of the results.*

We agree, and we have reduced the main figures from nine to eight. The NKG2D ligand histograms, previously Figure 5A, have been removed for the reason given in our response to the peer reviewer, Recommendation 4. The degranulation against wild-type and ΔVpr-infected targets, previously Figure 5B, and the degranulation and killing frequency measurements in mixed populations, previously Figure 3, have been moved to the supplementary material. The inhibitory receptor analyses have been reduced from approximately 1,800 words and more than 80 reported p-values to approximately 700 words and 24, with the detail retained in the supplemental tables. Each Results section now opens with a statement of the principal finding before the supporting data, and the Discussion synthesizes what the findings mean rather than restating them.

> *Figure 1 and Figure 1—figure supplement 2*
>
> *The observation that CD16dim NK cells responded more strongly by degranulation to K562 cells and HIV-1-infected cells could be due to the shedding of CD16 following activation. In other words, more strongly activated NK cells express higher levels of CD107 but also shed CD16, resulting in higher CD107 expression in CD16low NK cells. The authors should investigate this, for example by performing the degranulation assays shown in Figure 1 in the presence and absence of an ADAM17 inhibitor.*

We thank the reviewer for raising this important point, which we recognize is shared by all three reviewers and the editors, and which we address in full in the central response above. We note for clarity that the K562 data are not in Figure 1; they are presented in Figure 1—figure supplement 2, both in the reviewed preprint and in the revised manuscript. They were included to reproduce a previously established finding (Amand et al., Front Immunol 2017;8:699), and were not intended as a central experimental claim; the mechanistic focus of this study is the response to HIV-infected cells. Notably, that same study addressed the

question by sorting the CD56^{dim} subsets before stimulation rather than gating after, and our study applies the same approach and extends it to the HIV-infected setting. Four lines of evidence argue against the interpretation that CD16^{dim} degranulation reflects activation-induced CD16 shedding of CD16^{bright} cells:

(1) In cells sorted before target exposure, purified CD16^{dim} cells lyse HIV-infected targets approximately twice as efficiently as purified CD16^{bright} cells across the effector-to-target range, significantly so at 1:4 and above (Fig. 2; Supplemental Table 4); because the subsets are defined before any activation and the readout is direct target lysis rather than post-assay CD16 gating, this advantage cannot arise from shedding during the assay.

(2) The two subsets respond to ADAM17 inhibition in opposite directions, both in the magnitude of degranulation (Fig. 7B, now Figure 6B) and in the number of serial degranulation events per cell (Fig. 9, now Figure 8): ADAM17 inhibition increased degranulation in CD16^{bright} cells but decreased it in CD16^{dim} cells.

(3) Blocking NKG2D together with ADAM17 reduced CD16^{dim} degranulation below either treatment alone (Fig. 8A, now Figure 7A), indicating that the CD16^{dim} advantage is driven by NKG2D through a mechanism separable from ADAM17-mediated shedding.

(4) The subsets also differ before any stimulation, with NKG2D 1182 gMFI higher on CD16^{dim} cells in the no-target condition ($p < 0.0001$) and no corresponding difference in NKp46 under the same condition (Fig. 6, now Figure 5).

We will further strengthen these findings by expanding the sorted-subset experiments across additional donors, as described in the central response.

> *Figure 2*
>
> *The authors sorted CD16dim and bright NK cells for these experiments and observed higher lysis of HIV-1-infected CD4+ T cells. Important controls should be included in these experiments - how strong was the lysis of HIV-1-uninfected CD4+ T cells by these different NK cell subsets? It also appears that the results shown were derived using NK cells from one donor, and "representative of two independent sort experiments performed with separate donors, each yielding similar results". Why are the authors now showing the respective data? One or two experiments appear too few to come to these conclusions. To support the broad conclusions drawn by the reviewers, the experiments should be performed in a larger number of individuals.*

We thank the reviewer for these constructive points.

(1) Uninfected-target control. We agree this is an important control and will include lysis of uninfected autologous CD4 T cells by the sorted CD16^{dim} and CD16^{bright} subsets in Figure 2, confirming that the observed lysis is specific to HIV-infected targets. We note that the corresponding CD107a degranulation controls against uninfected targets are presented in Figure 1—Figure Supplement 4C of the revised manuscript.

(2) Number of donors and presentation of data. We agree that the conclusions require more than the representative donor shown. As described in the central response, we will expand these sorted-subset experiments to a larger number of individuals and will present the data from all donors rather than a single representative experiment. Because they require cell sorting and primary-cell work, these experiments will be completed within approximately six to eight weeks and provided with the revised manuscript.

> *Figures 3 and 4*
>
> *It appears that experiments were performed again using bulk NK cell populations, and superior degranulation and killing frequencies by CD16dim NK cells might reflect*

> *different levels of activation again, as described above for Figure 1. The same applies to Figure 4 - lower degranulation events in CD16bright NK cells are consistent with lower activation of these cells, resulting in less CD16 downregulation. Also, it is not clear to the reviewer why CD107a expression and killing frequencies decrease with higher effector-to-target ratios (Figure 3).*

(1) Activation-induced shedding in bulk experiments (Figs. 3 and 4, now Figure 2—figure supplement 1 and Figure 3). We agree that these figures use bulk NK cell populations gated by CD16, and we address the underlying shedding concern in full in the central response. The concern that the lower serial degranulation of $CD16^{bright}$ cells in the direct-killing assay simply reflects lower activation and therefore less shedding is addressed directly by our ADAM17-inhibition data. At 0 μg/mL VRC01, that is, in the absence of antibody, ADAM17 inhibition already affects the two subsets differently rather than in the same direction (Figs. 7B and 7C, now Figures 6B and 6C), as would be expected if they were one population differing only in activation level. This differential response is also seen across the antibody-dependent conditions in Figs. 7B and 9 (now Figures 6B and 8). As described in the central response, we will additionally repeat the specific-lysis and antibody-dependent degranulation measurements on subsets purified before target exposure across additional donors, and the serial degranulation assay as well if cell yields from the sort permit.

(2) Decrease in CD107a and killing frequency at higher effector-to-target ratios (Fig. 3, now Figure 2—figure supplement 1). This reflects the nature of the readout. CD107a mobilization is measured per effector cell, as the percentage of NK cells that degranulate, and is therefore maximized when targets are in excess. At low effector-to-target ratios, nearly every NK cell can encounter and engage a target, yielding a high percentage of CD107a-positive cells; at high ratios, targets become limiting, so a large fraction of NK cells never contact a target and remain unstimulated, and the rapid destruction of the limited target pool further reduces the stimulus available to the remaining cells. This lowers the measured per-effector degranulation frequency even as the absolute number of targets killed is maintained, and it is distinct from a lysis assay, which measures the fate of the target population and accordingly rises with increasing effector-to-target ratio. The same per-effector readout behavior applies to the degranulation data shown in Figs. 5C and 6C (now Figures 4A and 4B, and Figure 5C). This explanation has been added to the revised Discussion.

> *Pages 19-25*
>
> *It would be helpful if the authors could provide some conclusions regarding their findings - it is very difficult for the reader to follow the many reported frequencies and p-values. What does this actually mean? Overall, the results appear to follow prior observations that licensed (KIR3DL+) NK cells respond more strongly than unlicensed (KIR3DL1neg) NK cells. The consistent observation within these different subanalyses that CD16dim NK cells degranulate more than CD16bright NK cells is probably the result of activation-induced CD16 downregulation in these assays, as mentioned above. Providing two-way ANOVA analysis results for these very many observations would furthermore require, in the opinion of the reviewer, adjustments for multiple comparisons.*

We thank the reviewer, and we have addressed this in three ways.

(1) Readability. We agree that these sections were difficult to follow as presented. We have rewritten them, opening each with a statement of the principal finding before the supporting statistics, and reducing the inhibitory receptor section from approximately 1,800 words and more than 80 reported p-values to approximately 700 words and 24, with the detail retained in the supplemental tables. The Discussion now synthesizes what the findings mean.

(2) $CD16^{dim}$ degranulation in these subanalyses. The consistent observation that $CD16^{dim}$ cells degranulate more than $CD16^{bright}$ cells across these subanalyses is addressed in full in

the central response, where several lines of evidence, including subsets sorted before target exposure (Fig. 2) and the opposite responses of the two subsets to ADAM17 inhibition (Figs. 7B and 9, now Figures 6B and 8), argue against activation-induced CD16 downregulation as the explanation.

(3) Multiple comparisons. We agree, and we have re-analyzed these comparisons, applying the post-hoc test matched to each comparison structure: Dunnett's where every subset is compared against a single designated subset, Tukey's where all pairwise comparisons are of interest, and Šidák's where a prespecified subset of comparisons is of interest. Adjusted p-values are reported throughout, and the design and post-hoc test used for each figure and panel are given in a new supplemental table. The streamlining described above has also reduced the number of comparisons reported in the main text.

> *Figures 5 and 6*
>
> *These figures demonstrate that NK cell-mediated activation by HIV-1-infected cells depends on NKG2D ligands and can be inhibited by blocking this interaction - this is consistent with data presented by the Barker group and others previously, and does not provide new information.*

We agree that the dependence of NK-cell recognition of HIV-infected cells on NKG2D and its ligands is established, including in our own earlier work (Ward et al., PLoS Pathog 2009;5(10):e1000613) and by others, and we do not present that dependence as a novel finding.

On review, the histograms in Figure 5A were reproduced from that earlier study and should not have been included without attribution. We have removed that panel and cited the original finding in its place. Figures 5B and 5C are both new results from this study, and both are retained. Figure 5B, which shows that NK cells degranulate in response to wild-type HIV-infected targets but not to ΔVpr-infected or uninfected targets, establishing that the degranulation response in this system depends on Vpr, becomes Figure 4—figure supplement 1 in the revised manuscript. Figure 5C, the NKG2D blockade experiment, becomes Figure 4A and 4B.

We would also distinguish Figure 6 (now Figure 5), which we consider a substantive finding rather than a restatement of the established NKG2D-ligand dependence. That figure shows that NKG2D expression differs at the level of the individual subsets, and that the difference is present before stimulation and is specific to NKG2D. In the no-target condition, NKG2D was 1182 gMFI higher on $CD56^{dim}CD16^{dim}$ cells ($p < 0.0001$), approximately 1.6-fold, while NKp46 measured on the same cells in the same wells did not differ (mean difference 45.67 gMFI, $p = 0.0668$). This provides a candidate mechanism for the superior effector function of the $CD56^{dim}CD16^{dim}$ subset, in addition to their serial-degranulation capacity, and it bears directly on the central question of whether the two subsets differ intrinsically rather than as a consequence of activation. The revised text presents the established NKG2D-ligand dependence as context while making the subset-level NKG2D difference, and its mechanistic significance, more prominent.

> *Figure 7*
>
> *The authors extended their functional analyses of NK cells to ADCC function. It is very well established that CD16 is downregulated in the context of ADCC following activation of NK cells. Consistent with this, higher degranulation is observed by CD16dim NK cells.*

We agree that CD16 is downregulated during antibody-dependent responses, and this is precisely why we included the ADAM17-inhibition experiments within Figure 7 (now Figure 6), to determine whether the higher degranulation of $CD56^{dim}CD16^{dim}$ cells is a consequence of that shedding or a property of a distinct subset. As detailed in the central response, these

experiments argue against the shedding interpretation. In Fig. 7B (now Figure 6B), inhibiting ADAM17 affects the two subsets in opposite directions: it increases the degranulation of $CD56^{dim}CD16^{bright}$ cells while decreasing that of $CD56^{dim}CD16^{dim}$ cells. If the $CD16^{dim}$ cells were simply $CD16^{bright}$ cells that had shed CD16, blocking shedding would be expected to move the two in the same direction; the opposite responses instead indicate two distinct populations with opposite functional dependence on ADAM17 activity. The same opposition is seen when serial degranulation is resolved by the number of events per cell (Fig. 9, now Figure 8). Thus, while CD16 downregulation during antibody-dependent responses is well established, these data indicate that the superior response of the $CD56^{dim}CD16^{dim}$ subset is not explained by it. This interpretation is now explicit in the revised Discussion.

> *ADAM17-inhibition data (final figures)*
>
> *These data are of interest, but should be presented in a more structured way. First of all, does the addition of ADAM17 inhibitors change the overall proportion of CD16bright and dim NK cells following activation, independent of whether these cells degranulate or not? Overall, the proportion of CD16dim NK cells that degranulate appears to be reduced in the presence of the ADAM inhibitor, which is consistent with reduced CD16 shedding and maintenance of CD16 expression on activated NK cells - and this is supported by the increase in CD107a-positive NK cells that express CD16 (Figure 8a). Overall, the differences between CD16bright and dim NK cells in their level of activation appear to disappear in the presence of an ADAM17 inhibitor, based on the data shown in Figure 8b, suggesting that CD16 downregulation is occurring in response to activation of NK cells as a consequence of CD16 shedding, and can be inhibited by an ADAM17 inhibitor.*

We thank the reviewer for these suggestions, which we have used to present the ADAM17-inhibition data more clearly.

(1) Effect on subset proportions, independent of degranulation. This is shown in Fig. 8B (now Figure 7B). Because the two subsets differ greatly in baseline frequency, with $CD56^{dim}CD16^{bright}$ cells constituting the large majority of $CD56^{dim}$ NK cells before stimulation, a change in raw bulk proportion is small and difficult to interpret, for example a shift from roughly 95% to 92.5% of the bright population. To place the two subsets on comparable footing, the panel reports, for each subset, the frequency following target exposure minus its frequency in the matched unstimulated condition. Presented this way, ADAM17 inhibition clearly reduces the activation-associated change in subset proportions, consistent with reduced CD16 shedding. This normalization is stated in the legend and is now described in the Results text so that the analysis is not overlooked.

(2) Interpretation of the ADAM17-inhibition data. We agree that CD16 downregulation occurs as a consequence of activation-induced shedding and is prevented by ADAM17 inhibition; this is not in dispute. We would, however, offer an additional observation that bears on whether the between-subset functional difference is itself a product of that shedding. In Fig. 8A (now Figure 7A), combining ADAM17 inhibition with NKG2D blockade reduces $CD56^{dim}CD16^{dim}$ degranulation to 2.03%, below both anti-NKG2D alone at 5.24% and ADAM17 inhibition alone at 5.05% ($p < 0.0001$ and $p = 0.0001$ respectively). If the $CD16^{dim}$ advantage were solely a consequence of CD16 shedding, and if NKG2D blockade acted only by reducing that shedding, the combination could not reduce degranulation further than ADAM17 inhibition alone.

The same figure also shows that the two perturbations act in opposite directions within the $CD56^{dim}CD16^{bright}$ subset: anti-NKG2D reduced their degranulation from 2.58% to 0.92% ($p = 0.0263$), whereas ADAM17 inhibition increased it to 3.99% ($p = 0.0679$). NKG2D therefore supports the response of $CD56^{dim}CD16^{bright}$ cells while ADAM17 activity constrains it, the reverse of the pattern in $CD56^{dim}CD16^{dim}$ cells. Together with the opposite responses of the two subsets to ADAM17 inhibition described in the central response, this indicates that

NKG2D and ADAM17 contribute through separable mechanisms and that the two subsets are not one population at different stages of shedding. These data are now presented in a more structured form and the interpretation is explicit in the revised text.

> *Summary statement*
>
> *Taken together, many of the data presented in the manuscript are consistent with the very well-established downregulation of CD16 expression on activated NK cells, suggesting that the observed association between reduced CD16 expression on CD56dim NK cells and enhanced effector functions is a consequence of higher activation of these NK cells.*

We appreciate the reviewer articulating the central concern so clearly. We agree that CD16 downregulation on activated NK cells is well established and occurs in our assays; where we reach a different conclusion is on whether the enhanced function of the $CD56^{dim}CD16^{dim}$ subset is a consequence of that downregulation. As set out in the central response, three observations argue that it is not: the advantage is present in cells sorted into subsets before any target contact, where post-assay CD16 changes cannot apply (Fig. 2); the two subsets respond to ADAM17 inhibition in opposite directions, both in magnitude (Fig. 7B, now Figure 6B) and in the number of serial degranulation events per cell (Fig. 9, now Figure 8), which is difficult to reconcile with their being one population at different activation levels; and blocking NKG2D together with ADAM17 reduces $CD16^{dim}$ degranulation below either alone (Fig. 8, now Figure 7), indicating that the advantage is driven by NKG2D through a mechanism separable from shedding. We therefore interpret the association between low CD16 and enhanced function not as activation-induced downregulation of a single population, but as a property of a distinct, pre-existing subset. This interpretation is stated and defended explicitly in the revised Discussion, and will be strengthened with the expanded pre-sorted experiments.

> ***Reviewer #2 (Public review):***
>
> *(1) The central conclusion is weakened by the use of CD16 as a stable phenotypic marker. CD16 is well established to be rapidly downregulated following NK-cell activation and target cell (K562 or infected cells) engagement through ADAM17-mediated shedding. NK cell shedding regulates NK cell effector functions by promoting target cell detachment, boosting serial killing capacity, and preventing overstimulation. Therefore, NK cells displaying a CD56dimCD16dim phenotype after co-culture cannot be assumed to represent a pre-existing subset with intrinsically superior cytotoxic activity, but may instead correspond to activated CD56dimCD16bright NK cells that have downregulated CD16 during the assay. Because the vast majority of the functional experiments classified NK cell subsets based on post-assay CD16 expression, it is difficult to distinguish intrinsic functional differences between NK cell subsets from activation-induced phenotypic conversion. This limitation affects the interpretation of most of the study's principal findings.*

We thank the reviewer for this careful and well-articulated concern, which we recognize as the central issue of the review, and which we address in full in the central response above. We agree with the reviewer's premises: CD16 is rapidly shed by ADAM17 upon activation, and this shedding is itself functionally important, promoting target detachment, supporting serial engagement, and limiting overstimulation. Indeed, ADAM17-mediated shedding is integral to the serial degranulation mechanism we propose. We also agree that classifying subsets by post-assay CD16 expression alone cannot, on its own, distinguish a pre-existing subset from activation-induced conversion.

For this reason, our conclusion does not rest on post-assay classification. As detailed in the central response, the $CD56^{dim}CD16^{dim}$ advantage is demonstrated in cells sorted into subsets

before any target contact, where the readout is direct lysis rather than post-assay gating and where activation-induced shedding therefore cannot account for the difference (Fig. 2), an experiment both this reviewer and the peer reviewer identify as the strongest in the manuscript. This is reinforced by evidence that the two subsets are functionally distinct rather than one population caught at different stages of shedding: they respond to ADAM17 inhibition in opposite directions, both in the magnitude of degranulation (Fig. 7B, now Figure 6B) and in the number of serial degranulation events per cell (Fig. 9, now Figure 8); blocking NKG2D together with ADAM17 reduces $CD16^{dim}$ degranulation below either alone, indicating a mechanism separable from shedding (Fig. 8, now Figure 7); and the subsets differ before stimulation, with NKG2D 1182 gMFI higher on $CD16^{dim}$ cells and no corresponding difference in NKp46 (Fig. 6, now Figure 5). We will strengthen this further by expanding the sorted-subset experiments across additional donors, and the revised text rests the manuscript's conclusions explicitly on the pre-sorted data.

> *(2) The "killing frequency" analysis presented in Figure 3 is based on a mathematical estimate rather than a direct experimental measurement. Since total target cell killing is measured in mixed NK cell populations, it cannot be attributed to individual NK cell subsets. This experiment must be repeated using purified NK cell subsets.*

We agree that the killing frequency in Fig. 3 (now Figure 2—figure supplement 1C) is a mathematical estimate rather than a direct measurement. We would add that this is intrinsic to the metric: killing frequency is a derived quantity whether calculated from mixed or purified populations, so repeating it on purified subsets would not convert it into a direct measurement. This analysis has been moved to the supplementary material, and its limitations are stated in the Discussion, namely that killing frequency is an estimate and should be interpreted as such. Direct, subset-resolved killing is instead provided by Figure 2, in which NK cells sorted before target exposure show that purified $CD56^{dim}CD16^{dim}$ cells lyse HIV-infected targets more efficiently than purified $CD56^{dim}CD16^{bright}$ cells; this is the measurement on which our conclusion regarding direct killing rests, and it is the experiment we will expand across additional donors.

> *(3) The serial degranulation assay presented in Figure 4 does not directly measure serial target cell killing and therefore does not support the conclusion that CD56dimCD16dim NK cells possess superior serial killing capacity. Furthermore, the increased serial degranulation observed in the CD16dim population could simply reflect activation-induced CD16 downregulation rather than an intrinsic property of this subset. This experiment should therefore be repeated using purified NK cell subsets.*

We agree that Fig. 4 (now Figure 3) measures serial degranulation, not serial killing directly. The text has been revised throughout to describe this as serial degranulation rather than serial killing, so that our conclusions match what was measured. Regarding the concern that increased serial degranulation in $CD16^{dim}$ cells reflects activation-induced CD16 downregulation, we address this in the central response; the opposite responses of the two subsets to ADAM17 inhibition (Figs. 7B and 9, now Figures 6B and 8) argue against that interpretation. As the reviewer suggests, we will repeat the serial degranulation assay on subsets purified before target exposure if cell yields from the sort permit. We note that this assay requires four sequential labelling and washing steps and that the $CD56^{dim}CD16^{dim}$ subset constitutes fewer than 5% of $CD56^{dim}$ NK cells, so the number of sorted cells recovered may be limiting; we will report the outcome either way.

> *(4) The finding that CD56dimCD16dim NK cells exhibit greater ADCC activity is somewhat counterintuitive given the central role of CD16 in mediating ADCC. Moreover, these experiments are likely confounded by activation-induced CD16 downregulation, which is expected to be even more pronounced during ADCC. Thus, the apparent superiority of the CD56dimCD16dim subset may simply reflect the conversion of activated CD56dimCD16bright NK cells into the CD16dim gate rather than intrinsically greater*

> *ADCC activity. To directly compare the intrinsic ADCC capacity of each subset, these experiments should be repeated using purified NK cell populations prior to target-cell stimulation.*

We agree that the greater antibody-dependent response of $CD56^{dim}CD16^{dim}$ cells is counterintuitive given the central role of CD16, and we regard it as an informative finding rather than an artifact. As set out in our revised Discussion, the surface density of gp120 on HIV-infected primary T-cells is approximately 6.4×10^2 molecules per cell (Vasiliver-Shamis et al., 2008), two orders of magnitude below high-density antigens such as CD20 on Raji cells at approximately 5×10^4 molecules per cell (Lallemand et al., 2017). Antibody-dependent responses against HIV-infected cells therefore proceed under conditions of limiting antigen, and both $CD56^{dim}$ subsets face the same constraint. What differs between them is not the constraint but the NKG2D available to meet it: $CD56^{dim}CD16^{dim}$ cells carry higher NKG2D before target contact and respond more strongly, despite their lower CD16. Consistent with a requirement for a second signal under these conditions, ADAM17 inhibition reduced $CD56^{dim}CD16^{dim}$ degranulation even at 0 µg/mL VRC01 (Figs. 7B and 7C, now Figures 6B and 6C), where no antibody is present to engage CD16.

Regarding the concern that this superiority reflects conversion of $CD16^{bright}$ cells into the $CD16^{dim}$ gate, we address this in full in the central response; the opposite responses of the two subsets to ADAM17 inhibition, in both degranulation magnitude (Fig. 7B, now Figure 6B) and serial degranulation (Fig. 9, now Figure 8), argue against it. As the reviewer recommends, we will directly compare the intrinsic antibody-dependent capacity of each subset using cells purified before target-cell stimulation, extending the pre-sorted approach of Figure 2 to the antibody-dependent setting across additional donors.

> ***Recommendations for the authors:***
>
> ***Reviewer #2 (Recommendations for the authors):***
>
> *(1) As discussed in the public review, the majority of the functional assays should be repeated using purified NK cell subsets. This approach would eliminate the confounding effect of activation-induced CD16 downregulation and allow the intrinsic functional properties of each subset to be directly compared.*

We agree, and this is the central experimental commitment of our revision. As described in the central response, we will repeat the specific-lysis and antibody-dependent degranulation assays using NK cell subsets purified before target-cell exposure, so that the intrinsic functional properties of each subset are compared directly and are not subject to activation-induced changes in CD16 expression. We will also perform the serial degranulation assay on sorted subsets if cell yields permit; that assay requires four sequential labelling and washing steps, and the $CD56^{dim}CD16^{dim}$ subset constitutes fewer than 5% of $CD56^{dim}$ NK cells, so we cannot commit to it in advance of the sort. This extends the pre-sorted approach already used in Figure 2, which the reviewer identifies as the strongest evidence in the manuscript, across additional donors and across the functional readouts. These experiments require cell sorting and primary-cell work and will be completed within approximately six to eight weeks and provided with the revised manuscript.

> *(2) The experiments performed with purified NK cell subsets in Figure 2 provide the strongest evidence supporting the authors' conclusion that CD56dimCD16dim NK cells exhibit greater direct cytotoxicity against HIV-infected target cells. These data are the most convincing in the manuscript because they are not confounded by post-assay changes in CD16 expression. However, unlike the other functional assays, no representative gating strategy or raw flow cytometry plots are provided, and the results appear to be based on a single representative experiment. Given the importance of these data to the manuscript's central conclusion, this experiment should be expanded to*

> *include biological replicates from additional donors, representative flow cytometry plots, and validation using additional HIV-1 infectious molecular clones.*

We appreciate the reviewer identifying the sorted-subset experiments in Figure 2 as the strongest evidence for our conclusion, and we agree these data warrant expansion. In the revised manuscript we will:

(1) Expand the experiment to include biological replicates from additional donors, with all donors shown rather than a single representative experiment.

(2) Provide the representative gating strategy and flow cytometry plots for the sorted subsets. The reviewer is correct that these should be included, and we will add them, including for the expanded experiments.

(3) Validate the finding using additional HIV-1 strains. We note, for clarity, that the virus used throughout this study is a primary patient isolate (HIV-1^{SHM-1}), as stated in the Materials and Methods, rather than an infectious molecular clone. We have now compared NK cell degranulation against autologous $CD4^{positive}$ T-cells productively infected with HIV-1^{SHM-1}, with the X4-tropic infectious molecular clone HIV-1^{NL4-3}, and with the R5-tropic laboratory-adapted strain HIV-1^{BaL}, at three effector cell to target cell ratios. CD56 ^{dim} CD16 ^{dim} cells degranulated more than CD56 ^{dim}$CD16^{bright}$ cells against every virus at every ratio, in all nine comparisons at $p < 0.0001$. Both subsets responded less to HIV-1^{NL4-3} and HIV-1^{BaL} than to HIV-1^{SHM-1}, and did so in proportion: the ratio of CD56 ^{dim}$CD16^{dim}$ to CD56 ^{dim} $CD16^{bright}$ degranulation ranged from 2.7 to 3.8 across all nine conditions. The magnitude of the response therefore varies with the virus, whereas the relationship between the two subsets does not. These data are included in the revised manuscript as Figure 1—figure supplement 3, with the statistical analysis in a supplemental table.

The experiments described in points 1 and 2 require cell sorting and primary-cell work and will be completed within approximately six to eight weeks and provided with the revised manuscript.

> *(3) The mechanism underlying the enhanced effector function of CD56dimCD16dim NK cells remains unclear. Although the phenotypic characterization presented in Figure 5 (and related supplement figures) is informative, NK cell receptor expression was assessed after target cell stimulation, when it may already have been altered by activation and CD16 downregulation. Receptor expression should therefore be evaluated prior to stimulation. In addition to NKG2D, the authors should also consider assessing additional activating receptors, notably NKp30, which has recently been implicated in the elimination of autologous HIV-1-infected cells (PMID: 41079618).*

We agree that receptor expression should be assessed before stimulation, and in fact it is. In Fig. 6 (now Figure 5), the receptor gMFI data include the no-target condition, showing that $CD56^{dim}CD16^{dim}$ cells express 1182 gMFI more NKG2D than CD56 ^{dim}$CD16^{bright}$ cells before any target-cell contact ($p < 0.0001$), approximately 1.6-fold, and therefore before any activation-induced change in receptor expression. NKp46, measured on the same cells in the same wells, did not differ between the subsets under the same condition (mean difference 45.67 gMFI, $p = 0.0668$), indicating that the difference is specific to NKG2D rather than a general difference in activating receptor density. The baseline condition is now labelled explicitly as 1:0 in the revised figure and described as such in the Results text.

Regarding NKp30, we have assessed this receptor. Degranulation did not differ between NKp30 positive and NKp30 negative cells within either $CD56^{dim}$ subset, whereas both $CD56^{dim}CD16^{dim}$ groups exceeded both $CD56^{dim}CD16^{bright}$ groups regardless of NKp30 status, indicating that the enhanced degranulation of the subset is not attributable to NKp30, paralleling our finding for NKp46. These NKp30 data are included in the revised manuscript as

Figure 5—figure supplement 1, with the corresponding statistical analysis in a supplemental table. We note that this analysis addresses whether NKp30 accounts for the difference between the subsets; it does not exclude a role for NKp30 in NK-cell recognition of HIV-infected cells more generally, consistent with the study the reviewer cites, which we now discuss.

> *(4) In Figure 5, the histograms corresponding to the uninfected and ΔVpr conditions appear to be identical. If this is indeed the case, this represents a serious concern, as these are two distinct experimental conditions and should not be represented by the same flow cytometry plot. This raises the possibility of an inadvertent panel duplication. The authors should carefully verify the figure and replace the duplicated panel if necessary.*

We thank the reviewer for this careful observation. On review, the histograms in Figure 5A were reproduced from our earlier study (Ward et al., PLoS Pathog 2009;5(10):e1000613) and should not have been included without attribution. We have removed that panel and cite the original finding in its place.

Figures 5B and 5C are both new results from this study, and both are retained. Figure 5B, which shows that NK cells degranulate in response to wild-type HIV-infected targets but not to ΔVpr-infected or uninfected targets, becomes Figure 4—figure supplement 1 in the revised manuscript. Figure 5C, the NKG2D blockade experiment, becomes Figure 4A and 4B.

> *(5) The ADCC experiments and calculation require additional methodological clarification, particularly the analyses presented in Figure 7C. Although NK cell degranulation is commonly used as a surrogate marker of ADCC, the data presented in Figure 7 do not appear to isolate the antibody-dependent component of the response. To specifically quantify ADCC-mediated degranulation, the degranulation induced by HIV-infected target cells alone (i.e., in the absence of VRC01) should be subtracted from that measured in the presence of VRC01. Notably, in Figure 7C (DMSO), the CD56dimCD16dim population appears to exhibit similar levels of degranulation in the absence and presence of VRC01, suggesting that antibody-dependent degranulation may be limited in this subset, which does not support the author's conclusions.*

We thank the reviewer for raising this, and we agree that the antibody-dependent and antibody-independent components of the response should be distinguished. We would, however, respectfully argue against the subtraction as a means of doing so, and we believe the experiments already in the manuscript address the underlying question more directly.

The condition without VRC01 is not a background to be removed. It is the NKG2D-driven response of the same cells to the same infected targets, measured through the same degranulation machinery, and it is one of the principal findings of the study. Subtracting it treats the two components as though they were independent and additive, when both converge on a single immunological synapse and a single degranulation event per cell. The difference between the two conditions is therefore not the antibody-dependent response; it is the increment in total degranulation produced by adding antibody, which is a different quantity and one that carries no clean interpretation at the level of the individual cell.

The question the reviewer raises, whether the antibody-dependent component differs between the subsets, is answered directly by the two-way ANOVA of these data. Across the VRC01 titration, the effect of NK cell subset accounts for 85.91% of the total variation ($F(1, 16) = 424.0$, $p < 0.0001$) and the effect of VRC01 concentration for 10.18% ($F(3, 16) = 16.74$, $p < 0.0001$), while the subset × VRC01 interaction is not significant ($F(3, 16) = 1.112$, $p = 0.3732$) and accounts for 0.68% (Supplemental Table 20 in the revised manuscript). The absence of an interaction means that adding antibody raises the response of both subsets by a comparable amount, and that the difference between the subsets is the same at every VRC01

concentration tested. This is a statistical statement about the antibody-dependent component, obtained without subtracting one condition from another.

We agree with the implication the reviewer draws from this, and we state it plainly in the revised Discussion: the antibody-dependent increment is modest in both subsets. We attribute this to the very low surface density of gp120 on HIV-infected primary T-cells, approximately 6.4×10^2 molecules per cell (Vasiliver-Shamis et al., 2008), which is two orders of magnitude below high-density antigens such as CD20 on Raji cells, approximately 5×10^4 molecules per cell (Lallemand et al., 2017). Under these conditions the antibody-dependent signal available to any NK cell is limited, and this applies equally to both subsets.

Where we differ from the reviewer is on the conclusion this supports. That the antibody-dependent increment is modest in both subsets does not weaken our central claim, which is comparative: at every VRC01 concentration tested, including in the presence of antibody, $CD56^{dim}CD16^{dim}$ cells degranulate more than $CD56^{dim}CD16^{bright}$ cells against antibody-coated HIV-infected targets. That comparison is what the manuscript reports, and it is unaffected by how the response is partitioned between its antibody-dependent and antibody-independent components.

We also note that the experiments in Figs. 7B and 7C (now Figures 6B and 6C) do isolate a component of the response experimentally rather than arithmetically. Inhibiting ADAM17 removes the contribution that depends on CD16 turnover, and it does so in opposite directions in the two subsets, reducing $CD56^{dim}CD16^{dim}$ degranulation and increasing that of $CD56^{dim}CD16^{bright}$ cells at every VRC01 concentration. These are direct experimental manipulations of the antibody-dependent pathway, and they are more informative than the arithmetic difference between two conditions.

Finally, we take the reviewer's point that the analyses in Fig. 7C require clearer explanation. In the revised manuscript we state explicitly what is plotted, namely the percentage of each CD16 subset among CD107a positive $CD56^{dim}$ NK cells, we describe the background subtraction that applies to all CD107a data in this study, and we report the statistical analysis of each panel in full.

> *(6) It is also unclear how the authors interpret the effects of ADAM17 inhibition. While ADAM17 inhibition increases the ADCC activity of the CD56dimCD16bright population, it simultaneously decreases that of the CD56dimCD16dim population. An alternative explanation is that inhibition of CD16 shedding prevents activated CD56dimCD16bright NK cells from transitioning into CD56dimCD16dim during the assay. This possibility should be discussed and experimentally addressed, as it provides a plausible alternative interpretation of the observed phenotype.*

We thank the reviewer for articulating this alternative, which we address in full in the central response. We agree that the opposite effects of ADAM17 inhibition on the two subsets are central to interpreting these experiments, and we interpret them as evidence that the two are distinct populations rather than one transitioning into the other.

The reviewer's alternative, that ADAM17 inhibition prevents $CD56^{dim}CD16^{bright}$ cells from transitioning into the $CD56^{dim}CD16^{dim}$ gate, predicts that blocking shedding should reduce the $CD56^{dim}CD16^{dim}$ population by cutting off its supply from $CD16^{bright}$ cells. Three observations argue against this being the explanation for the functional difference. First, the effect is not merely a change in population size but a change in per-cell function in opposite directions: ADAM17 inhibition increases the number of serial degranulation events in $CD56^{dim}CD16^{bright}$ cells while decreasing them in $CD56^{dim}CD16^{dim}$ cells (Fig. 9, now Figure 8), which is difficult to explain if the dim cells were simply bright cells prevented from converting. Second, blocking NKG2D together with ADAM17 reduces $CD56^{dim}CD16^{dim}$ degranulation below either treatment alone (Fig. 8A, now Figure 7A); if NKG2D blockade

acted only by reducing the shedding that drives the putative transition, the combination could not exceed the effect of ADAM17 inhibition alone. Third, we have tracked the fate of each subset sorted before target exposure: at one hour, when degranulation is maximal, only approximately 4% of sorted CD16^{bright} cells were found in the CD16^{dim} gate, while approximately 35% had moved to the CD16^{negative} gate (Author response image 1 accompanying this response). Shedding therefore directs CD16^{bright} cells past the CD16^{dim} gate rather than into it.

We discuss this alternative explicitly in the revised Discussion and will address it further experimentally by repeating these assays on subsets purified before target exposure, where no transition can occur during the assay.

> ***Reviewing Editor Comments:***
>
> *The conclusion that CD56dimCD16dim NK cells are intrinsically superior effectors against HIV-infected target cells requires additional evidence because CD16 is rapidly downregulated following NK-cell activation. Throughout most of the study, NK-cell subsets are classified after target-cell encounter, making it difficult to distinguish pre-existing CD56dimCD16dim cells from activated CD56dimCD16bright cells that have undergone ADAM17-mediated CD16 shedding. The authors should repeat functional experiments using NK-cell subsets purified before target-cell exposure and determine the extent to which ADAM17 inhibition alters subset frequencies and functional readouts. These experiments are essential to establish whether the observed functional differences reflect intrinsic biology rather than activation-induced phenotypic conversion.*

We thank the editor for this clear synthesis of the central concern, which we address in full in the central response above. In brief, our conclusion does not rest on post-encounter classification: the CD56^{dim}CD16^{dim} advantage is established in cells sorted into subsets before any target contact, using direct lysis as the readout (Fig. 2), and is reinforced by the opposite responses of the two subsets to ADAM17 inhibition in both degranulation magnitude (Fig. 7B, now Figure 6B) and serial degranulation (Fig. 9, now Figure 8), by the separable contributions of NKG2D and ADAM17 (Fig. 8, now Figure 7), and by pre-stimulation differences between the subsets, with NKG2D 1182 gMFI higher on CD16^{dim} cells and no corresponding difference in NKp46 (Fig. 6, now Figure 5). We agree these questions are central and will repeat the functional experiments on subsets purified before target exposure, and the effect of ADAM17 inhibition on subset frequencies is presented explicitly in Figs. 7C and 8B (now Figures 6C and 7B).

> *Major conclusions should be supported by more rigorous experimental validation. In particular, the sorted NK-cell experiments should be expanded using multiple independent donors, include killing of uninfected target cells as controls and provide representative gating strategies and flow cytometry plots. Likewise, the current analyses of killing frequency, serial killing, and ADCC should be strengthened by direct measurements using purified NK-cell subsets rather than mathematical estimates or analyses performed in mixed NK-cell populations.*

We agree and will strengthen the validation as follows. The sorted-subset experiments will be expanded across multiple independent donors, with all donors shown. Uninfected-target controls will be included for the sorted-cell lysis experiments (Fig. 2); the corresponding CD107a controls against uninfected targets are already presented in Figure 1—Figure Supplement 4C of the revised manuscript. Representative gating strategies and flow cytometry plots will be provided for the sorted-cell experiments, as for our other assays. Regarding direct measurement: the killing-frequency metric (Fig. 3, now Figure 2—figure supplement 1C) is a mathematical estimate whether derived from mixed or purified populations, and it has been moved to the supplementary material with this limitation noted in the Discussion, while direct, subset-resolved killing is provided by the pre-sorted lysis

experiment (Fig. 2), which we will expand; the serial degranulation assay (Fig. 4, now Figure 3) is now described as serial degranulation rather than serial killing, and will be repeated on purified subsets if cell yields from the sort permit; and the antibody-dependent comparison will be performed on subsets purified before stimulation.

> *Some aspects of the data analysis and presentation require clarification. The authors should evaluate receptor expression before target-cell stimulation, clarify the ADCC analyses and interpretation of ADAM17 inhibition, verify the apparent duplicated flow-cytometry panel, apply appropriate statistical corrections for multiple comparisons where necessary, and streamline the presentation by emphasizing the principal conclusions rather than extensive descriptive analyses.*

We have addressed each of these. Receptor expression before stimulation is shown in the gMFI data of Fig. 6 (now Figure 5) at the no-target condition, where $CD56^{dim}CD16^{dim}$ cells carry 1182 gMFI more NKG2D than $CD56^{dim}CD16^{bright}$ cells ($p < 0.0001$) with no corresponding difference in NKp46 ($p = 0.0668$); this condition is now labelled explicitly as 1:0 in the figure and described as such in the Results text. The antibody-dependent analyses and the interpretation of ADAM17 inhibition are clarified in the revised text, as detailed in our responses to the three reviewers and the central response.

On the duplicated panel: the histograms in Figure 5A were reproduced from Ward et al. (2009) and should not have been included without attribution. That panel has been removed and the original finding is cited in its place. Figures 5B and 5C are both new results and are retained, becoming Figure 4—figure supplement 1 and Figures 4A and 4B respectively.

We have applied appropriate multiple-comparison corrections, using the post-hoc test matched to each comparison structure and reporting adjusted p-values throughout; the design and post-hoc test used for each figure and panel are given in a new supplemental table. Finally, we have streamlined the presentation by opening each Results section with a statement of the principal finding before the supporting data, and by reducing the inhibitory receptor section from approximately 1,800 words and more than 80 reported p-values to approximately 700 words and 24, with the detailed data retained in the supplemental tables and their significance synthesized in the Discussion.

References

Amand M, Iserentant G, Poli A, Sleiman M, Fievez V, Sanchez IP, Sauvageot N, Michel T, Aouali N, Janji B, Trujillo-Vargas CM, Seguin-Devaux C, Zimmer J. 2017. Human $CD56^{dim}CD16^{dim}$ cells as an individualized natural killer cell subset. Frontiers in Immunology 8:699. doi:10.3389/fimmu.2017.00699.

Lallemand C, Liang F, Staub F, Simansour M, Vallette B, Huang L, Ferrando-Miguel R, Tovey MG. 2017. A novel system for the quantification of the ADCC activity of therapeutic antibodies. Journal of Immunology Research 2017:3908289. doi:10.1155/2017/3908289.

Vasiliver-Shamis G, Tuen M, Wu TW, Starr T, Cameron TO, Thomson R, Kaur G, Liu J, Visciano ML, Li H, Kumar R, Ansari R, Han DP, Cho MW, Dustin ML, Hioe CE. 2008. Human immunodeficiency virus type 1 envelope gp120 induces a stop signal and virological synapse formation in noninfected CD4+ T cells. Journal of Virology 82:9445-9457. doi:10.1128/JVI.00835-08.

Ward J, Davis Z, DeHart J, Zimmerman E, Bosque A, Brunetta E, Mavilio D, Planelles V, Barker E. 2009. HIV-1 Vpr triggers natural killer cell-mediated lysis of infected cells through activation of the ATR-mediated DNA damage response. PLoS Pathogens 5(10):e1000613. doi:10.1371/journal.ppat.1000613.

https://doi.org/10.7554/eLife.112322.1.sa0